Table of contents

Název práce: Vedené vlny v periodických strukturách a jejich senzorové aplikace.
Autor: Milan Vala
Katedra (ústav): Katedra chemické fyziky a optiky, MFF UK
Vedoucí diplomové práce: Ing. Jiří Homola, CSs., *Ústav radiotechniky a elektroniky, Akademie věd České republiky*
e-mail vedoucího: homola@ure.cas.cz
Abstrakt: Práce je uvedena popisem základních vlastností povrchových plazmonů šířících se podél rozhraní kov-dielektrikum a podél struktury s tenkým kovovým filmem obklopeným z obou stran dielektriky se shodným indexem lomu. Je ukázáno, že na symetrické struktuře s tenkou vrstvou kovu lze vybudit dva typy vidů vázaných povrchových plazmonů - long-range povrchový plazmon a short-range povrchový plazmon. Dále je poskytnuta stručná rešerše věnována použití těchto typů povrchových plazmonů v optických senzorech. Je navržena difraktivní vrstevnatá struktura, ve které se vázané vidy povrchových plazmonů excitují na struktuře tvořené tenkým zlatým filmem obklopeným dielektriky s podobnými indexy lomu. S použitím rigorózní integrální metody je difraktivní struktura optimalizována pro aplikaci v senzoru s povrchovými plazmony. Difraktivních struktury s optimálními parametry jsou připraveny a charakterizovány opticky a s použitím mikroskopu atomových sil. V závěru je demonstrována aplikace připravených difraktivních struktur v senzoru s povrchovými plazmony a modulací vlnové délky.
Klíčová slova: senzor s povrchovými plazmony, long-range povrchový plazmon, difrakční mřížka

Title: Guided waves in periodical structures and their sensor applications.
Author: Milan Vala
Department: Department of Chemical Physics and Optics
Supervisor: Ing. Jiří Homola, CSc., *Institute of Radio Engineering and Electronics, Czech Academy of Sciences*
Supervisor's e-mail address: homola@ure.cas.cz
Abstract: This work is introduced by the description of fundamental properties of surface plasmons, propagating along the metal-dielectric interface and along the structure with thin metal film surrounded by the dielectrics with identical refractive indices. It is shown, that the excitation of two coupled modes (long-range surface plasmon - LRSP and short-range surface plasmon - SRSP) on symmetrical structure with a thin metal film is possible. Further, a brief overview of surface plasmons applications in optical sensors is presented. The diffractive multi-layer structure supporting LRSP and SRSP modes, which consists of the thin gold film surrounded by the dielectrics with slightly different refractive indices is designed. The diffractive structure is optimized using rigorous integral method for an application in SPR sensor. Diffractive structures with optimal parameters are prepared and characterized optically and using atomic force microscopy. In the end, an application of developed diffractive structure in SPR sensor with wavelength modulation is demonstrated.
Keywords: SPR sensor, long-range surface plasmon, diffraction grating

1. Introduction

During several last decades, attention devoted to development of high-resolution sensors for biological and chemical sensing in medicine, food industry, warfare etc. has been growing significantly. Up to now, a wide range of sensing techniques were studied giving rise to a variety of sensors – electromechanical [1], electrochemical [2] or optical [3]-[11].
Optical sensors represents fast growing branch of research and together with the progress in optics, chemistry, material sciences and related disciplines, they find a place in numerous applications. Up to now, optical sensors employing techniques such as Raman scattering spectroscopy [3], surface enhanced Raman scattering spectroscopy [4], fluorescence intensity measurement [5], grating coupler [6], [7], interferometry [8], [9], colorimetry [10] or surface plasmon resonance (SPR) [11] were developed.
Since the 80's of 20th century SPR sensors have been widely used due to their ability to perform a real time, „in situ" monitoring of refractive index changes near the sensor surface and their high resolution. Advantageous is also that SPR is a label-free technique [11]. Several types of SPR sensors were reported including fiber optical [35], integrated optical SPR sensor [40], prism [29] or grating [44] coupler-based SPR sensor.
In this thesis theoretical study, fabrication and characterization of a new sensing structure for SPR sensor based on grating coupler with interrogation of special modes of surface plasmon (SP) called long-range and short-range SP is described. By employing these special SP modes, improvement in resolution compared to "standard" grating-coupled SPR sensors is expected. Besides that, possible simplification of the sensor instrumentation is motivation of this work.

1.1 Phenomenon of surface plasmon

Surface plasmon (SP) is a lossy electromagnetic surface wave propagating along the boundary between a metal and a dielectric. SP is generated by collective coherent oscillations of free electrons at the metal surface (see Fig. 1). These coherent charge density oscillations can be excited optically (see Chapter 1.4) or by fast electrons [15].

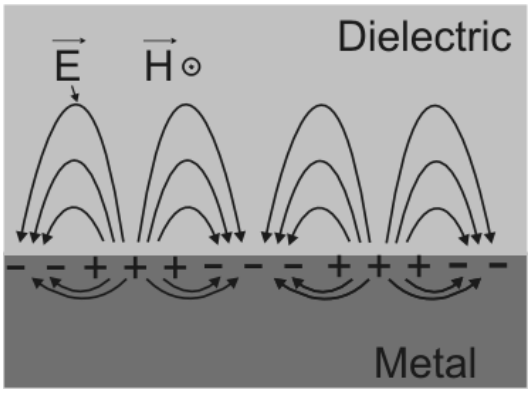

Fig. 1 Coherent charge density oscillations on metal-dielectric boundary.

The phenomenon of surface plasmon resonance was first observed in the beginning of the 20th century by Wood, who observed anomalous dark bands in spectrum of light reflected from metallic gratings [12], [13]. Later, these anomalies were found to be related to the excitation of surface waves on the metal surface by Fano [14]. In 50's, Ritchie studied excitation of surface plasmons on thin metallic films by fast electrons [15]. Later, in 60's Otto, Kretschmann and Raether introduced the attenuated total reflection method for coupling of light to surface plasmons [16], [17], which increased applicability of SPs dramatically.

1.2 Fundamental properties of surface plasmon

Let us describe fundamental properties of SP guided along a plane metal-dielectric interface. In general, in such geometry transverse electric (TE) modes (electric intensity vector perpendicular to the direction of propagation and parallel to the interface) and transverse magnetic (TM) modes (magnetic intensity vector perpendicular to direction of propagation and parallel to the interface) can propagate. Specially, let us consider the geometry consisting of a plane boundary between semi-infinite non-magnetic homogenous isotropic metal and dielectric, with complex permittivity ε_M ($\varepsilon_M = \varepsilon_M' + i\varepsilon_M''$) and ε_D, respectively. Properties of electromagnetic modes propagating along the metal dielectric boundary can be found by solving Maxwell equations with standard boundary conditions, see [18]. There can be shown, that there exists only one guided electromagnetic mode supported by this geometry. This mode is referred as to a surface plasmon (SP) and it is TM polarized with its field decaying exponentially from the interface.

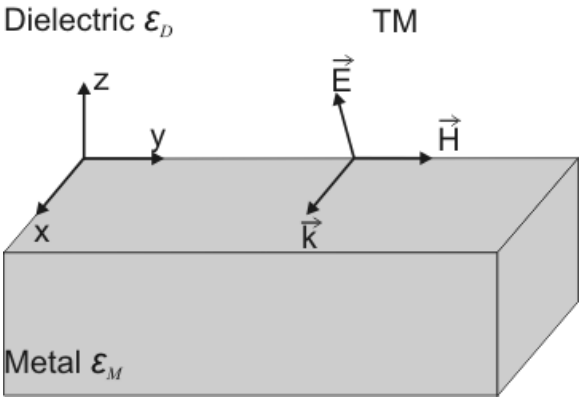

Fig. 2 Transversal magnetic mode guided along metal-dielectric interface.

Further, let us assume Cartesian coordinates with *z* axis perpendicular to the metal surface and *x* and *y* axis within metal-dielectric interface, see Fig. 2. Metal occupies the region z<0 and dielectric medium occupies the region z>0. If we assume propagation of TM-polarized surface plasmon in *x* direction, its electromagnetic field can be described as [18]:

$$\begin{aligned}
\mathbf{r}\\
E_D &= (E_x, 0, E_z) = (1, 0, \frac{ib}{a_D}) A \exp\{-a_D z + i(b x - wt)\} \quad ,\\
\mathbf{r}\\
H_D &= (0, H_y, 0) = (0,1,0) \frac{-iAwe_D}{c^2 a_D m_0} \exp\{-a_D z + i(b x - wt)\} \quad ,\\
a_D^2 &= b^2 - \left(\frac{w}{c}\right)^2 e_D \quad ,
\end{aligned} \tag{1.1}$$

$$\begin{aligned}
\mathbf{r}\\
E_M &= (E_x, 0, E_z) = (1, 0, \frac{ib}{a_M}) A \exp\{-a_M z + i(b x - wt)\} \quad ,\\
\mathbf{r}\\
H_M &= (0, H_y, 0) = (0,1,0) \frac{-iAwe_M}{c^2 a_M m_0} \exp\{-a_M z + i(b x - wt)\} \quad ,\\
a_M^2 &= b^2 - \left(\frac{w}{c}\right)^2 e_M \quad ,
\end{aligned} \tag{1.2}$$

where $\vec{E}$ is the electric intensity vector, $\vec{H}$ is the magnetic intensity vector, β is the longitudinal propagation constant, α is the transversal propagation constant, μ_0 is the permeability of vacuum, A is a normalization constant, ω is the angular frequency, c denotes speed of light in vacuum and t is time. Indices „$_D$“ (z>0) and „$_M$“ (z<0) denote dielectric and metal, respectively. By solving Maxwell equations with boundary condition at the interface, one can obtain the propagation constant of surface plasmon β as [18]:

$$b = \frac{w}{c}\sqrt{\frac{e_D e_M}{e_D + e_M}} = \frac{w}{c} N_{SP}, \tag{1.3}$$

where N_{SP} is the effective refractive index of surface plasmon. The solution described by (1.3) exists when the real part of permittivity of metal is negative ($e_M' < 0$) and inequality $|e_M'| > e_D$ is fulfilled. For instance, this condition is valid for gold and silver in VIS and NIR region of spectrum. When describing the permittivity ε_M with Drude model, this condition is transformed to $w < w_P / \sqrt{1+e_D}$, where $w_p = \sqrt{4pNe^2 / m_0}$ (N is free electron density in metal, e is electron charge and m_0 is electron mass). Dispersion relation of SP is shown in Fig. 3.

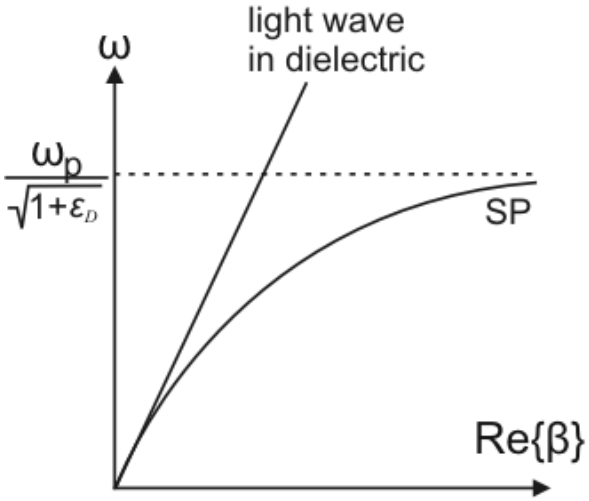

Fig. 3 Dispersion relation of SP.

As the permittivity ε_M is complex, the propagation constant β is complex as well. Its real part corresponds to the momentum of surface plasmon and it can be expressed for $|e_M''| < e_M'$ as:

$$\mathrm{Re}\{b\} = \frac{w}{c}\sqrt{\frac{e_D e_M^{'}}{e_D + e_M^{'}}}\,. \tag{1.4}$$

Imaginary part of β determines attenuation of SP in direction of propagation. The propagation length (distance where intensity of SP falls to 1/e) is then given by:

$$L_p = \frac{1}{\left|2\,\mathrm{Im}\{b\}\right|} = \frac{c}{w}\left(\frac{e_D e_M^{'}}{e_D + e_M^{'}}\right)^{-3/2}\frac{e_M^{'2}}{e_M^{''}}. \tag{1.5}$$

As SP is a surface wave, its field amplitude exponentially decays from surface into metal and dielectric media (see Fig. 4). Important parameter of SP is its penetration depth into these media. It is defined as the depth where amplitude of field falls to 1/e of its maximal value on the metal-dielectric boundary. Using equations (1.1), (1.2) and (1.3) propagation depths into dielectric L_D and metal L_M can be expressed as:

$$L_D = \frac{1}{|a_D|} = \frac{c}{w}\sqrt{\frac{e_M^{'} + e_D}{e_D^2}} \quad , \quad L_M = \frac{1}{|a_M|} = \frac{c}{w}\sqrt{\frac{e_M^{'} + e_D}{(e_M^{'})^2}}. \tag{1.6}$$

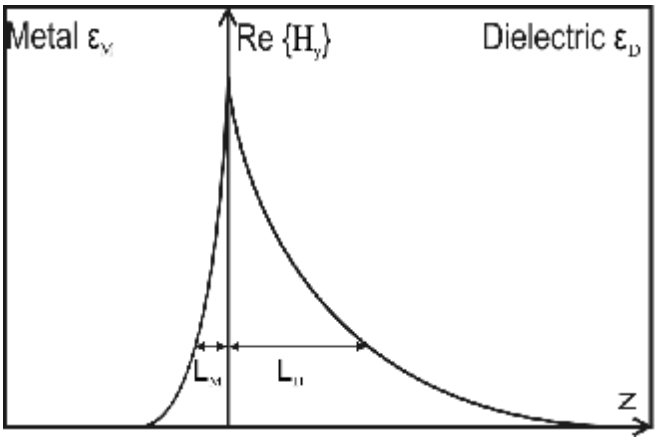

Fig. 4 Field profile of H_y component of SP.

Examples of propagation length and penetration depth of surface plasmon propagating along the boundary of dielectric ($\varepsilon_D = 1.74$) and two noble metals (gold and silver) calculated for wavelength λ=630 nm and λ=850 nm are shown in Table 1.

	Gold		Silver	
Wavelength [nm]	630	850	630	850
Penetration depth into dielectric L_D [nm]	162	400	219	443
Penetration depth into metal L_M [nm]	29	25	24	23
Propagation length L_P [μm]	2	24	19	57

Table 1. Penetration depth and propagation length of SP calculated for wavelengths 630, 850 nm and for gold and silver. Data are taken from [19].

1.3 Surface plasmon modes on a very thin metal film

Until now, we studied SP on interface between semi-infinite metal and dielectric media. Further, let us assume geometry in which a metal film of finite thickness is embedded between two semi-infinite dielectrics with permittivities ε_{D1} and ε_{D2}. In this case SPs can exist on both sides of the metal (see Fig. 5). If the metal layer thickness d_M is much larger than penetration depth of SP into metal $d_M >> L_M$, we can describe the propagation of SPs on both interfaces as in the previous chapter. However, when decreasing the metal film thickness to $d_M \sim L_M$ (see Fig. 5), electromagnetic field of SPs on opposite sides of the film can overlap giving rise to the coupling between these modes, [18].

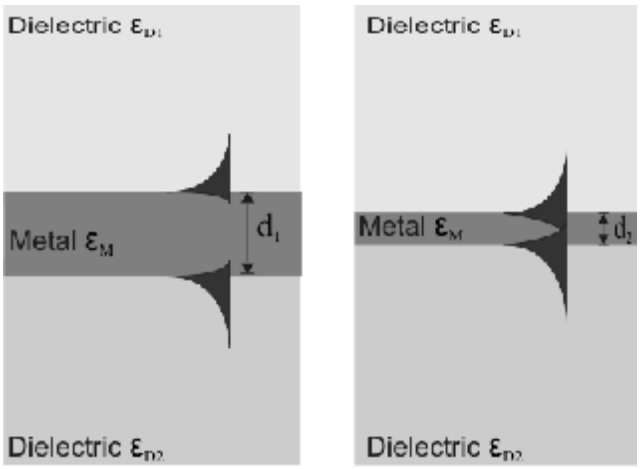

Fig. 5 Interaction between surface plasmons on the opposite sides of the metal film.

The interaction between SPs on opposite sides of the metal film can occur when ε_{D1} *and* ε_{D2} are close to each other. This interaction gives rise to existence of two coupled modes, denoted usually as "symmetrical" and "anti-symmetrical". For $\varepsilon_{D1} = \varepsilon_{D2}$ dispersion relation of these modes can be expressed as (see [18]):

$$e_M a_D + e_D a_M \tanh\left(\frac{1}{2i} a_M d\right) = 0, \tag{1.7}$$

$$e_M a_D + e_D a_M \coth\left(\frac{1}{2i} a_M d\right) = 0 \,, \tag{1.8}$$

where equations (1.7) and (1.8) describes the dispersion relation of symmetrical and anti-symmetrical mode, respectively. Example of dispersion relation of coupled SP modes guided by a thin metal film with thickness d=20 and 50 nm surrounded with a dielectric with refractive index 1.33 is shown in Fig. 6. It reveals that when decreasing the metal layer thickness, the split between the dispersion relation of symmetrical and anti-symmetrical surface plasmon mode increases.

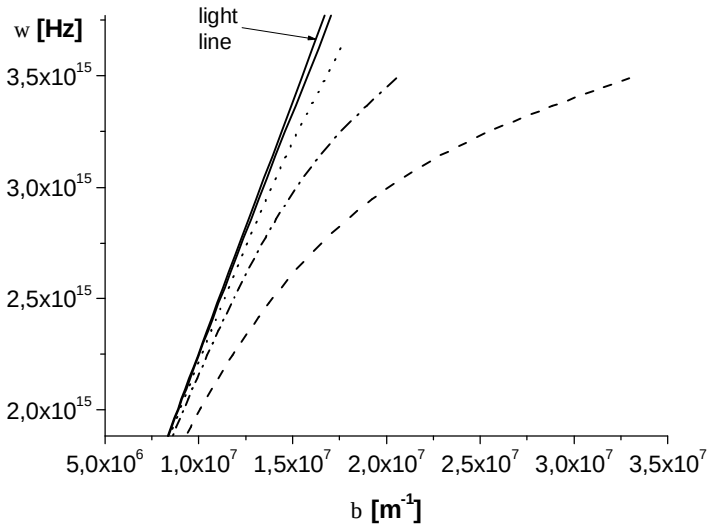

Fig. 6 Dispersion relation of SP modes on thin gold film embedded between semi-infinite dielectric with permittivity ε_D=1.33 calculated for gold film thickness 20 nm (——— symmetrical, – – – anti-symmetrical) and 50 nm (..... symmetrical, — . – anti-symmetrical).

In Fig. 7, field distribution of magnetic intensity H_y of symmetrical and anti-symmetrical mode is shown. The anti-symmetrical mode with field more localized in lossy metal (see Fig. 7) has lower propagation length than symmetrical mode with field more stretched in dielectric (see Table 2). Hence, the symmetrical mode is usually denoted as long-range surface plasmon (LRSP) and anti-symmetrical mode as short-range surface plasmon (SRSP).

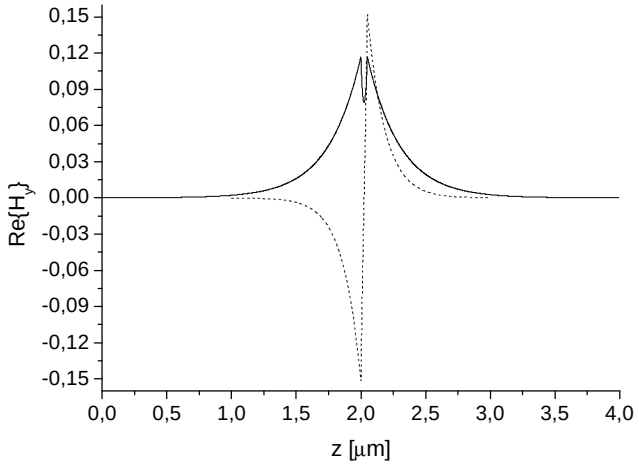

Fig. 7 Distribution of Re{H_y} of long-range (____) and short-range (.....) SP guided along a thin gold film with thickness 50 nm embedded between dielectric with refractive index n=1.33, $\omega=3x10^{15}$ (free space wavelength λ=630 nm).

In Table 2, examples of propagation lengths and penetration depths of long-range and short-range surface plasmons on thin gold film calculated for wavelengths 630 and 850 nm are presented.

Wavelength [nm]	630	850
Penetration depth of SRSP into dielectric [nm]	146	320
Penetration depth of LRSP into dielectric [nm]	251	524
Propagation length of SRSP[μm]	1,6	13
Propagation length of LRSP[μm]	13	97

Table 2 Penetration depths and propagation lengths of SP guided by the structure consisting of 50 nm thick gold film embedded in semi-infinite dielectric media with refractive index n_D =1.33 calculated for wavelengths 630 and 850 nm.

1.4 Excitation of surface plasmon

For efficient coupling of an optical wave into SP, these two waves need to be phase-matched along the metal surface. This condition is fulfilled, when the component of wave vector of light that is parallel to the interface is equal to the propagation constant of SP. As SP is a guided mode, its propagation constant is always larger than the wave vector of light in adjacent dielectric (see Fig. 3). Therefore, on plane metal surface it is not possible to optically excite SP directly from the adjacent dielectric.

In order to couple light into SP, a coupler providing enhancement of propagation constant of light needs to be used. Most commonly used couplers are prism couplers and diffraction grating couplers.

1.4.1. Excitation of surface plasmons using prism coupler

In prism coupler, attenuated total reflection (ATR) method is used (see Fig. 8, Fig. 9) to match the optical wave's wave vector with that of SP. An optical wave propagates through a dielectric prism with refractive index n_P on which base it totally reflects. Upon the reflection, evanescent field is generated at the prism base. For excitation of SP, this field is made overlapped with the region in which SP propagates along an interface between metal and dielectric with lower refractive index n_D. As the refractive index of the prism is higher then the one of the dielectric ($n_P > n_D$), the phase-matching of SP and the light wave can be achieved when:

$$\frac{w}{c} n_p \sin q = \mathrm{Re}\{b\}, \tag{1.9}$$

where θ is the angle of incidence of the light wave reflected at the prism base and β is the propagation constant of SP.

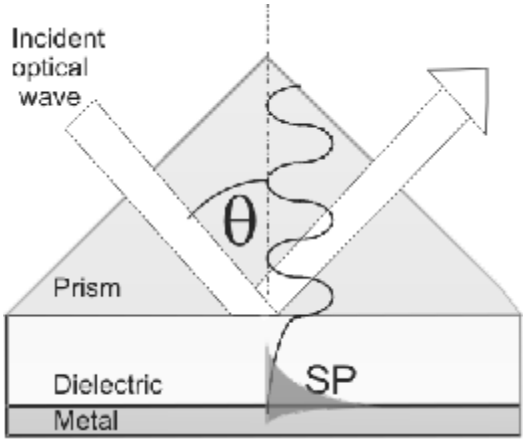

Fig. 8 Excitation of SP using prism coupler in Otto configuration.

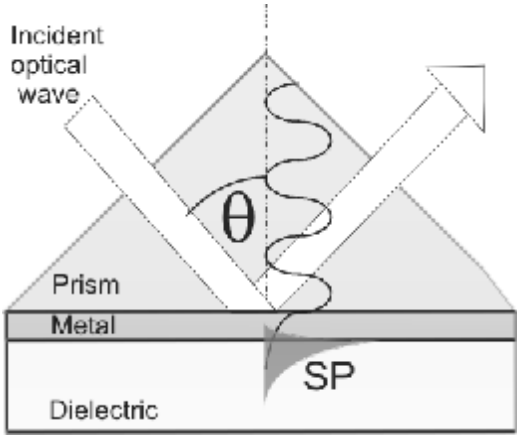

Fig. 9 Excitation of SP using prism coupler in Kretschmann configuration.

Prism coupler-based excitation of SPs can be realized in Otto or Kretschmann configuration. In Otto configuration SPs are excited through a dielectric with refractive index n_D (see Fig. 8) while in Kretschmann configuration they are excited through a thin metal film (see Fig. 9). The efficiency of the coupling between the optical wave in prism and SP can be controlled by the distance d_{PM} between prism base and the metal surface

along which SP propagates. There can be shown, that the total energy transfer between the incident optical wave and SP can occur only for certain distance d_{PM}^{opt}.

The coupling of light to SP is manifested as a narrow dip in the wavelength or angular reflectivity spectrum. This SPR dip is centered at the wavelength (for fixed angle of incidence) or angle of incidence (for fixed wavelength) described by the phase-matching condition (1.9). An example of excitation of SP in Kretschmann configuration is given in Fig. 10. In Fig. 10, angular reflectivity spectra of TM polarized wave with wavelength 800 nm exciting SP for angle of incidence about 66 degrees are shown. The structure consist of a prism with refractive index n_P=1.51, gold film with thickness 40, 50, 60 and 70 nm, and dielectric with refractive index n_D=1.33. It shows that maximum coupling of light into SP occurs for gold film thickness of about 50 nm.

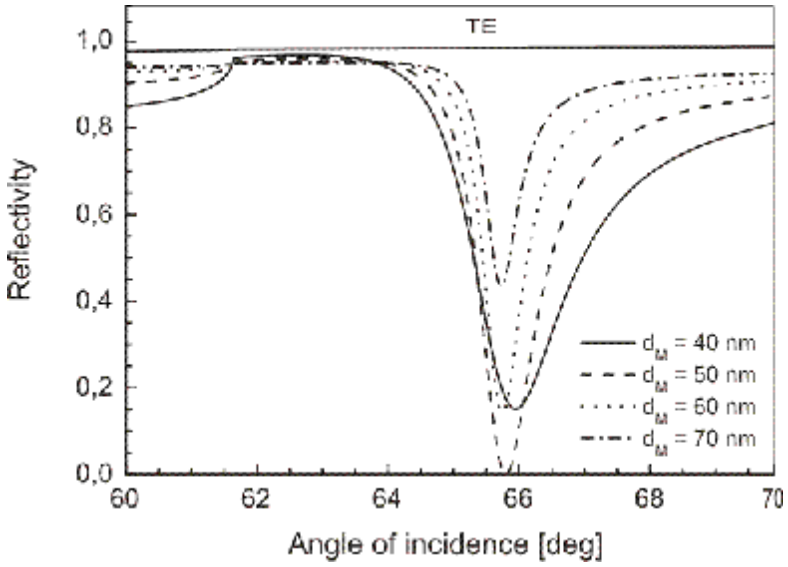

Fig. 10 Angular spectra of reflectivity of TM polarized wave calculated for Kretschmann configuration and thickness of gold film between 40 and 70 nm. Incident light wavelength λ=800 nm, n_P=1.51, n_D=1.33. TE reflectivity is shown for comparison.

1.4.2. Excitation of surface plasmon using grating coupler

Another approach to coupling of an optical wave to SP is based on grating coupler. By using grating coupler, incident light's wave vector can be enhanced to match the SP propagation constant by the diffraction of light on a periodically corrugated metal surface where the SP propagates, see Fig. 11.

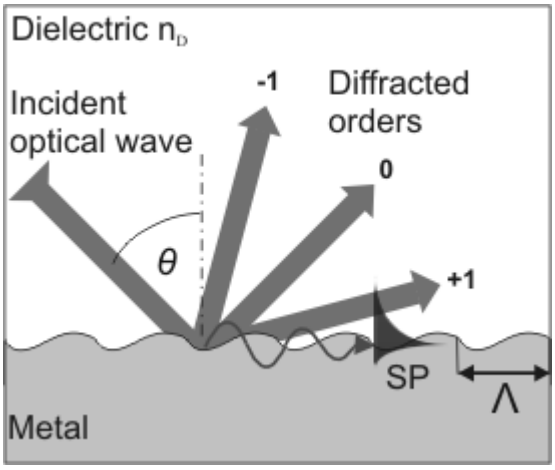

Fig. 11 Excitation of SP using a grating coupler.

If the light wave is made incident under an angle of incidence θ on periodically corrugated surface of diffraction grating with plane of incidence perpendicular to the grating grooves, reflected light splits into series of diffracted orders [20] with components of wave vectors parallel to the surface given by:

$$k_m = \frac{w}{c} n_D \sin q + mK_G, \tag{1.10}$$

where n_D denotes the refractive index of incidence dielectric, m is integer which indexes diffracted orders. K_G is the grating wave vector, which may be expressed as:

$$K_G = \frac{2p}{\Lambda}, \tag{1.11}$$

where Λ denotes spatial period of the grating. From (1.10) and (1.11) it follows, that the momentum of an optical wave can be enhanced using diffraction grating. Therefore, phase-matching between optical wave and SP can be achieved through m^{th} diffracted order:

$$\frac{w}{c} n_D \sin q + m\frac{2p}{\Lambda} = \pm \mathrm{Re}\{b\}. \tag{1.12}$$

Similarly to the ATR method, the coupling of optical wave into SP using grating coupler can be observed as narrow dip in wavelength or angular spectrum of intensity of reflected orders. The efficiency of this coupling can be controlled through the grating profile.
An example of excitation of SP using grating coupler is given in Fig. 11. This figure shows calculated reflectivity spectra of TM polarized wave, which impinges on a sinusoidal metallic grating under an angle of incidence 6 degrees (in air). The structure consist of a semi-infinite metal with periodically modulated surface (Λ=670 nm, modulation depth 10, 30, 50 and 70 nm) and dielectric with refractive index n_D=1.33. The maximum coupling of light into SP in this configuration occurs when the depth of modulation of the metal surface is about 30 nm.

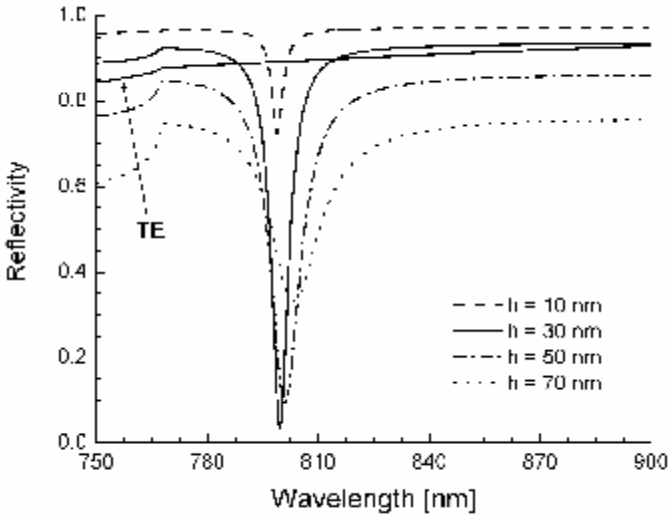

Fig. 12 Reflectivity spectra of TM polarized wave reflected from metal grating with sinusoidal profile for four different depths of modulation *h*.

1.5 Surface plasmon resonance sensors

In surface plasmon resonance (SPR) sensors, surface plasmons are used to probe the refractive index (RI) changes at the sensor surface. A thin sensitive layer is placed on the sensor surface to convert variations in a quantity of interest (for example humidity [21], pressure[22], gas concentration [34], electric field [23], concentration of biological analyte [24]-[28] etc.) into changes in RI or thickness of sensitive layer. As majority of SP energy is carried in the dielectric adjacent to the metal surface, propagation constant of SP is extremely sensitive to variations in the refractive index at the sensor surface, see (1.4). In SPR sensors, changes in optical properties of sensitive layer alter the propagation constant of SP which affects its interaction with the optical wave. Therefore,

a change in the quantity of interest can be observed as a change in one of the characteristics of the optical wave exciting surface plasmons, see Fig. 14.

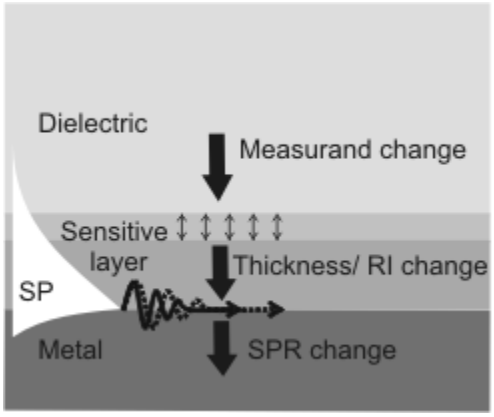

Fig. 13 Surface of an SPR sensor with a sensitive layer probed by surface plasmon.

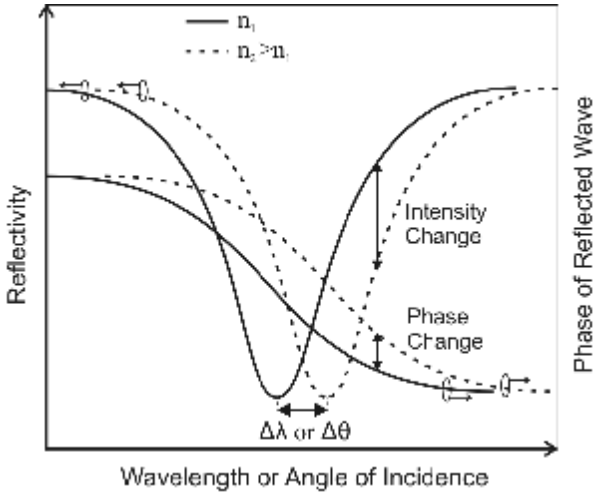

Fig. 14 SPR change caused by a refractive index change in spectrum of reflected wave characteristics.

SPR sensors relying on measurements of various characteristics of light exciting SPs were investigated [19]:

- Angular modulation (SPR is monitored using monochromatic optical wave under multiple angles of incidence. Variations of RI in sensing area are measured by tracking changes in position of SPR dip in angular reflectivity spectrum.)
- Wavelength modulation (SPR is monitored using polychromatic optical wave under fixed angle of incidence. Variations of RI in sensing area are measured by tracking changes in position of SPR dip in reflectivity spectrum of wavelength.)
- Intensity modulation (SPR is monitored using monochromatic optical wave under fixed angle of incidence. Changes of RI in sensing area are determined from variations of intensity of reflected optical wave.)
- Phase modulation (SPR is monitored using monochromatic optical wave under fixed angle of incidence. Changes of RI in sensing area are determined by measuring the variations of phase of reflected optical wave.)
- Polarization modulation (SPR is monitored using monochromatic optical wave under fixed angle of incidence. Changes of RI in sensing area are determined by measuring the reflected optical wave polarization changes.)

Majority of SPR sensors is used for detection of biological analytes. Up to now number of SPR sensors capable of measuring various analytes such as toxins [24], [25] herbicides [26], [27] and bacteria [28] were reported. In SPR biosensors, a sensitive layer with biological recognition elements, able to capture selected analyte, is used, see Fig. 15.

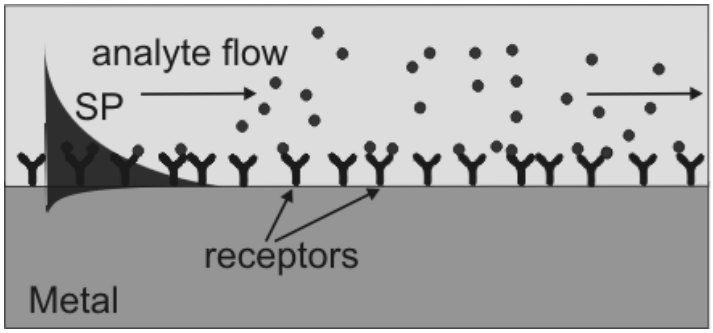

Fig. 15 Surface of SPR biosensor with layer of receptors as biological recognition element.

Up to now, SPR sensor devices were carried out using various optical arrangements. These include prism-based SPR sensors [29]-[33], grating-coupled SPR sensors [34], [44], [46]-[48], integrated optical SPR sensors [40]-[43] and optical fiber SPR sensors [35]-[39].

1.5.1 Prism-based SPR sensors

The configuration based on prism coupler was employed in first SPR sensors pioneered in the beginning of 80's [30] and later it has become the most popular one [29], [31], [32]. In these sensors, Kretschmann geometry for excitation of SPs is used as it allows bringing the samples in contact with the sensor surface directly (see Fig. 16, Fig. 17). In prism-based SPR sensors, numerous SPR modulations were employed. In Fig. 16 and Fig. 17, SPR sensors based on prism coupler with angular and wavelength modulation, respectively, are shown. In prism coupler-based SPR sensor with angular modulation of SPR, monochromatic light wave is made incident on the prism base under different angles of incidence. Changes in the resonant angle of incidence are measured from variations in the angular distribution of intensity of reflected light. In prism coupler-based SPR sensors with wavelength modulation (Fig. 17), collimated polychromatic wave is used to excite SPs. Changes in SPR are measured by the spectral analysis of the reflected light using a spectrograph.
Prism-based SPR sensor with angular modulation was demonstrated to be capable of measurements of refractive index changes as low as $3x10^{-7}$ RIU (refractive index units) [53].

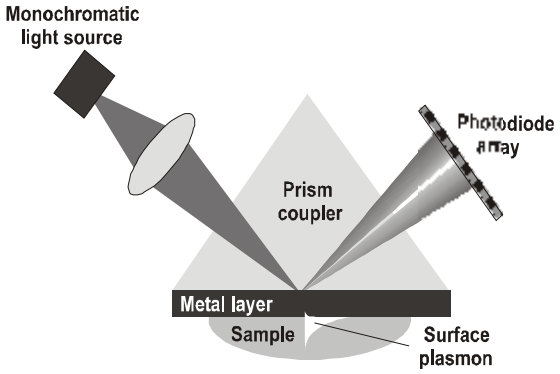

Fig. 16 SPR sensor with prism coupler and angular modulation (reproduced from [19]).

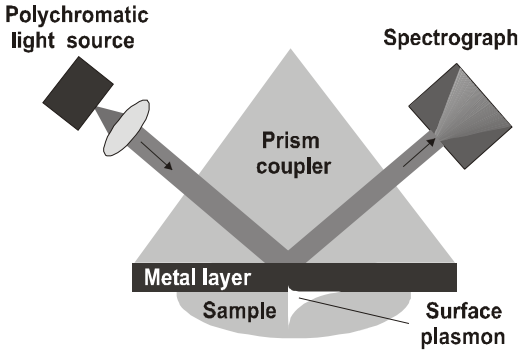

Fig. 17 SPR sensor with prism coupler and wavelength modulation (reproduced from [19]).

1.5.2 Optical fiber SPR sensors

SPR sensors based on optical fibers were investigated in order to exploit their potential for design of miniaturized and remote operating sensors. Up to now, numerous optical fiber SPR sensors based on multi-mode [35], [36] and single-mode [37]-[39] optical fibers were developed since the beginning of the nineties of the last century. In these sensors, surface plasmons are excited by guided modes of an optical fiber when the cladding of the fiber is locally removed and replaced by the SPR active metal layer. Example of sensing area of SPR sensor based on single-mode optical fiber is presented in Fig. 18. The resolution of optical fiber SPR sensor as low as $1x10^{-6}$ RIU, was achieved with SPR sensor based on single-mode optical fiber and wavelength modulation [39].

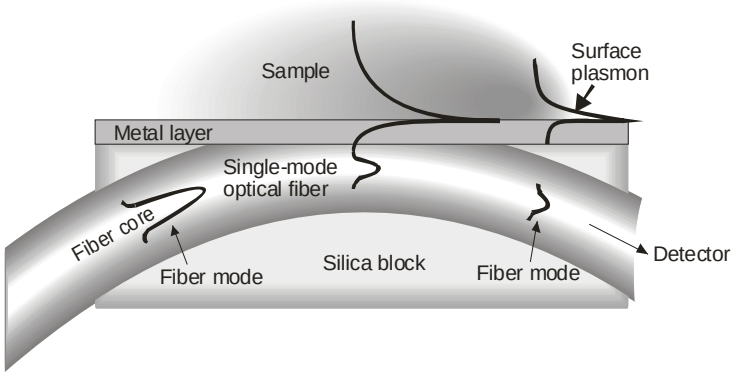

Fig. 18 Sensing structure of fiber optics SPR sensor (reproduced from [39]).

1.5.3 Integrated optical SPR sensors

The principle of integrated optical SPR sensors is similar to fiber optical SPR sensors. SPs are excited by guided mode of a waveguide such as slab or channel waveguide. Sensing structure used in this type of sensors is depicted in Fig. 19.

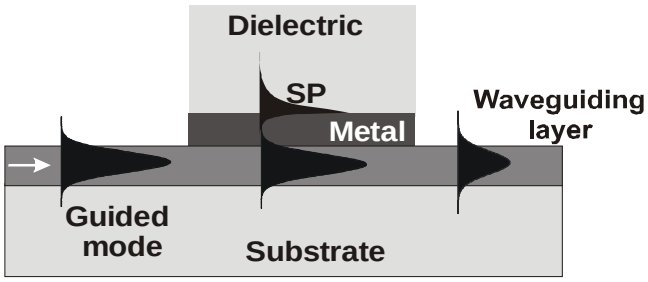

Fig. 19 Excitation of SP in integrated optics wave-guiding structure.

This type of sensor was first demonstrated in 1987 [40]. Later, several integrated optical SPR sensors were developed [41], [42]. Using integrated-optical sensor with wavelength modulation (see Fig. 20) resolution as low as 1.2×10^{-6} RIU was achieved [43].

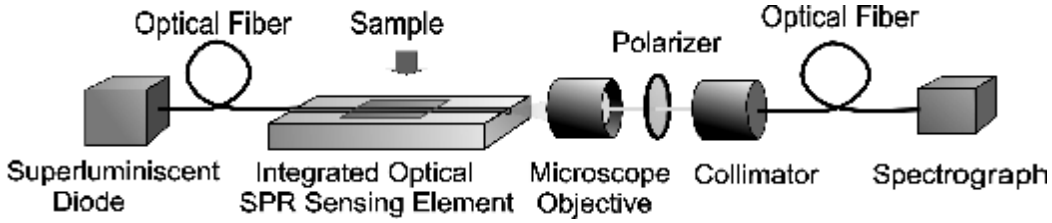

Fig. 20 Integrated optical SPR sensor with wavelength modulation (reproduced from [43]).

1.5.4 Diffraction grating-based SPR sensors

So far, diffraction gratings have been exploited in SPR sensors to a lesser extend than prism couplers. The reason for this lower interest is due to more complicated design of diffraction gratings. In addition, the necessity of excitation of SPs through analyzed samples can be assumed as a disadvantage. On the other hand, diffraction grating structures offer numerous features advantageous for applications in SPR sensors. These include the higher versatility of coupling of light to surface plasmons and possibility of integration of multiple diffraction-based optical components on the sensor chip. Additionally, the sensor chip can be fabricated from plastics by mass-production compatible technologies such as hot embossing or injection molding, [45].
Scheme of example of grating-based SPR sensor with wavelength interrogation is depicted in Fig. 21.

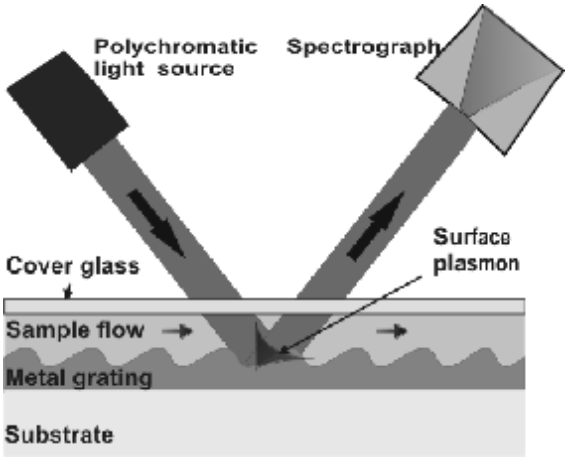

Fig. 21 SPR sensor with diffraction grating and wavelength modulation.

The first reported SPR sensor with diffraction grating relied on intensity modulation of SPR [44]. Later, wavelength and angular modulation was introduced to diffraction grating-based SPR sensors to achieve higher accuracy in SPR measurements [46]-[49]. Grating-based SPR sensor with wavelength modulation and improvement of resonant momentum detection using acousto-optical modulator was demonstrated to be capable to recognize refractive index changes as small as $1x10^{-6}$ RIU [54].

1.5.5 SPR sensors with long-range surface plasmons

So far, majority of SPR sensors employed SPs propagating along a single metal dielectric interface. In order to improve the accuracy of SPR sensors, excitation of long-range surface plasmons guided along thin metal films was explored.

In prism coupler-based SPR sensors, employing of long-range surface plasmons was shown to improve the sensor resolution, because this SP mode allows closer matching of its dispersion relation with that of excitation optical wave. This results in narower SPR reflectivity dip, which yields in higher accuracy in determination of SPR position [57]. In 2001, Nenninger et. al. demonstrated prism-based SPR sensor with long-range SPs allowing measurements of refractive index changes as small as 2.6×10^{-7} RIU [33]. Most recently, Slavík reported SPR sensor based on prism coupler and wavelength interrogation of long-range SPs capable of resolution of refractive index changes down to 4×10^{-8} RIU [60]. Further, prism-based SPR sensor based on long-range SPs imaging was reported in 2005 [61].

On diffraction gratings, possibility of excitation of LRSPs on asymmetric structure for sensor applications was demonstrated by Lyndin et. al. in 1999 [59]. However, no grating coupler-based SPR sensor with long-range surface plasmons was reported yet.

2. Aim of the work

Aim of this work investigation of special surface plasmon modes - long-range surface plasmon (LRSP) and short-range surface plasmon (SRSP) - for applications in grating-coupled surface plasmon resonance (SPR) sensors with wavelength modulation of SPR. The introduction of long-range surface plasmons to SPR sensors is expected to provide several important benefits. As losses of LRSP are lower then the ones of the conventional SP, narrower resonance can be observed in the wavelength spectrum of light exciting this mode. Therefore, measurement of changes in the resonant wavelength can be performed more precisely, which yields in higher resolution of SPR sensor. Furthermore, more sensing channels can be encoded in certain wavelength band in SPR sensors relying on wavelength division multiplexing (WDM) of sensing channels. In addition, the coupling of SP modes through the thin metal layer allows excitation of LRSP and SRSP through the substrate. This feature allows simplification of grating-coupled SPR sensor instrumentation, as the light does not need to pass through the flow-cell and analyzed sample.

This work encompasses both theoretical and experimental analysis of diffractive structure for excitation of LRSP and SRSP modes. In the theoretical part of this work, presented in Chapter 3, characteristics and optical excitation of LRSP and SRSP modes guided by slightly refractive index asymmetric structure is investigated. Furthermore, sensitivity of LRSP and SRSP to refractive index changes at the sensor surface is evaluated. In the experimental part of the work, presented in Chapter 4, fabrication and characterization of the diffractive structure followed is described. Finally, application of prepared diffractive structures for an SPR sensor is demonstrated.

3. Theory

In this chapter, theoretical analysis and optimization of multi-layer diffractive structure for SPR sensor with LRSP and SRSP modes is carried out. At first, theoretical analysis of guided modes supported by the slightly asymmetrical structure consisting of buffer layer (refractive index close to water), thin gold film and water-like medium is presented, followed by the optimization of grating profile parameters in order to achieve an optimal coupling between an optical wave and SP modes. After, the minimal thickness of AlF_3 layer and the sensitivity of considered sensor to refractive index changes are determined.
All numerical calculations in this chapter were made by using the commercial computer program "PC-Grate" [55] based on the modified rigorous integral method [50]. The SP field profiles were calculated by the computer program CAMFR [56] (Cavity Modeling Framework) based on the eigen-mode expansion method [56].
Because the proposed SPR sensor is considered to operate with aqueous samples, the dielectric "buffer" layer with refractive index close to that of water needs to be added into the diffractive structure (see Fig. 22). In this work, aluminum fluoride (AlF_3) is chosen to form the buffer layer as it has suitable mechanical and optical qualities.
In the following calculations, normal incidence of excitation optical wave is considered. The grating spatial period is chosen to establish the maximum coupling of SP with optical wave at λ=800 nm, where the gold exhibits smallest losses. Modulation profile of gold film surfaces is considered to be sinusoidal. Dispersion relations of materials, which are used in numerical model, are included in Appendix.

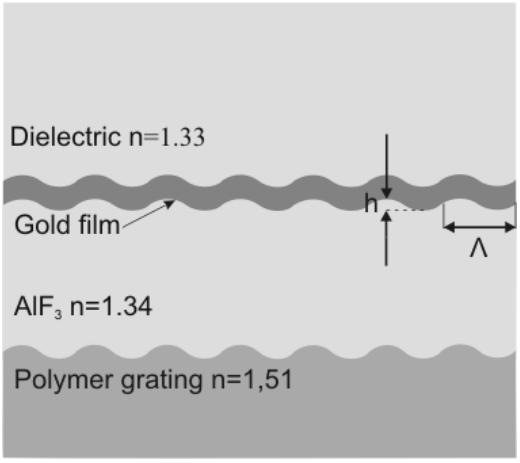

Fig. 22 Multi-layer diffractive structure, Λ denotes grating period, h is modulation depth. Refractive indices are given for λ=800 nm.

3.1 Modeling of SPR on metallic diffraction grating using integral method

Let us assume the geometry with Cartesian coordinates (see Fig. 23), consisting of semi-infinite metal (permittivity ε_M) with periodically modulated surface and semi-infinite dielectric (permittivity ε_D). The metal surface cross-section by the plane *xz* is described by a periodic function z=*f(x)*, which is invariant along the *y* coordinate. Further, if we assume incident monochromatic plane wave impinging on grating in the plane of incidence *xz*, diffraction problem can be treated in two dimensions, because of the system homogeneity in *y* direction.

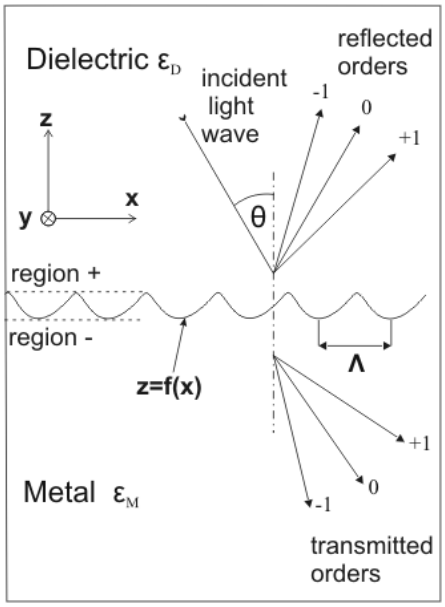

Fig. 23Geometry of diffraction problem on a metallic grating.

In general, total field in space above the grating can be expressed as superposition of incident and diffracted field. In case of TM polarization (magnetic intensity vector parallel to the grating grooves), magnetic intensity field can be expressed as:

$$H_y^{tot} = H_y^i + H_y^d, \tag{2.1}$$

where H_y^{tot}, H_y^{inc} and H_y^d denotes total, incident and diffracted magnetic field, respectively, θ is angle of incidence. Diffracted field in regions denoted as "+" (*z > max[f(x)]) and* "-" (*z < min[f(x)])* (Fig. 23) can be described in the form of Rayleigh expansion [52]:

$$H_y^{d+} = \sum_{m=-\infty}^{+\infty} R_m \exp[-i(k_{xm}x + k_{zm}^{+}z)], \tag{2.2}$$

$$H_y^{d-} = \sum_{m=-\infty}^{+\infty} T_m \exp[-i(k_{xm}x + k_{zm}^{-}z)], \tag{2.3}$$

where R_m and T_m are amplitudes of m^{th} reflected and transmitted order, respectively ,k_{xm} is x-component of m^{th} diffracted order, k_{zm}^{+} and k_{zm}^{-} are z-components of the m^{th} order in region "+" and "-", respectively. Components of wave vectors k_{xm}, k_{zm}^{+} and k_{zm}^{-} can be expressed as:

$$\begin{aligned} k_{xm} &= \frac{w}{c}\sqrt{e_D}\sin q + m\frac{2p}{\Lambda}, \\ k_{zm}^{+} &= \sqrt{e_D\left(\frac{w}{c}\right)^2 - k_{xm}^2}, \\ k_{zm}^{-} &= \sqrt{e_M\left(\frac{w}{c}\right)^2 - k_{xm}^2}, \end{aligned} \tag{2.4}$$

where ε_D, ε_M denotes permittivity of top (dielectric) and bottom (metal) medium, respectively and Λ is period of function $f(x)$. In order to find amplitudes of diffracted orders in Rayleigh expansion (2.2), (2.3), rigorous integral method (see [50]-[52]) was used. In the rigorous integral method, diffracted field is considered to be formed by a current flowing along the grating surface. This current is induced by the incident electromagnetic field. Diffraction problem is then reduced to finding the expression for the unknown surface current. Diffracted magnetic field in the dielectric medium can be expressed in the form of Helmholz-Kirchhoff integral (see [50]), when the integration is done over one grating period with respect to Floquet theorem [52]:

$$\mathrm{H_y^d} = \int_{\Lambda} \mathrm{G^+(x, x', y, f(x'))\Psi(x', f(x'))dx'}. \tag{2.5}$$

Here, function $\Psi(x,f(x))$ represents transformed current on the grating surface and G^+ is the so-called Green function of upper half space. Unknown scalar function $\Psi(x,f(x))$, which knowledge is necessary for retrieve the diffracted field by solving eq. (2.5), can be obtained when boundary conditions for total field and its normal derivatives on the metal-dielectric interface are taken into account. This yields in integral equation from which the function Ψ can be numerically calculated when the incident field, material constants and grating profile are known. When function Ψ is found, the Helmholz-Kirchhoff integral can be solved using point matching method (collocation method) [50]. For solving the

diffraction problem on multi-layer structures, integral method was extended to “modified integral method” [50], [51] few years ago.

3.2 Surface plasmon modes guided along slightly asymmetric structure

In this chapter, properties of long-range and short-range SP modes guided by the structure consisting of gold layer embedded between two semi-infinite dielectric media with refractive indices 1.33 and 1.34 RIU are presented.
Gold film thickness determines the coupling strength between SP modes propagating on the opposite sides of the metal film, which affects the propagation constant of long-range and short-range SP modes (see equations (1.7), (1.8) and Fig. 24). From TM reflectivity spectra, shown in Fig. 25 for three different thicknesses of the gold film, one can see that with decreasing the gold film thickness, difference in spectral position of reflectivity dips associated to LRSP (at lower wavelength) and SRSP (at larger wavelegth) are increasing which is in agreement with Fig. 24. Further, reflectivity dip caused by the resonance with LRSP exhibits smaller width with decreasing the gold film thickness, while the SRSP mode exhibits opposite dependence. This feature is given by the different distribution of LRSP and SRSP field (see Fig. 26). While the portion of LRSP field localized in lossy metal is decreasing with decreasing gold film thickness, the SRSP mode is localized more in metal for smaller gold film thicknesses which causes broadening of the SPR dip.

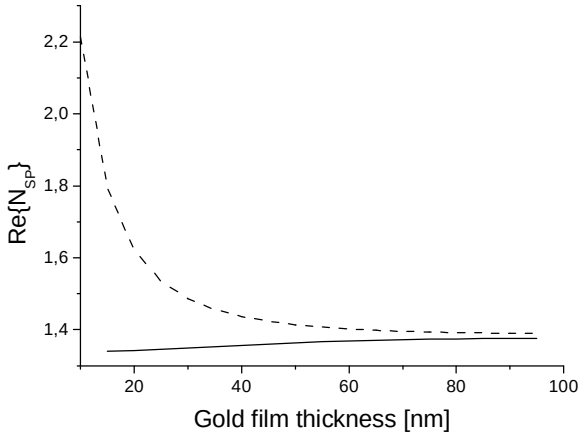

Fig. 24 Real part of effective refractive index of long-range (———) and short-range (– – –) SP modes as function of gold film thickness. Calculated at λ=800 nm, for structure consisting of semi-infinite dielectric with refractive index n=1,33 RIU, gold film and semi-infinite dielectric with refractive index n=1,34 RIU.

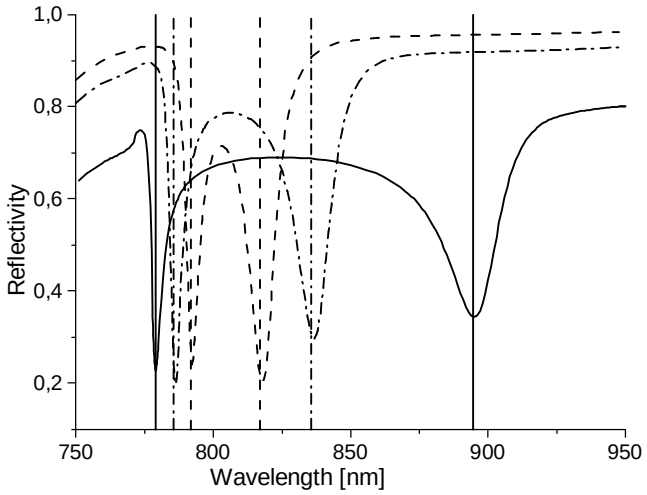

Fig. 25 Spectra of TM polarized normal incident optical wave, reflected from the structure consisting of 20 (____), 35 (_ . _) and 50 (_ _ _) nm thick gold film with periodically modulated surfaces, surrounded by two semi-infinite dielectric media with refractive indices 1.33 and 1.34 RIU. Parameters of grating profile: period Λ=580 nm, modulation depth h=30 nm. Vertical lines represent the resonant wavelength of LRSP (lower wavelengths) and SRSP (larger wavelengths) in resonance with normal incident optical wave calculated using equations (1.7), (1.8) and (1.12) on structure consisting of periodically modulated gold film (Λ=580 nm) with thickness 20 (____), 35 (_ . _) and 50 (_ _ _) nm surrounded by the semi-infinite dielectric medium with refractive index n_D=1.335.

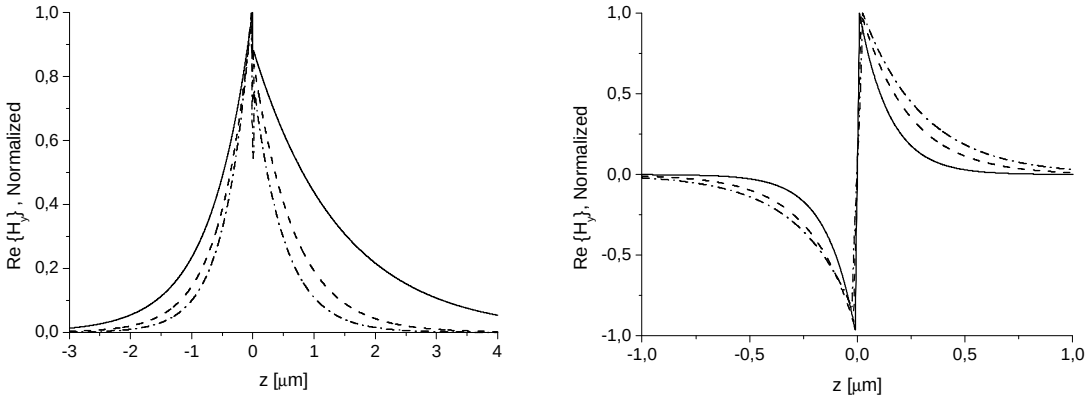

Fig. 26 Normalized real part of LRSP (left) and SRSP (right) magnetic intensity field calculated for structure consisting of dielectric (n=1.33 RIU), gold film with thickness 20 (____), 35 (_ _ _) and 50 nm (_ . _) and dielectric (n=1.34) (from left to right).

3.3 Optimization of grating profile parameters

In order to excite SPs on desired wavelength, dependence of resonant wavelength on the grating spatial period was calculated for long-range and short-range mode on structure with 40 nm thick gold film embedded between semi-infinite AlF_3 and water media (see Fig. 27). This dependence was determined from positions of reflectivity dips, calculated using the integral method for several values of grating period Λ.

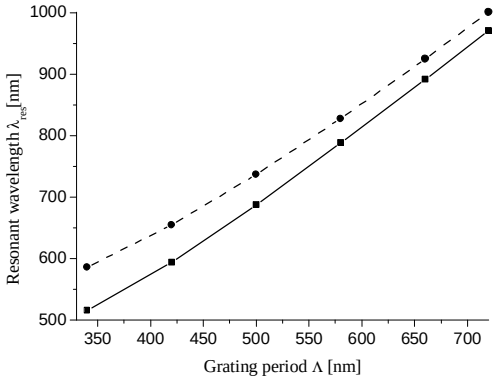

Fig. 27 Resonant wavelength of LRSP (——) and SRSP (– – –) mode as function of grating spatial period Λ in normal incidence geometry.

Efficiency of coupling between light wave and SP can be controlled through modulation depth of the grating. For purposes of SPR sensing, sharp and deep resonances in reflectivity spectrum are preferred as they allow determination of the resonant wavelength more precisely. Reflectivity spectra in normal incidence geometry were calculated for structures consisting of semi-infinite AlF_3 layer, gold film with periodically modulated surface (thickness 20 and 50 nm) and semi-infinite water. For each grating period, a set of reflectivity spectra with different modulation depths was calculated and parameters δR_{LR} and δR_{SR} (for illustration see Fig. 28) describing the depth of reflectivity dip caused by the coupling to long-range and short-range SPs respectively were determined.

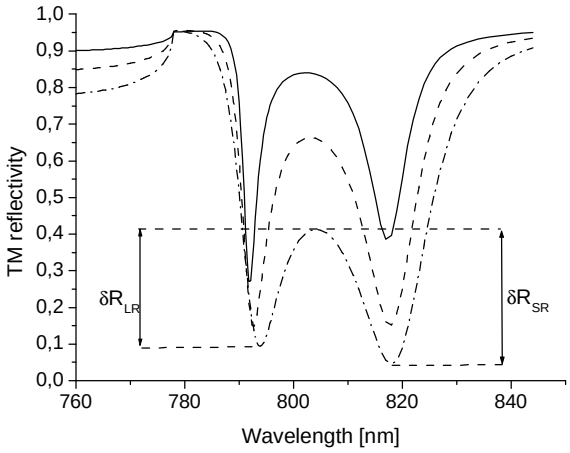

Fig. 28 Reflectivity spectra of TM polarized light wave in normal incidence geometry on structure consisting of gold film (thickness 50 nm) with periodically modulated boundaries (period of modulation 580 nm, modulation depth 20 (——), 30 (– – –) and 40 (– · –) nm) embedded in semi-infinite dielectric media -AlF_3 and water.

From calculated sets of spectra optimal modulation depths h were determined as those, for which parameters δR_{LR} (describing the coupling to long-range SP) and δR_{SR} (describing the coupling to short-range SP) are maximal. Obtained optimal modulation depths calculated for gold film thickness 20 and 50 nm at λ=800 nm are presented in Table 3.

	Optimal modulation depth h [nm]	
	LRSP	SRSP
Gold thickness 20 nm	25	45
Gold thickness 50 nm	22	27

Table 3 Optimal grating modulation depth calculated for gold film thickness 20 and 50 nm at the wavelength λ=800 nm.

3.4 Effect of finite thickness of aluminum fluoride layer

As in real sensing structure, AlF_3 is used to form the layer between the substrate and the gold layer, let us explore the effect of finite thickness of AlF_3 on SPR reflectivity. Objective of this chapter is to determine the minimal thickness of the AlF_3 layer, for which almost entire SP field is localized inside the AlF_3 – gold – sample structure. This condition should assure the independence of SPR on the AlF_3 layer thickness. For this purpose, the dependence of SPR properties on AlF_3 layer thickness was calculated for several values of thickness of the gold layer. The set of theoretical reflectivity spectra in

normal incidence configuration was calculated for each thickness of gold film with thickness of AlF_3 layer varying from 100 to 1500 nm. Then, we observed the value of reflectivity in the minimum of the spectral dip, caused by the coupling of light into long-range SP. Dependence of these resonant reflectivities on the thickness of AlF_3 layer is shown in Fig. 29 for several gold film thicknesses. The modulation of described curves in Fig. 29 is caused by the multiple reflections of light on the boundaries of aluminum fluoride with gold and substrate.

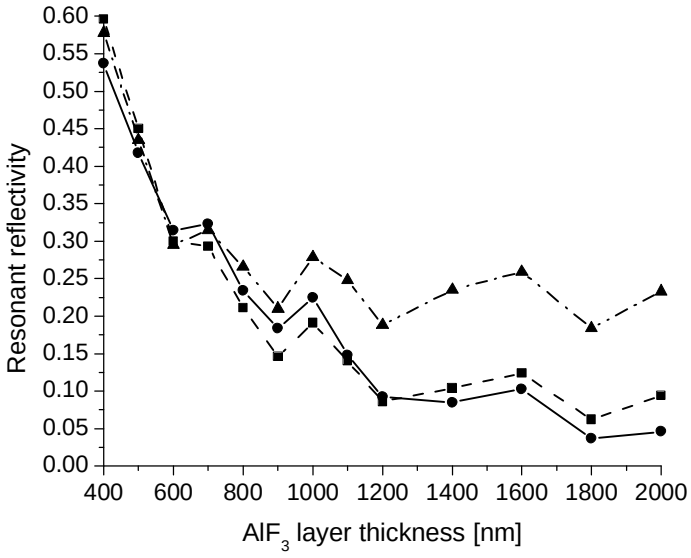

Fig. 29 Reflectivity of normal incident TM polarized optical wave in resonance with LRSP as function of the AlF_3 layer thickness. Diffractive structure consists of substrate (semi- infinite, refractive index 1.51RIU), AlF_3 layer with thickness 400-2000 nm, gold film with thickness 20 (——), 40 (– – –), 60 (– · –) nm. Period of grating profile modulation Λ was chosen to excite LRSP near the the desired wavelength (λ=800 ± 5 nm, Λ=595 ± 5 nm), grating modulation depth is 30 nm.

From data presented in Fig. 29, we assumed that in designed multi-layer diffractive structure, AlF_3 layer with thickness 1000 nm is sufficient to assure the localization of majority of LRSP field in AlF_3 - gold – sample structure.

3.5 Sensitivity of long-range and short-range SP modes to refractive index changes

In SPR sensor with wavelength interrogation, sensitivity of the sensor to refractive index changes is defined as:

$$S = \frac{d\,l_{res}}{d\,n}, \tag{2.6}$$

where $\delta\lambda_{res}$ denotes change in resonant wavelength caused by the small change in refractive index of sensed dielectric δn. Further, one can distinguish sensitivity to bulk refractive index changes (S_B, bulk sensitivity) and sensitivity to refractive index changes within a thin layer near the sensor surface with the thickness much smaller than SP penetration depth into dielectric (S_S, surface sensitivity). In order to evaluate the bulk sensitivity of SPR sensor based on studied diffractive structure, resonant wavelengths were calculated for two slightly different refractive indices of sample medium. This calculation was done for both SP modes - LRSP and SRSP, when the resonant wavelengths were set to be in interval λ_{res}=(800±5) nm. Bulk sensitivities calculated for the metal film thickness varying from 20 to 50 nm are shown in Fig. 30. The surface sensitivity was calculated for the same resonant wavelength and gold film thickness values, but change in refractive index was assumed to occur only within the 15 nm thick dielectric layer attached to the sensor surface (see Fig. 31).

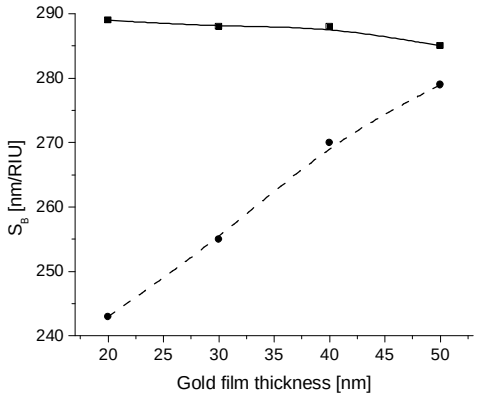

Fig. 30 Sensitivity of resonant wavelength to bulk refractive index changes as function of gold film thickness calculated for normal incident light wave in resonance with long-range (____) and short-range (_ _ _) SP, λ=800 nm. Sensing structure consists of semi-infinite AlF_3, gold film and semi-infinite sample (refractive index was varied from n=1.33 to n=1.34 RIU).

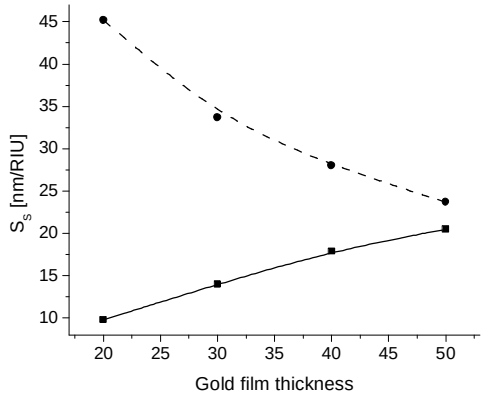

Fig. 31 Sensitivity of resonant wavelength to surface refractive index changes as function of gold film thickness calculated for normal incident light wave in resonance with long-range (____) and short-range (_ _ _) SP, λ=800 nm. Sensing structure consists of semi-infinite AlF_3, gold film, 15 nm sample (refractive index was varied from n=1.33 RIU to n=1.43 RIU) and semi-infinite dielectric (n=1.33 RIU).

Calculated dependences of sensitivities of long-range and short-range SP modes to bulk and surface refractive index changes correspond to the different field distribution of these SP modes. Long-range SP exhibit higher sensitivity to bulk RI changes than the SRSP as it has larger portion of its field stretched in sensed dielectric, while the SRSP mode has larger surface sensitivity, because its field is localized near the sensor surface.
Furthermore, the dependence of bulk sensitivity of LRSP and SRSP modes on resonant wavelength was calculated for normal incident excitation optical wave, while the gold film thickness was set to 20 nm. Different values of resonant wavelength were obtained by changing the grating spatial period *Λ*. Obtained dependence is shown in Fig. 32.

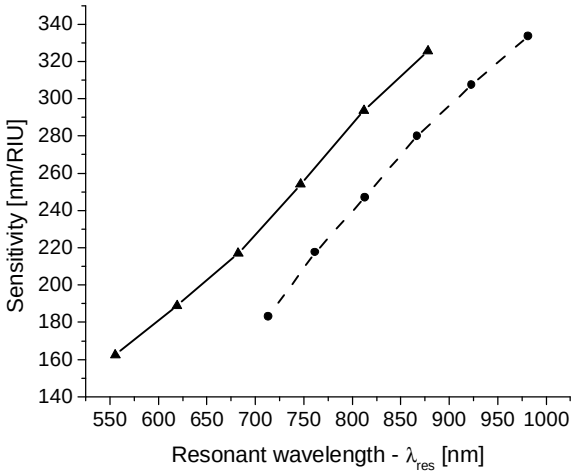

Fig. 32 Bulk sensitivity of SPR sensor with LRSP(——) and SRSP (– – –) modes as a function of resonant wavelength calculated on structure consisting of semi-infinite AlF_3 layer, gold film (thickness 20 nm) and semi-infinite dielectric (refractive index was varied from n=1.33 to n=1.34 RIU).

4. Experimental

In this chapter, fabrication and characterization of diffractive structure is presented. At the end of this chapter, prepared sensing structure is evaluated for SPR sensing in model refractometric experiment.

4.1 Fabrication of the multi-layer diffractive structure

The procedure of fabrication of the multi-layer diffractive structure consists of several steps including holographical preparation of master diffraction grating, its replication using soft-lithographical method and preparation of layers which supports the propagation of long-range and short-range SP modes by means of thermal evaporation in vacuum.

4.1.1 Master grating preparation

Master diffraction grating was prepared holographically into photoresist layer (SF 1813 from Shipley, USA) deposited on substrate - polished BK7 glass slide with dimensions 32x15x1,5 mm (from Schott glass technologies, Duryea, USA).
Before the photoresist deposition, substrates were cleaned with acetone and then placed into an ozone cleaner (UVO cleaner 42-220 from Jelight Company) for 20 minutes. The photoresist layer was deposited on substrate by means of spin-coating. Sufficient amount (200 μl) of photoresist was dropped on a rotating substrate while the rotation speed was set to 3500 rpm and rotation time to 15 s. Resulting thickness of photoresist layer was about 1 μm. After the deposition, substrates with photoresist layer were dried for 30 minutes at temperature 90°C.
The holographical exposition of the photoresist layer was realized using Mach – Zehnder interferometer arrangement. Substrate slides with photoresist layer on the front side were painted with black paint on its back side to avoid the back reflections during the holographical exposition. Such prepared samples were exposed to incidence of two coherent laser beams which were made incident on photoresist with angles of incidence $\theta/2$ and $-\theta/2$ (see Fig. 33). As source of the coherent light, an argon ion laser (type 165 from Spectra Physics, USA) operating at λ_L=457,9 nm was used. Exposition time was set to 2 minutes and intensity of optical wave in both interferometer arms were set to 13 $\mu W/cm^2$.

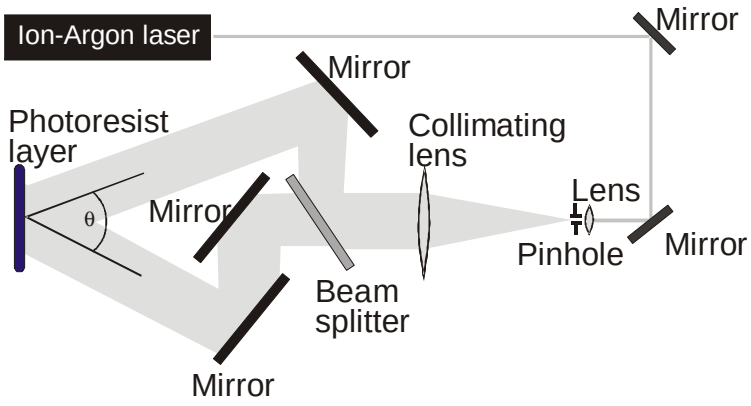

Fig. 33 Arrangement of the holographical grating exposition using Mach-Zehnder interferometer.

The grating period is given by the distance of interference fringes in the interference region, which is dependent on the angle of intersection of the laser beams θ and operation wavelength of laser λ_L:

$$\Lambda = \frac{l_L}{2\sin(q/2)}. \tag{3.1}$$

Substrates coated by the photoresist layer with recorded grating were developed in AZ 303 developer diluted in ratio 1:9 with distilled water. During the development, modulation depth of grating profile was controlled by measuring the efficiency of -1st diffracted order, which was compared with efficiency calculated using integral method for different modulation depths of the grating. The efficiency of -1st diffracted order was measured using Littrow configuration, when intensities of -1st and 0th diffracted order were measured (see Fig. 34) with He-Ne laser, operating at 632,8 nm. The total development time was varied from 30 to 100 s to obtain a desired modulation depth for each individual grating.

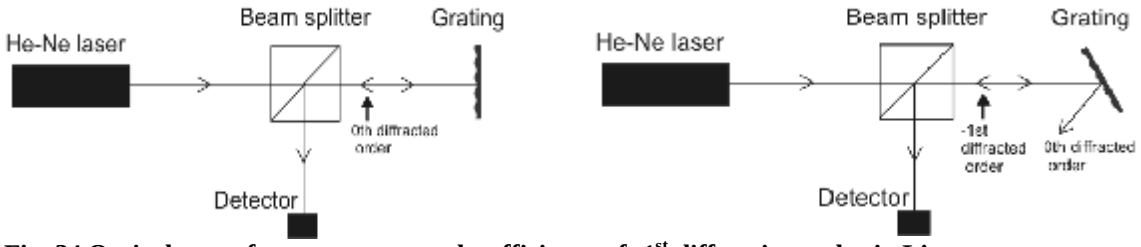

Fig. 34 Optical setup for measurement the efficiency of -1st diffraction order in Littrow configuration.

4.1.2 Replication of master diffraction grating

During the multi-layered structure preparation, samples are exposed to high temperatures (~250 °C). Because the photoresist layer instability at such temperatures, replication of master grating to polymer layer with higher thermal stability was used. Furthermore, this replication technique based on soft lithographic method make the process of the grating preparation less time consuming.
The replication procedure consists of several steps. At first, master grating profile was copied into special stamp, which was consequently used to imprint the grating profile to polymer layer, prepared on another substrate. For purpose of transfer the master grating profile to stamp, master grating was cast in liquid mixture of polymethyldisiloxane (PDMS, Sylgard 184 from Dow Cornig, USA) and curing agent, mixed with ratio 9:1. Then, the liquid PDMS was degassed and cured for 6 hours at 60°C to produce elastic PDMS stamp. These PDMS stamps were used to copy the master grating modulation profile to polymer (UV curable OG 146 from Epotek, USA) layer coated on cleaned glass slides. The polymer layer was deposited by spin-coating (rotation speed 10000 rpm, rotation time 10s), and then - in contact with PDMS stamp - was cured after the thermal stabilization in UV for 30 minutes using a mercury lamp. After this procedure, the PDMS stamp was removed and replica grating was heated for 30 minutes at 150°C to undergo the glass transition of OG 146 layer. Main steps in grating replication procedure are illustrated in Fig. 35.

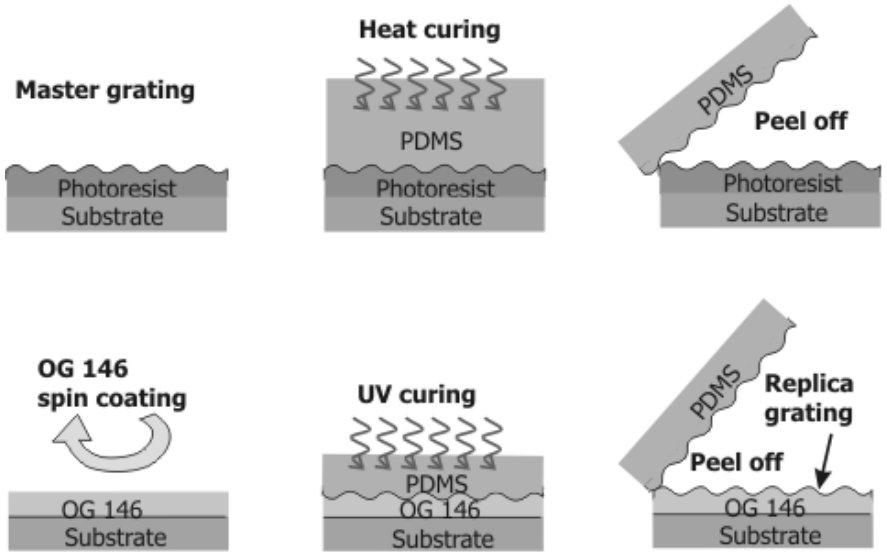

Fig. 35 Scheme of grating replication procedure. First row of pictures illustrates the transfer of master grating to PDMS stamp. Second row shows the imprinting of the PDMS stamp grating profile into replica grating.

4.1.3 Deposition of aluminum fluoride and gold layers

Aluminum fluoride (from Cerac, USA) and gold layers were both prepared by the thermal evaporation technique in PFEIFFER PLS 570 deposition chamber in vacuum better than 10^{-7}mbar. Thicknesses of deposited layers were continuously controlled by the quartz crystal oscillator. The AlF_3 layer was evaporated from molybdenum crucible (with deposition speed 0,2-0,3 nm/s) designed specially to reduce the spitting of evaporated material. Temperature was kept at 250 °C. After the deposition, sample was let for 30 minutes at the same temperature. Deposition of gold layer was done from wolfram crucible in the same vacuum while the temperature was decreased to 150 °C. Deposition speed was 0,4-0,5 nm/s. In order to establish better adhesion between AlF_3 and gold layers, several sensing structures were made with adhesion promoting titanium layer that was deposited AlF_3 layer by means of electron-beam gun. After deposition of Ti, gold layer was evaporated in the same manner as it is described above.

4.2 Characterization of developed sensing structure

In this chapter, characterization of developed sensing structures by means of measuring the reflectivity spectra or study of the surface quality of AlF_3 and gold layers by the atomic force microscope is given. The optimization of diffractive structure parameters presented in Chapter 3, resulted to structure consisting of substrate (RI=1.51), polymer layer with refractive index very close to that of substrate (thickness approximately 1 μm), AlF_3 layer with thickness 1 μm and gold layer (thickness 30-40 nm). The period of grating modulation profile was chosen to be about 600 nm to excite LRSP and SRSP modes near the desired wavelength λ=800 nm. Grating modulation depth was chosen to be 30-35 nm to reach optimal coupling of optical wave and SP modes.

4.2.1 Characterization of grating profile using atomic force microscopy

In order to characterize the properties of prepared multi-layer diffractive structure, surface of deposited layers – AlF_3 and gold were analysed using AFM (MultimodeTM from Veeco, USA). The set of several diffraction gratings was made with different modulation depth of the surface modulation to evaluate the smoothing of the original grating modulation profile after the evaporation of AlF_3 and gold layers. All measured gratings with original modulation depth from 38 to 65 nm exhibited after deposition of 1 μm thick AlF_3 layer and 30 nm gold layer lowering of the grating modulation depth by approximately 10 percent. Also the roughness properties of studied gratings did not change after the deposition of AlF_3 and gold layers significantly. The rms of the roughness of the polymer grating profile and gold grating profile were determined to be about 10 nm in both cases. Detail of grating surface before and after the deposition of AlF_3 and gold layers is in Fig. 36.

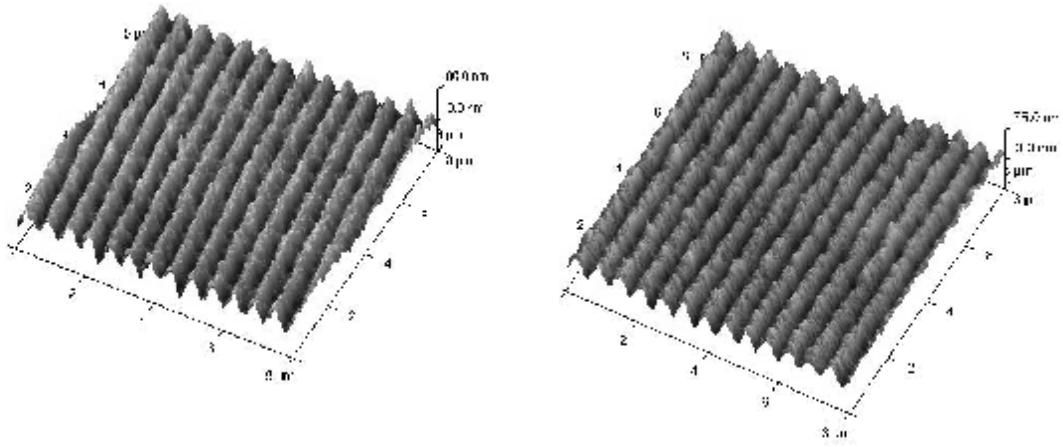

Fig. 36 AFM pictures of grating profile of replica grating before (left picture) and after (right picture) the deposition of AlF_3 and gold layers.

4.2.2 Characterization of long-range and short-range surface plasmon on diffraction grating

For purposes of evaluation of SPR on the developed diffractive structure, reflectivity of light wave in normal incidence was measured when the sensing structure was in contact with water. The experimental setup is shown in Fig. 37. Light from a polychromatic light source was coupled into a multi-mode optical fiber (FT-200 EMT from Thorlabs, USA) and on the fiber output was collimated using "Glass optics for parallel beam" (from Zeiss, Germany). Collimated beam was then passed through a polarizer (Polarcor 800-HC from Corning, USA) and a cube beam-splitter (from Linos, UK), where it hit the diffractive structure in contact with water. Optical wave reflected from the sensing structure was coupled into an optical fiber (FT-200 EMT from Thorlabs, USA) and transmitted to a spectrograph (MCS 500 spectrometer module from Zeiss, Germany) connected to a computer, where it was analysed.

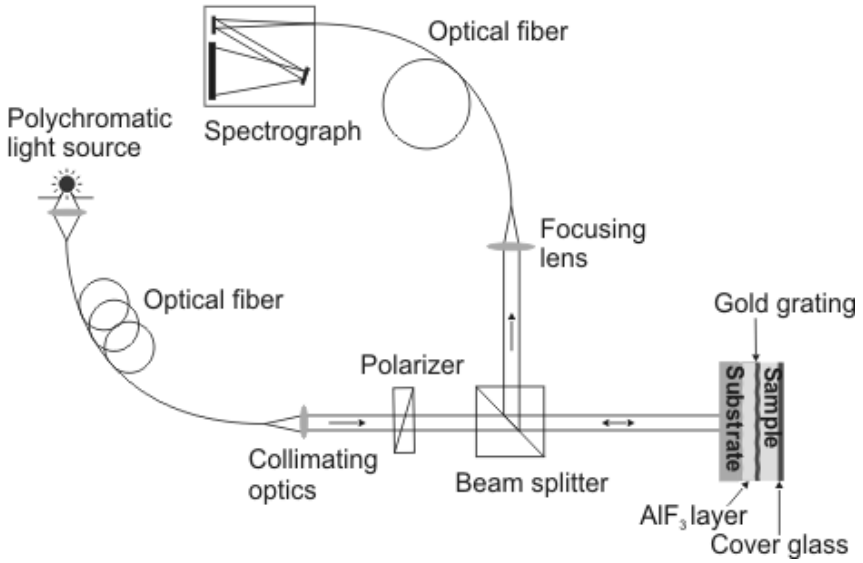

Fig. 37 Experimental setup used to observe excitation of LRSP and SRSP modes on a gold diffraction grating.

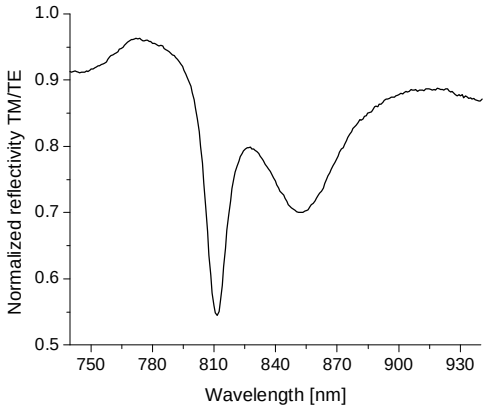

Fig. 38 Normalized reflectivity spectrum measured in normal incidence geometry on diffractive structure consisting of substrate (RI=1.51), polymer layer (RI = 1.51), AlF_3 layer (thickness 1µm), Ti layer (thickness ~ 0.5 nm) and gold layer (thickness 35 nm, modulation depth 31 nm, grating period 600 nm) in contact with water.

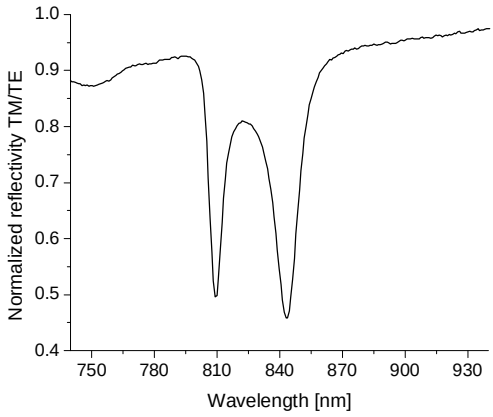

Fig. 39 Normalized reflectivity spectrum measured in normal incidence geometry on diffractive structure consisting of substrate (RI=1.51), polymer layer (RI = 1.51), AlF_3 layer (thickness 1µm) and gold layer (thickness 42 nm, modulation depth 31 nm, grating period 600 nm) in contact with water.

From measured spectra (Fig. 38, Fig. 39), one can see, that employing the lossy adhesion layer into sensing structure affects the SPR significantly even though the thickness of the fabricated layer has been chosen to be as low as possible (~0.5 nm). Besides that, we can see that influence of the titanium layer is stronger in case of SRSP mode due to its electromagnetic field localized mainly in the vicinity of the gold layer surface, where the

Ti layer is placed. While the full width at half a minimum (FWHM) of the resonant dip associated to LRSP changes approximately from 6 to 9.5 (see Table 4) nm by employing the Ti layer, FWHM of resonant dip caused by the SRSP will change from 11 to 25 nm. When we compare the reflectivity spectrum measured on a diffractive structure without the Ti layer with the spectrum calculated using integral method on the same structure (semi-infinite substrate – RI=1.51 / AlF_3 layer – thickness 1000 nm / gold layer – thickness 42 nm, grating period 596 nm, modulation depth 31 nm / semi-infinite sample - water) shown in Fig. 40, we can see that in comparison with theoretical model, measured reflectivity dips are shallower and have larger widths. This effect is probably caused by the grating inhomogeneity, roughness of the grating surface and also by a quality of optical wave collimation.

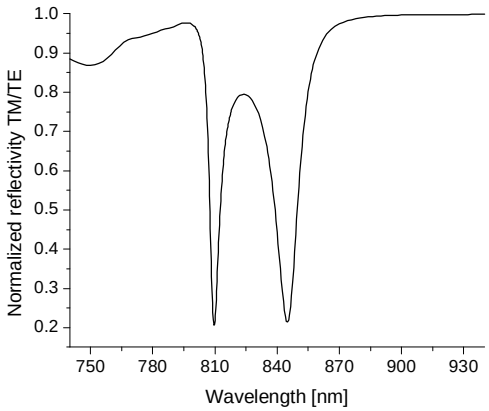

Fig. 40 Normalized reflectivity spectrum calculated in normal incidence geometry on structure consisting of semi-infinite substrate – RI=1.51, AlF_3 layer – thickness 1000 nm, gold layer – thickness 42 nm, grating period 596 nm, modulation depth 31 nm and semi-infinite sample – water.

	FWHM of LRSP	FWHM of SRSP [nm]
Theoretical (without Ti)	5.0	10.7
Measured (without Ti)	6.2	10.7
Measured (with Ti)	9.5	25.1

Table 4 Comparison of calculated and measured reflectivity dip widths (FWMH) for LRSP and SRSP modes. Data in second, third and fourth row of the table are determined from Fig. 40, Fig. 39 and Fig. 38, respectively.

4.3 SPR sensor based on developed sensing structure

In this chapter, we report results of model refractometric experiments based on developed diffractive sensing structure. The measurements were performed using sensor setup shown in Fig. 41, which is similar to one, that is described in Chapter 4.2.2. The samples with different refractive indices were made flow along the sensor surface by means of peristaltic pump (Reglo from Ismatec, Switzerland) with flow rates from 40 to 70 µl/min. Spectral properties of out-coming light were determined by the SD 2000 spectrometer (from Ocean optics, USA) with CCD array consisting of 2048 elements. The spectrometer working range was 740-975 nm. The spectra measured by the spectrograph were further processed using computer program, which tracks changes in the position of spectral dips [58].

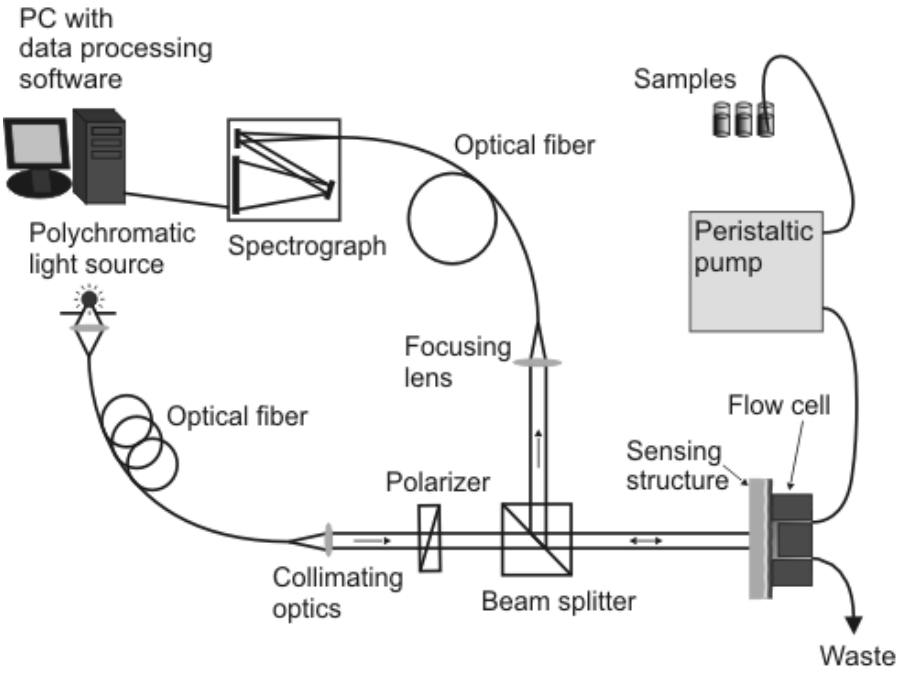

Fig. 41 Arrangement of grating-coupled SPR sensor setup with wavelength interrogation.

These model experiments were realized using two sensing structures, both fabricated from the same master grating, without (Fig. 42) and with the adhesion promoting titanium layer (Fig. 43).
The resonant wavelength was determined using special data processing software for SPR sensors based on tracking centroid method [58]. Typically, 50 spectra measured by the spectrometer during 5 seconds were averaged to obtain raw spectrum. The raw spectrum

was further smoothed and resonant wavelength was determined by the tracking centroid algorithm.

Measured data are shown in Fig. 42 and Fig. 43, where changes in positions of both resonances – caused by the LRSP and SRSP modes – were monitored, while the different mixtures of water and ethylene glycol with RI = 1.3330 1.3360, 1.3390 and 1.3419 were flowed along the sensor surface.

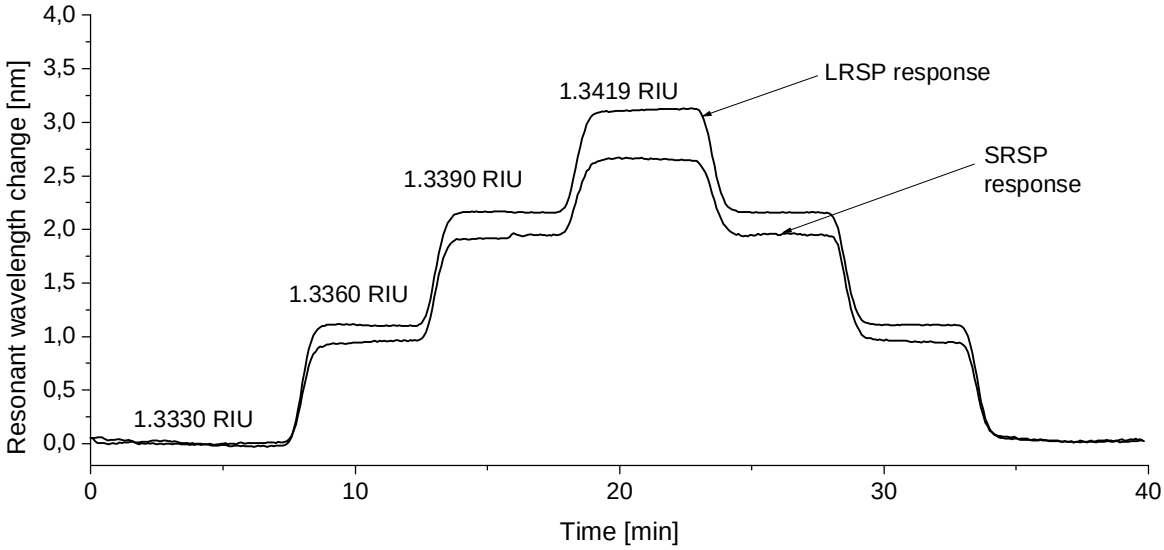

Fig. 42 Resonant wavelength of LRSP and SRSP as function of time, when samples with different refractive indices were flowed along the sensor surface. Used sensing structure consisted of substrate, OG 146 polymer layer (~1µm), AlF_3 layer (~1µm) and gold film (~40nm) and was illuminated by the normal incident optical wave through the substrate.

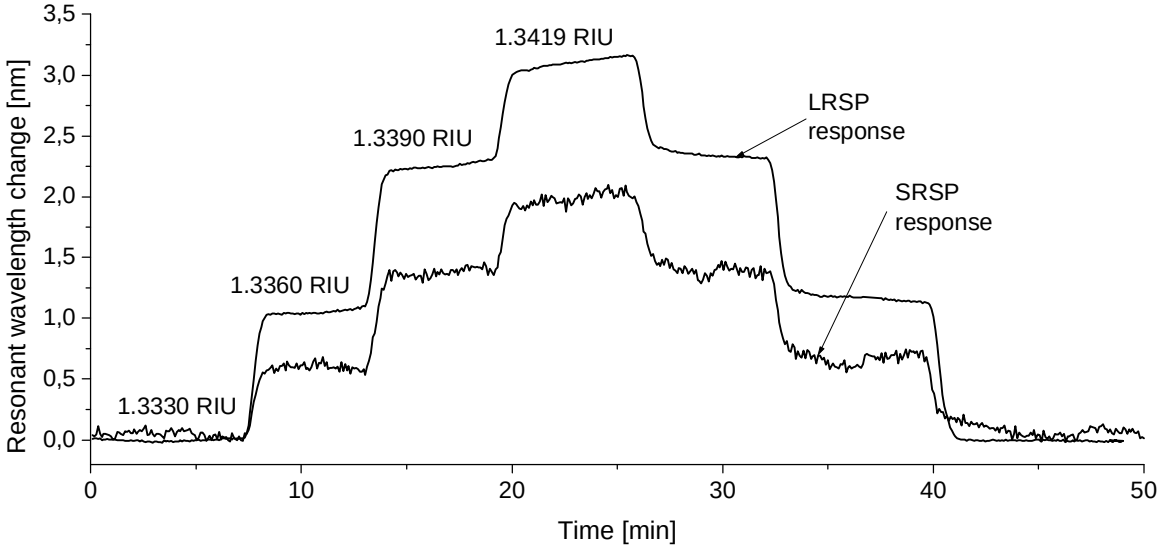

Fig. 43 Resonant wavelength of LRSP and SRSP as function of time, when samples with different refractive indices flowed along the sensor surface. Used sensing structure consisted of substrate, OG 146 polymer layer (~1µm), AlF_3 layer (~1µm), Ti (~0.5nm) and gold film (~35nm) and was illuminated by the normal incident optical wave through the substrate.

From measured sensor responses shown in Fig. 42 and Fig. 43, sensitivity to bulk refractive index changes S_B of SRSP and LRSP modes were determined for two fabricated sensing structures – with and without the Ti layer. The resolution of the sensor defined as a ration of the standard deviation of noise - N_{SD} and sensitivity: $RES = N_{SD} / S_B$, was also determined. Measured sensitivities, standard deviations of noise and resolutions associated to the LRSP and SRSP modes are summarized in Table 5.

	S_B [nm/RIU]	N_{SD} [nm]	Resolution [RIU]
LRSP, without Ti	350	0.002	$5{,}7 \times 10^{-6}$
SRSP, without Ti	330	0.005	$1{,}5 \times 10^{-5}$
LRSP, with Ti	350	0.005	$1{,}43 \times 10^{-5}$
SRSP, with Ti	~250	0.03	1.2×10^{-4}

Table 5. Measured sensitivities to bulk refractive index changes and sensor resolutions determined by the experiment on grating-coupled SPR sensor with interrogation of LRSP and SRSP modes and based on two different sensing structures – with and without adhesion promoting Ti layer.

Data presented in second and third row of Table 5 shows, that sensitivity of long-range SP propagating along structure without Ti to bulk refractive index changes is slightly larger than that of SRSP. Presence of the adhesion layer does not affect the sensitivity of LRSP mode, but noise characteristics of the sensor gets worse more than two times,

which is caused by the broadening the SPR dip and thus larger uncertainty in SPR dip position determination. The influence of Ti layer to SRSP properties is much more significant, because of the larger portion of its field is localized in Ti layer when compared to LRSP mode. This feature results in a decrease of sensitivity of SRSP mode as well as an increase of standard deviation of noise (almost ten times).
Unfortunately, sensing structures prepared without the Ti layer were not mechanically stable, which makes them less practical for SPR sensors.

5. Conclusions

Special surface plasmon (SP) modes- LRSP and SRSP, excited using a grating coupler on a thin gold film, were theoretically and experimentally studied for application in a surface plasmon resonance (SPR) sensor. For this purpose, a multi-layer diffractive structure with aluminum fluoride and thin gold layers, which supports coupled surface plasmon modes – long-range and short-range SP, was developed.

In the theoretical part of the work, excitation of coupled surface plasmons on the diffractive structure was simulated using the rigorous integral method. The analysis was focused on optimization of the diffractive structure in order to achieve the optimal coupling of light into SP modes and optimal properties of SP modes with respect to the sensor performance. Based on the carried out optimization of diffractive structure parameters, multi-layer diffractive structures with and without an adhesion promoting Ti layer were prepared and characterized.

Finally, the developed diffractive structure was tested in SPR sensor with wavelength modulation. The sensor based on LRSP interrogation, with diffractive sensing structure without Ti exhibited good resolution of bulk refractive index changes ($5{,}7 \times 10^{-6}$ RIU) comparable with standard grating-coupled SPR sensors. Unfortunately, due to the rather limited adhesion between AlF_3 and gold layers, this structure is not sufficiently stable for sensing applications. A thin (~0.5 nm) Ti layer was demonstrated to promote the adhesion between these two layers. The presence of lossy Ti in this multi-layer structure negatively affects the sensor resolution.

Currently, this structure is tested for biosensing applications [62]. Further development of this structure will be focused on finding alternative ways to improve the adhesion between AlF_3 and gold layers.

6. References

[1] J. Raiteri, M. Grattarola, H. J., P. Skladal: Micromechanical cantilever-based biosensors. *Sensors and Actuators B*, 79 (2001) 115-126.

[2] J. Shah, E. Wilkins: Electrochemical Biosensors for Detection of Biological Warfare Agents. *Electroanalysis*, 15 (2003), 157-167.

[3] Nguyen Quy Dao and M. Jouan: The Raman laser fiber optics (RLFO) method and its applications. *Sensors and Actuators B,* 11 (1993) 147-160.

[4] Ch. R. Yonzon, Ch. L. Haynes, X. Zhang, J. T. Walsh,Jr. And R. P.Van Duyne: A Glucose Biosensor on Surface-Enhanced Raman Scattering: Improved Partition Layer, Temporal Stability, Reversibility and Resistance to Serum Protein Interference. *Analytical Chemistry*, 76 (2004) 78-85.

[5] W. Trettnak, O. S. Wolfbeis: Fully reversibe fibre-optic glucose biosensor based on the intrinsic fluorescence of glucose oxidase. *Analytical Chimica Acta*, 221 (1989) 1995-203.

[6] D. Clerc and W. Lukosz: Integrated optical output grating coupler as refractometer and (bio-)chemical sensor. *Sensors and Actuators B,* 11 (1998) 461-465.

[7] J. Piehler, A. Brandenburg, A. Brecht, E. Wagner, and G. Gauglitz: Characterization of grating couplers for affinity-based pesticide sensing. *Applied Optics,* Vol. 36, No. 25 (1997) 6554-6562.

[8] A. Y. Johannes S. Kanger, R. Wijn, P. V. Lambeck, J. Greve: Development of a multichannel integrated interferometer immunosensor. *Sensors and Actuators B,* 83 (2002) 1-7.

[9] X. Liu, Z. Cao, Q. Shen, and S. Huang: Optical sensor based on Fabry-Perot resonance modes. *Applied Optics*, Vol. 42, No. 36 (2003) 7137-7140.

[10] B. Cunnigham, P. Li, B. Lin, J. Pepper: Colorimetric resonant reflection as a direct biochemical assay technique. *Sensors and Actuators B,* 81 (2002) 316-328.

[11] J. Homola, S. Yee, G. Gauglitz: Surface plasmon resonance sensors: review. *Sensors and Actuators B,* 54 (1999) 3-15.

[12] R. W. Wood: On a remarkable case of uneven distribution of light in a diffraction grating spectrum. *Phil. Magm.* 4, (1902) 396-402.

[13] R. W. Wood: Anomalous Diffraction Gratings. *Physical Review, 48 (1935)* 928-936.

[14] U. Fano: The Theory of Anomalous Diffraction Gratings and of Quasi-Stationary Waves on Metallic Surfaces (Sommerfeld's Waves), *J.O.S.A.*, 31 (1941) 215-222.

[15] R.H. Ritchie: Plasma losses by fast electrons in thin films, *Physical Review,* 106 (1957) 874-881.

[16] A. Otto: Excitation of nonradiative surface plasma waves in silver by the method of frustrated total reflection. *Z.Phys* , 216 (1968) 398-410.

[17] E. Kretschmann, H. Raether: Radiative decay of nonradiative surface plasmon excited by light. *Z.Naturf,* 23A: (1968) 2135-2136.

[18] H. Raether: Surface Plasmons on Smooth and Rough Surfaces and on Gratings. Springer tracks in modern physics, Vol 111, *Springer-Verlag, Berlin* (1983).

[19] J. Homola, S. S. Yee, D. Myszka: Surface plasmon resonance biosensors. In: Optical biosensors: Present and future. (Editor: F. S. Ligler), *Elsevier, Amsterdam* (2002) 207-251.

[20] M. C. Hutley: Diffraction gratings. *Academic press* (1982).

[21] J. Homola, G. Schwotzer, H.Lehman, R.Willish, W. Ecke, H. Barlert: A New Optical Fiber Sensor for Humidity Measurement. *Photonics' 95, Prague, Czech Republic, August 1995, EOS Annual Meeting Digest Series*, 2A, 225-248.

[22] A. Schilling, O.Yavas, J. Bischof, J. Boneberg, and P. Leiderer: Absolute pressure measurement on nanosecond scale using surface plasmons, *Appl. Phys. Lett.*, 69 (1996).

[23] B. Moslehi, M. W. Foster, P. Harvey: Optical Magnetic and Electric Field Sensors Based on Surface Plasmon Polariton Resonance Coupling, *Electronic Letters*, 27 (1991).

[24] A. Rasooly: Surface plasmon resonance analysis of staphylococcal enterotoxin B in food. *Journal of Food Protection*, 64 (2001) 37-43.

[25] J. Homola, J. Dostálek, S Chen, A. Rasooly, S Jiang and S. S. Yee: Spectral surface plasmon biosensor for detection of staphylococcal enterotoxin B in milk. *International Journal of Food Microbiology*, 75 (2002) 61-69.

[26] M. Minunni and M. Mascini: Detection of pesticide in drinking water using real-ime biospecific interaction analysis. *Analytical Letters*, 26 (1993).

[27] C. Mouvet, R. D. Harris, C. Maciag, B. J. Luff, J. S. Wilkinson, J. Piehler, A. Brecht, G. Gauglitz, R. Abuknesha and G. Ismail: Detemination of simazine in water samples by waveguide surface plasmon resonance. *Analytica Chimica Acta*, 338 (1997) 109-117.

[28] P. M. Fratamico T. P. Strobaugh, M. B. Medina and A. G. Gehring: Detection of Escherichia coli O157:H7 using a surface plasmon resonance biosensor. *Biotechnology Techniques*, 12 (1998) 571-576.

[29] B. Liedberg, I. Lundstrom and E. Stenberg: Principles of biosensing with an extended coupling matrix and surface plasmon resonance. *Sensors and Actuators B,* 11 (1993) 63–72.

[30] B. Liedberg, C. Nylander and I. Lundström, Surface Plasmon Resonance for Gas Detection and Biosensing, *Sensors and Actuators*, 4, (1983), 299-304.

[31] M. Zhang, D. Uttamchandani: Optical chemical sensing employing surface plasmon resonance. *Electronic Letters*, (1988) Vol.24 No.23, L.

[32] K. Matsubara, S. Kawata, S. Minami: Optical chemical sensor based on surface plasmon measurement. *Applied Optics* Vol.27 No.6 (1988).

[33] G. G. Nenninger, P. Tobiška, J. Homola, S. S. Yee: Long-range surface plasmons for high-resolution surface plasmon resonance sensors. *Sensors and Actuators B*, 74 (2001) 145-151.

[34] M. J. Jory, P. S. Vukusic and J. R. Sambles: Development of a prototype gas sensor using surface plasmon resonance on gratings. *Sensors and Actuators B,* 17 (1994) 1203–1209.

[35] R. C Jorgenson, S. S Yee, A fiber-optic chemical sensor based on surface plasmon resonance, *Sensors and Actuators B*, 12 (1993) 213-220.

[36] A. Trouillet, C. Ronot-Trioli, C. Veillas, and H. Gagnaire, Chemical Sensing by Surface Plasmon Resonance in a Multimode Optical Fiber, *Pure Applied Optics*, 5 (1996) 227 - 237.

[37] R. E. Dessy, W. J. Bender, Feasibility of a Chemical Microsensor Based on Surface Plasmon Resonance on Fiber Optics Modified by Multilayer Vapor Deposition, *Analytical Chemistry*, 66 (1994) 963 – 970.

[38] J. Homola: Optical Fiber Sensor Based on Surface Plasmon Excitation. *Sensors and Actuators* B, 29 (1995) 401 - 405.

[39] R. Slavík, J. Homola, E. Brynda: A miniature fiber optic surface plasmon resonance sensor for fast detection of staphylococcal enterotoxin B. *Biosensors and Bioelectronics,* 17 (2002) 591-595.

[40] H. J. M. Kreuewel, P. V. Lambeck, J. van Gent, T. J. A. Popma: Surface plasmon dispersion and luminiscence quenching applied to a planar waweguide sensors for measurement of chemical concentrations. *Proc. SPIE* , 789 (1987) 218–224.

[41] C. R. Lavers and J. S. Wilkinson: A waveguide-coupled surface-plasmon sensor for an aqueous environment. *Sensors and Actuators B,* 22 (1994) 75-81.

[42] C. Mouvet, R. D. Harris, C. Maciag, B. J. Luff, J. S. Wilkinson, J. Piehler, A. Brecht, G. Gauglitz, R. Abuknesha, G. Ismail: Determination of simazine in water samples by waveguide surface plasmon resonance. *Analytica Chimica Acta,* 338 (1997) 109-117.

[43] J. Dostálek, J. Čtyroký, J. Homola, E. Brynda, M. Skalský, P. Nekvindová, J. Špirková, J. Škvor, J. Schrőfel: Surface plasmon resonance biosensor based on integrated optical waveguide. *Sensors and Actuators B,* 76 (2001) 8-12.

[44] D. C. Cullen, R. G. Brown, C. R. Lowe: Detection of Immuno-complex Formation via Surface Plasmon Resonance on Gold-coated Diffraction Gratings. *Biosensors* 3 (1987/88) 211-225.

[45] M. T. Gale: Replication technique for diffractive optical elements. *Microelectronic Engineering*, 34 (1997) 321-339.

[46] M. J. Jory, G. W. Bradberry, P. S. Cann and J. R. Sambles: A surface-plasmon-based optical sensor using acousto-optics. *Meas. Sci. Technology*. 6 (1995) 1193-1200.

[47] J. M. Brockman, S. M. Fernandez: Grating-coupled surface plasmon resonance for rapid, label-free, array-based sensing. *Am. Laboratory* 33 (2001) 37-40.

[48] J. Dostálek, J. Homola, M. Miler: Rich information format surface plasmon resonance biosensor based on array of diffraction gratings. *Sensors and Actuators B*, 107, (2005) 154-161.

[49] P. Adam, J. Dostálek, J. Homola: Multiple surface plasmon spectroscopy for study of biomolecular systems. *Sensor and Actuators B*, 113 (2006) 774-781.

[50] L. I. Goray: Modified integral method for weak convergence problems of light scattering on relief grating. *Proc. SPIE,* 4291 (2001) 1-12.

[51] L. I. Goray and J. F. Seely: Efficiencies of master, replica, and multilayer gratings for the soft-x-ray–extreme-ultraviolet range: modeling based on the modified integral method and comparisons with measurements. *Applied Optics*, 41 (2002) 1434-1445.

[52] R. Petit: Electromagnetic theory of gratings. *Springer–Verlag Berlin Heidelberg New York* (1980).

[53] R. Karlsson, R. Stahleberg: Surface plasmon resonance detection and multispot sensing for direct monitoring of interactions involving low-molecular-weight analytes and for determination of low affinities. *Anal. Biochem.* 228 (1995) 274–280.

[54] M. J. Jory, G. W. Bradberry, P. S. Cann, J. R. Sambles: A surface plasmon-based optical sensor using acousto-optics. *Meas. Sci. Technol.* 6 (1995) 1193–1200.

[55] http://pcgrate.com

[56] http://camfr.sourceforge.net

[57] J. Homola, I. Koudela, S. S. Yee: Surface plasmon resonance sensor based on difraction gratings and prism couplers: sensitivity comparison. *Sensors and Actuators B*, 54 (1999) 16-24.

[58] G.G. Nenninger, M. Piliarik and J. Homola: Data analysis for optical sensors based on spectroscopy of surface plasmons. *Measurement Science and Technology*, 13 (2002) 2038-2046.

[59] N. M. Lyndin, I. F. Salakhutinov, V.A. Sychugov, B. A. Usievich, F. A.Pudonin, O. Parriaux: Long-range surface plasmons in asymmetric layered metal dielectric structures. *Sensors and Actuators B*, 54 (1999) 37-42.

[60] R. Slavík, J. Homola: A new surface plasmon resonance sensor with an ultra=high resolution: *Europt(r)ode VIII, Tubingen, Germany, April 2 – 5, 2006, Book of Abstracts*, pp. 112.

[61] A. W. Wark, H. J. Lee and R. M. Corn: Long-range surface plasmon resonance imaging for bioaffinity sensors. *Analytical Chemistry*, 77 (2005) 3904-3907.

[62] M. Vala, J. Dostálek, J. Homola: Long-range surface plasmon resonance biosensor based on difraction gratings. *The ninth world congress on biosensors, May 10-12, 2006 Sheraton Centre Toronto, Ontario, Canada, Accepted for presentation.*

[63] G. M. Hale, M. R. Querry: Optical constants of water in the 200-nm to 200-μm wavelength region, *Applied Optics*, Vol. 12, No.3, (1973) 555-562.

Appendix

Dispersion relations

Water:

$$e_{H_2O}(l) = (1.429331 - 0.403306\times10^{-2}\, l + 0.650493\times10^{-4}\, l^2 - 0.487305\times10^{-6}\, l^3 + 0.137143\times10^{-8}\, l^4)^2 ,$$

Ethylene glycol:

$$e_{EG}(l) = \left[1.42099 + 0.01516 \exp\left(-\frac{l - 439.06012}{173.61282}\right)\right]^2 ,$$

Gold:

$$\varepsilon_{Au}(\lambda) = [41.56403 - 0.2106\lambda + 3.98641\times10^{-4}\lambda^2 - 3.3293\times10^{-7}\lambda^3 + 1.03534\times10^{-10}\lambda^4 + i(-20.95173 + 0.0945\,\lambda + 1.44797\times10^{-4}\lambda^2 + 1.0889\times10^{-7}\lambda^3 - 3.09932\times10^{-11}\lambda^4)]^2 ,$$

AlF_3:

$$\varepsilon_{AlF_3}(\lambda) = (-0.36277 + 0.00932\lambda - 1.83679\times10^{-5}\lambda^2 + 1.5643\times10^{-8}\,\lambda^3 - 4.88843\times10^{-12}\lambda^4)^2 ,$$

Dispersion relation of water is taken from [63], while the dispersion relation of ethylene glycol is derived from data provided by the producer. Dispersion relations of gold and aluminum fluoride thin layers were determined using ellipsometer SE-850 (Sentech Instruments, Germany).

Table of contents

Název práce: Vedené vlny v periodických strukturách a jejich senzorové aplikace.
Autor: Milan Vala
Katedra (ústav): Katedra chemické fyziky a optiky, MFF UK
Vedoucí diplomové práce: Ing. Jiří Homola, CSs., *Ústav radiotechniky a elektroniky, Akademie věd České republiky*
e-mail vedoucího: homola@ure.cas.cz
Abstrakt: Práce je uvedena popisem základních vlastností povrchových plazmonů šířících se podél rozhraní kov-dielektrikum a podél struktury s tenkým kovovým filmem obklopeným z obou stran dielektriky se shodným indexem lomu. Je ukázáno, že na symetrické struktuře s tenkou vrstvou kovu lze vybudit dva typy vidů vázaných povrchových plazmonů - long-range povrchový plazmon a short-range povrchový plazmon. Dále je poskytnuta stručná rešerše věnována použití těchto typů povrchových plazmonů v optických senzorech. Je navržena difraktivní vrstevnatá struktura, ve které se vázané vidy povrchových plazmonů excitují na struktuře tvořené tenkým zlatým filmem obklopeným dielektriky s podobnými indexy lomu. S použitím rigorózní integrální metody je difraktivní struktura optimalizována pro aplikaci v senzoru s povrchovými plazmony. Difraktivních struktury s optimálními parametry jsou připraveny a charakterizovány opticky a s použitím mikroskopu atomových sil. V závěru je demonstrována aplikace připravených difraktivních struktur v senzoru s povrchovými plazmony a modulací vlnové délky.
Klíčová slova: senzor s povrchovými plazmony, long-range povrchový plazmon, difrakční mřížka

Title: Guided waves in periodical structures and their sensor applications.
Author: Milan Vala
Department: Department of Chemical Physics and Optics
Supervisor: Ing. Jiří Homola, CSc., *Institute of Radio Engineering and Electronics, Czech Academy of Sciences*
Supervisor's e-mail address: homola@ure.cas.cz
Abstract: This work is introduced by the description of fundamental properties of surface plasmons, propagating along the metal-dielectric interface and along the structure with thin metal film surrounded by the dielectrics with identical refractive indices. It is shown, that the excitation of two coupled modes (long-range surface plasmon - LRSP and short-range surface plasmon - SRSP) on symmetrical structure with a thin metal film is possible. Further, a brief overview of surface plasmons applications in optical sensors is presented. The diffractive multi-layer structure supporting LRSP and SRSP modes, which consists of the thin gold film surrounded by the dielectrics with slightly different refractive indices is designed. The diffractive structure is optimized using rigorous integral method for an application in SPR sensor. Diffractive structures with optimal parameters are prepared and characterized optically and using atomic force microscopy. In the end, an application of developed diffractive structure in SPR sensor with wavelength modulation is demonstrated.
Keywords: SPR sensor, long-range surface plasmon, diffraction grating

1. Introduction

During several last decades, attention devoted to development of high-resolution sensors for biological and chemical sensing in medicine, food industry, warfare etc. has been growing significantly. Up to now, a wide range of sensing techniques were studied giving rise to a variety of sensors – electromechanical [1], electrochemical [2] or optical [3]-[11].
Optical sensors represents fast growing branch of research and together with the progress in optics, chemistry, material sciences and related disciplines, they find a place in numerous applications. Up to now, optical sensors employing techniques such as Raman scattering spectroscopy [3], surface enhanced Raman scattering spectroscopy [4], fluorescence intensity measurement [5], grating coupler [6], [7], interferometry [8], [9], colorimetry [10] or surface plasmon resonance (SPR) [11] were developed.
Since the 80's of 20th century SPR sensors have been widely used due to their ability to perform a real time, „in situ" monitoring of refractive index changes near the sensor surface and their high resolution. Advantageous is also that SPR is a label-free technique [11]. Several types of SPR sensors were reported including fiber optical [35], integrated optical SPR sensor [40], prism [29] or grating [44] coupler-based SPR sensor.
In this thesis theoretical study, fabrication and characterization of a new sensing structure for SPR sensor based on grating coupler with interrogation of special modes of surface plasmon (SP) called long-range and short-range SP is described. By employing these special SP modes, improvement in resolution compared to "standard" grating-coupled SPR sensors is expected. Besides that, possible simplification of the sensor instrumentation is motivation of this work.

1.1 Phenomenon of surface plasmon

Surface plasmon (SP) is a lossy electromagnetic surface wave propagating along the boundary between a metal and a dielectric. SP is generated by collective coherent oscillations of free electrons at the metal surface (see Fig. 1). These coherent charge density oscillations can be excited optically (see Chapter 1.4) or by fast electrons [15].

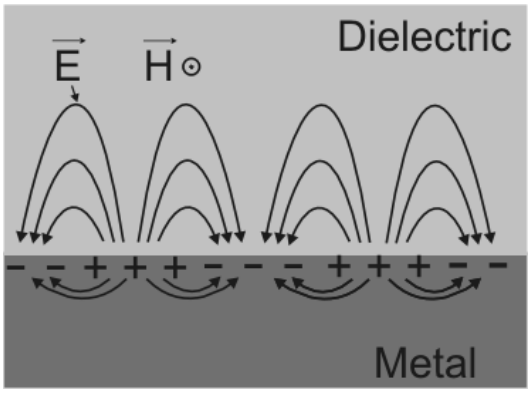

Fig. 1 Coherent charge density oscillations on metal-dielectric boundary.

The phenomenon of surface plasmon resonance was first observed in the beginning of the 20th century by Wood, who observed anomalous dark bands in spectrum of light reflected from metallic gratings [12], [13]. Later, these anomalies were found to be related to the excitation of surface waves on the metal surface by Fano [14]. In 50's, Ritchie studied excitation of surface plasmons on thin metallic films by fast electrons [15]. Later, in 60's Otto, Kretschmann and Raether introduced the attenuated total reflection method for coupling of light to surface plasmons [16], [17], which increased applicability of SPs dramatically.

1.2 Fundamental properties of surface plasmon

Let us describe fundamental properties of SP guided along a plane metal-dielectric interface. In general, in such geometry transverse electric (TE) modes (electric intensity vector perpendicular to the direction of propagation and parallel to the interface) and transverse magnetic (TM) modes (magnetic intensity vector perpendicular to direction of propagation and parallel to the interface) can propagate. Specially, let us consider the geometry consisting of a plane boundary between semi-infinite non-magnetic homogenous isotropic metal and dielectric, with complex permittivity ε_M ($\varepsilon_M = \varepsilon_M' + i\varepsilon_M''$) and ε_D, respectively. Properties of electromagnetic modes propagating along the metal dielectric boundary can be found by solving Maxwell equations with standard boundary conditions, see [18]. There can be shown, that there exists only one guided electromagnetic mode supported by this geometry. This mode is referred as to a surface plasmon (SP) and it is TM polarized with its field decaying exponentially from the interface.

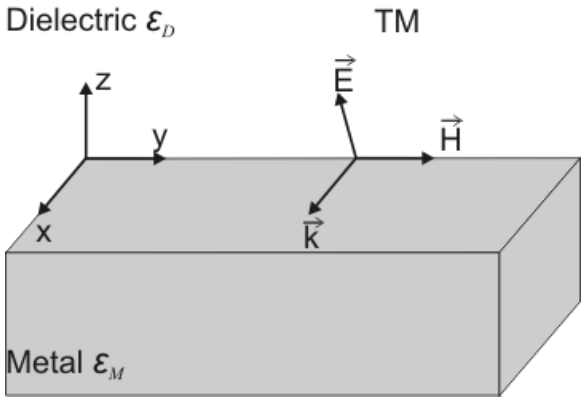

Fig. 2 Transversal magnetic mode guided along metal-dielectric interface.

Further, let us assume Cartesian coordinates with *z* axis perpendicular to the metal surface and *x* and *y* axis within metal-dielectric interface, see Fig. 2. Metal occupies the region z<0 and dielectric medium occupies the region z>0. If we assume propagation of TM-polarized surface plasmon in *x* direction, its electromagnetic field can be described as [18]:

$$\begin{aligned}
\mathbf{r}\\
E_D &= (E_x, 0, E_z) = (1, 0, \frac{ib}{a_D}) A \exp\{-a_D z + i(b x - wt)\} \quad ,\\
\mathbf{r}\\
H_D &= (0, H_y, 0) = (0,1,0) \frac{-iAwe_D}{c^2 a_D m_0} \exp\{-a_D z + i(b x - wt)\} \quad ,\\
a_D^2 &= b^2 - \left(\frac{w}{c}\right)^2 e_D \quad ,
\end{aligned} \tag{1.1}$$

$$\begin{aligned}
\mathbf{r}\\
E_M &= (E_x, 0, E_z) = (1, 0, \frac{ib}{a_M}) A \exp\{-a_M z + i(b x - wt)\} \quad ,\\
\mathbf{r}\\
H_M &= (0, H_y, 0) = (0,1,0) \frac{-iAwe_M}{c^2 a_M m_0} \exp\{-a_M z + i(b x - wt)\} \quad ,\\
a_M^2 &= b^2 - \left(\frac{w}{c}\right)^2 e_M \quad ,
\end{aligned} \tag{1.2}$$

where $\vec{E}$ is the electric intensity vector, $\vec{H}$ is the magnetic intensity vector, β is the longitudinal propagation constant, α is the transversal propagation constant, μ_0 is the permeability of vacuum, A is a normalization constant, ω is the angular frequency, c denotes speed of light in vacuum and t is time. Indices „$_D$“ (z>0) and „$_M$“ (z<0) denote dielectric and metal, respectively. By solving Maxwell equations with boundary condition at the interface, one can obtain the propagation constant of surface plasmon β as [18]:

$$b = \frac{w}{c}\sqrt{\frac{e_D e_M}{e_D + e_M}} = \frac{w}{c} N_{SP}\,, \tag{1.3}$$

where N_{SP} is the effective refractive index of surface plasmon. The solution described by (1.3) exists when the real part of permittivity of metal is negative ($e_M' < 0$) and inequality $\left|e_M'\right| > e_D$ is fulfilled. For instance, this condition is valid for gold and silver in VIS and NIR region of spectrum. When describing the permittivity ε_M with Drude model, this condition is transformed to $w < w_P/\sqrt{1+e_D}$, where $w_p = \sqrt{4pNe^2/m_0}$ (N is free electron density in metal, e is electron charge and m_0 is electron mass). Dispersion relation of SP is shown in Fig. 3.

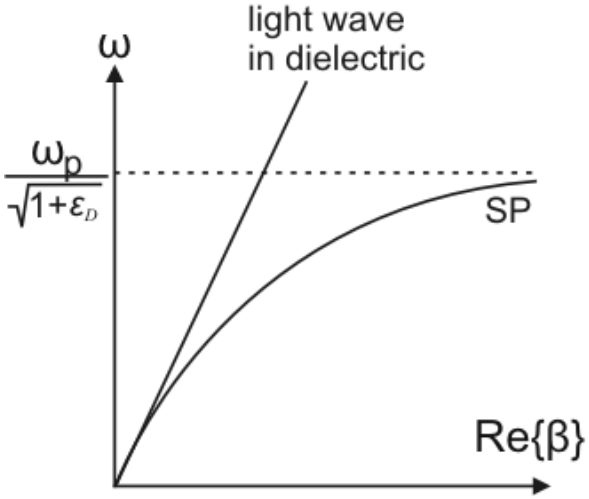

Fig. 3 Dispersion relation of SP.

As the permittivity ε_M is complex, the propagation constant β is complex as well. Its real part corresponds to the momentum of surface plasmon and it can be expressed for $\left|e_M''\right| < e_M'$ as:

$$\mathrm{Re}\{b\} = \frac{w}{c}\sqrt{\frac{e_D e_M'}{e_D + e_M'}}\,. \tag{1.4}$$

Imaginary part of β determines attenuation of SP in direction of propagation. The propagation length (distance where intensity of SP falls to 1/e) is then given by:

$$L_p = \frac{1}{|2\,\mathrm{Im}\{b\}|} = \frac{c}{w}\left(\frac{e_D e_M'}{e_D + e_M'}\right)^{-3/2}\frac{e_M'^{\,2}}{e_M''}. \tag{1.5}$$

As SP is a surface wave, its field amplitude exponentially decays from surface into metal and dielectric media (see Fig. 4). Important parameter of SP is its penetration depth into these media. It is defined as the depth where amplitude of field falls to 1/e of its maximal value on the metal-dielectric boundary. Using equations (1.1), (1.2) and (1.3) propagation depths into dielectric L_D and metal L_M can be expressed as:

$$L_D = \frac{1}{|a_D|} = \frac{c}{w}\sqrt{\frac{e_M' + e_D}{e_D^2}} \quad , \quad L_M = \frac{1}{|a_M|} = \frac{c}{w}\sqrt{\frac{e_M' + e_D}{(e_M')^2}}. \tag{1.6}$$

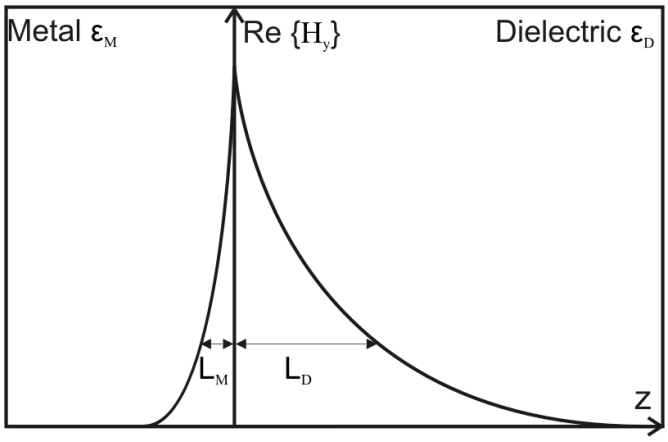

Fig. 4 Field profile of H_y component of SP.

Examples of propagation length and penetration depth of surface plasmon propagating along the boundary of dielectric ($\varepsilon_D = 1.74$) and two noble metals (gold and silver) calculated for wavelength λ=630 nm and λ=850 nm are shown in Table 1.

	Gold		Silver	
Wavelength [nm]	630	850	630	850
Penetration depth into dielectric L_D [nm]	162	400	219	443
Penetration depth into metal L_M [nm]	29	25	24	23
Propagation length L_P [μm]	2	24	19	57

Table 1. Penetration depth and propagation length of SP calculated for wavelengths 630, 850 nm and for gold and silver. Data are taken from [19].

1.3 Surface plasmon modes on a very thin metal film

Until now, we studied SP on interface between semi-infinite metal and dielectric media. Further, let us assume geometry in which a metal film of finite thickness is embedded between two semi-infinite dielectrics with permittivities ε_{D1} and ε_{D2}. In this case SPs can exist on both sides of the metal (see Fig. 5). If the metal layer thickness d_M is much larger than penetration depth of SP into metal $d_M >> L_M$, we can describe the propagation of SPs on both interfaces as in the previous chapter. However, when decreasing the metal film thickness to $d_M \sim L_M$ (see Fig. 5), electromagnetic field of SPs on opposite sides of the film can overlap giving rise to the coupling between these modes, [18].

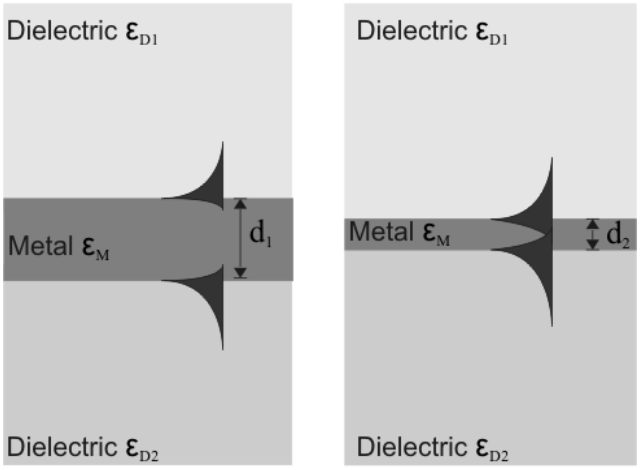

Fig. 5 Interaction between surface plasmons on the opposite sides of the metal film.

The interaction between SPs on opposite sides of the metal film can occur when ε_{D1} *and* ε_{D2} are close to each other. This interaction gives rise to existence of two coupled modes, denoted usually as "symmetrical" and "anti-symmetrical". For $\varepsilon_{D1} = \varepsilon_{D2}$ dispersion relation of these modes can be expressed as (see [18]):

$$e_M a_D + e_D a_M \tanh\left(\frac{1}{2i} a_M d\right) = 0, \tag{1.7}$$

$$e_M a_D + e_D a_M \coth\left(\frac{1}{2i} a_M d\right) = 0 \,, \tag{1.8}$$

where equations (1.7) and (1.8) describes the dispersion relation of symmetrical and anti-symmetrical mode, respectively. Example of dispersion relation of coupled SP modes guided by a thin metal film with thickness d=20 and 50 nm surrounded with a dielectric with refractive index 1.33 is shown in Fig. 6. It reveals that when decreasing the metal layer thickness, the split between the dispersion relation of symmetrical and anti-symmetrical surface plasmon mode increases.

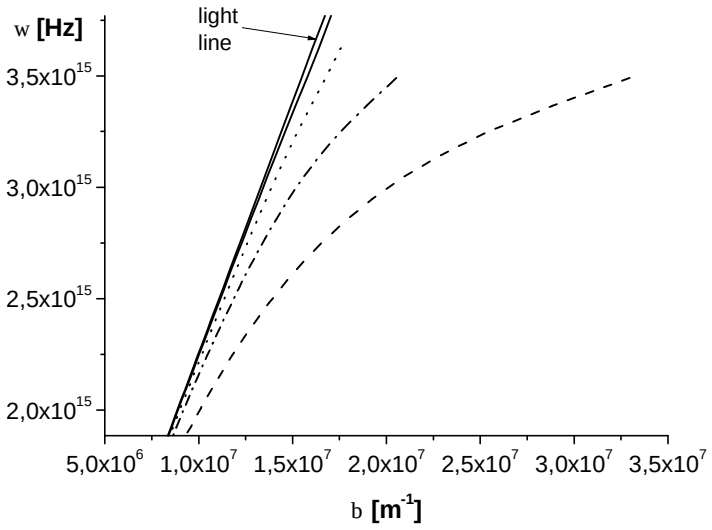

Fig. 6 Dispersion relation of SP modes on thin gold film embedded between semi-infinite dielectric with permittivity ε_D=1.33 calculated for gold film thickness 20 nm (—— symmetrical, – – – anti-symmetrical) and 50 nm (..... symmetrical, — . – anti-symmetrical).

In Fig. 7, field distribution of magnetic intensity H_y of symmetrical and anti-symmetrical mode is shown. The anti-symmetrical mode with field more localized in lossy metal (see Fig. 7) has lower propagation length than symmetrical mode with field more stretched in dielectric (see Table 2). Hence, the symmetrical mode is usually denoted as long-range surface plasmon (LRSP) and anti-symmetrical mode as short-range surface plasmon (SRSP).

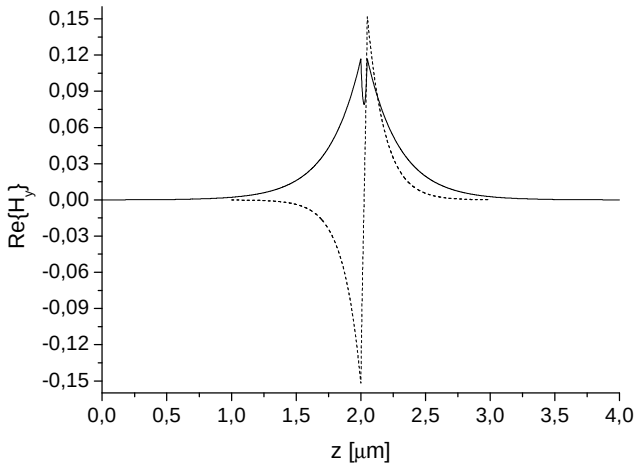

Fig. 7 Distribution of Re{H_y} of long-range (____) and short-range (.....) SP guided along a thin gold film with thickness 50 nm embedded between dielectric with refractive index n=1.33, $\omega=3x10^{15}$ (free space wavelength λ=630 nm).

In Table 2, examples of propagation lengths and penetration depths of long-range and short-range surface plasmons on thin gold film calculated for wavelengths 630 and 850 nm are presented.

Wavelength [nm]	630	850
Penetration depth of SRSP into dielectric [nm]	146	320
Penetration depth of LRSP into dielectric [nm]	251	524
Propagation length of SRSP[μm]	1,6	13
Propagation length of LRSP[μm]	13	97

Table 2 Penetration depths and propagation lengths of SP guided by the structure consisting of 50 nm thick gold film embedded in semi-infinite dielectric media with refractive index n_D =1.33 calculated for wavelengths 630 and 850 nm.

1.4 Excitation of surface plasmon

For efficient coupling of an optical wave into SP, these two waves need to be phase-matched along the metal surface. This condition is fulfilled, when the component of wave vector of light that is parallel to the interface is equal to the propagation constant of SP. As SP is a guided mode, its propagation constant is always larger than the wave vector of light in adjacent dielectric (see Fig. 3). Therefore, on plane metal surface it is not possible to optically excite SP directly from the adjacent dielectric.

In order to couple light into SP, a coupler providing enhancement of propagation constant of light needs to be used. Most commonly used couplers are prism couplers and diffraction grating couplers.

1.4.1. Excitation of surface plasmons using prism coupler

In prism coupler, attenuated total reflection (ATR) method is used (see Fig. 8, Fig. 9) to match the optical wave's wave vector with that of SP. An optical wave propagates through a dielectric prism with refractive index n_P on which base it totally reflects. Upon the reflection, evanescent field is generated at the prism base. For excitation of SP, this field is made overlapped with the region in which SP propagates along an interface between metal and dielectric with lower refractive index n_D. As the refractive index of the prism is higher then the one of the dielectric ($n_P > n_D$), the phase-matching of SP and the light wave can be achieved when:

$$\frac{w}{c} n_p \sin q = \mathrm{Re}\{b\}, \tag{1.9}$$

where θ is the angle of incidence of the light wave reflected at the prism base and β is the propagation constant of SP.

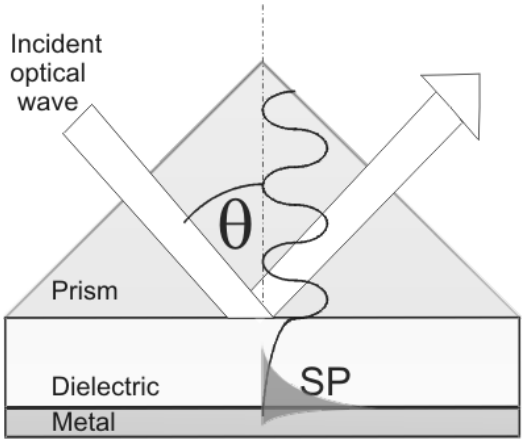

Fig. 8 Excitation of SP using prism coupler in Otto configuration.

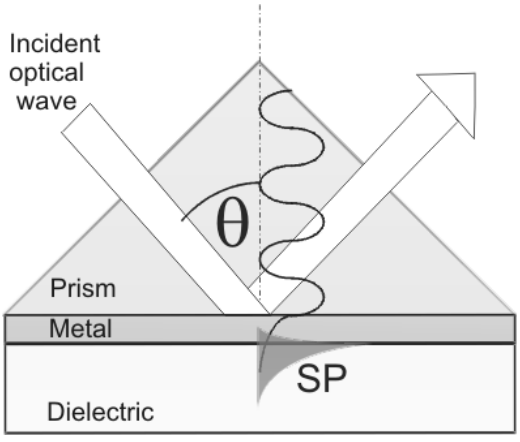

Fig. 9 Excitation of SP using prism coupler in Kretschmann configuration.

Prism coupler-based excitation of SPs can be realized in Otto or Kretschmann configuration. In Otto configuration SPs are excited through a dielectric with refractive index n_D (see Fig. 8) while in Kretschmann configuration they are excited through a thin metal film (see Fig. 9). The efficiency of the coupling between the optical wave in prism and SP can be controlled by the distance d_{PM} between prism base and the metal surface

along which SP propagates. There can be shown, that the total energy transfer between the incident optical wave and SP can occur only for certain distance d_{PM}^{opt}.

The coupling of light to SP is manifested as a narrow dip in the wavelength or angular reflectivity spectrum. This SPR dip is centered at the wavelength (for fixed angle of incidence) or angle of incidence (for fixed wavelength) described by the phase-matching condition (1.9). An example of excitation of SP in Kretschmann configuration is given in Fig. 10. In Fig. 10, angular reflectivity spectra of TM polarized wave with wavelength 800 nm exciting SP for angle of incidence about 66 degrees are shown. The structure consist of a prism with refractive index n_P=1.51, gold film with thickness 40, 50, 60 and 70 nm, and dielectric with refractive index n_D=1.33. It shows that maximum coupling of light into SP occurs for gold film thickness of about 50 nm.

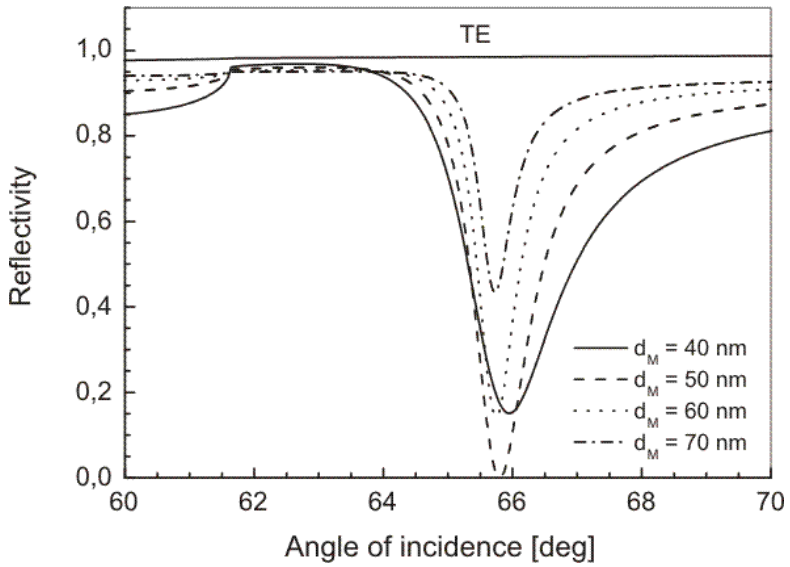

Fig. 10 Angular spectra of reflectivity of TM polarized wave calculated for Kretschmann configuration and thickness of gold film between 40 and 70 nm. Incident light wavelength λ=800 nm, n_P=1.51, n_D=1.33. TE reflectivity is shown for comparison.

1.4.2. Excitation of surface plasmon using grating coupler

Another approach to coupling of an optical wave to SP is based on grating coupler. By using grating coupler, incident light's wave vector can be enhanced to match the SP propagation constant by the diffraction of light on a periodically corrugated metal surface where the SP propagates, see Fig. 11.

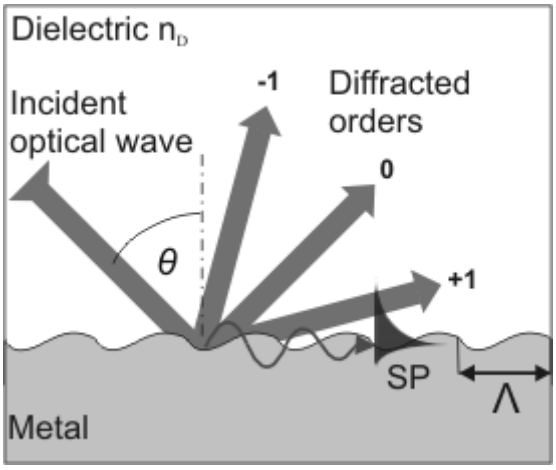

Fig. 11 Excitation of SP using a grating coupler.

If the light wave is made incident under an angle of incidence θ on periodically corrugated surface of diffraction grating with plane of incidence perpendicular to the grating grooves, reflected light splits into series of diffracted orders [20] with components of wave vectors parallel to the surface given by:

$$k_m = \frac{w}{c} n_D \sin q + mK_G, \tag{1.10}$$

where n_D denotes the refractive index of incidence dielectric, m is integer which indexes diffracted orders. K_G is the grating wave vector, which may be expressed as:

$$K_G = \frac{2p}{\Lambda}, \tag{1.11}$$

where Λ denotes spatial period of the grating. From (1.10) and (1.11) it follows, that the momentum of an optical wave can be enhanced using diffraction grating. Therefore, phase-matching between optical wave and SP can be achieved through m^{th} diffracted order:

$$\frac{w}{c} n_D \sin q + m\frac{2p}{\Lambda} = \pm \mathrm{Re}\{b\}. \tag{1.12}$$

Similarly to the ATR method, the coupling of optical wave into SP using grating coupler can be observed as narrow dip in wavelength or angular spectrum of intensity of reflected orders. The efficiency of this coupling can be controlled through the grating profile.
An example of excitation of SP using grating coupler is given in Fig. 11. This figure shows calculated reflectivity spectra of TM polarized wave, which impinges on a sinusoidal metallic grating under an angle of incidence 6 degrees (in air). The structure consist of a semi-infinite metal with periodically modulated surface (Λ=670 nm, modulation depth 10, 30, 50 and 70 nm) and dielectric with refractive index n_D=1.33. The maximum coupling of light into SP in this configuration occurs when the depth of modulation of the metal surface is about 30 nm.

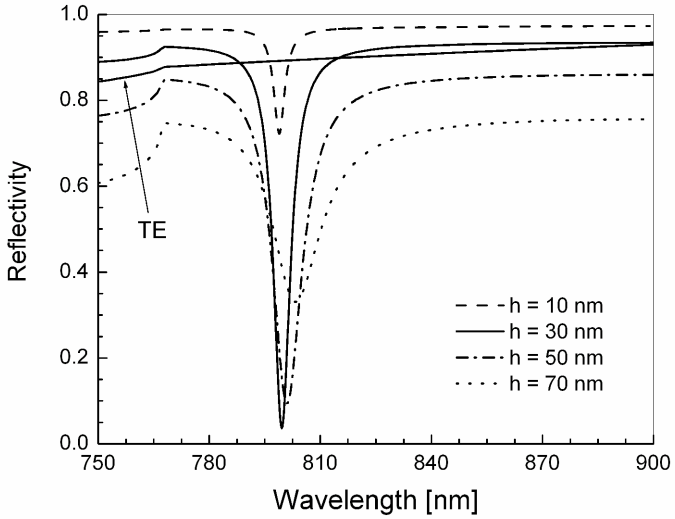

Fig. 12 Reflectivity spectra of TM polarized wave reflected from metal grating with sinusoidal profile for four different depths of modulation *h*.

1.5 Surface plasmon resonance sensors

In surface plasmon resonance (SPR) sensors, surface plasmons are used to probe the refractive index (RI) changes at the sensor surface. A thin sensitive layer is placed on the sensor surface to convert variations in a quantity of interest (for example humidity [21], pressure[22], gas concentration [34], electric field [23], concentration of biological analyte [24]-[28] etc.) into changes in RI or thickness of sensitive layer. As majority of SP energy is carried in the dielectric adjacent to the metal surface, propagation constant of SP is extremely sensitive to variations in the refractive index at the sensor surface, see (1.4). In SPR sensors, changes in optical properties of sensitive layer alter the propagation constant of SP which affects its interaction with the optical wave. Therefore,

a change in the quantity of interest can be observed as a change in one of the characteristics of the optical wave exciting surface plasmons, see Fig. 14.

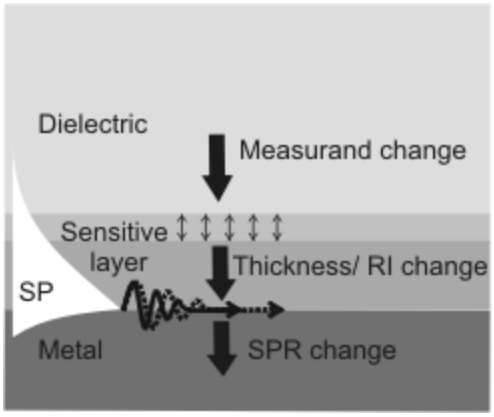

Fig. 13 Surface of an SPR sensor with a sensitive layer probed by surface plasmon.

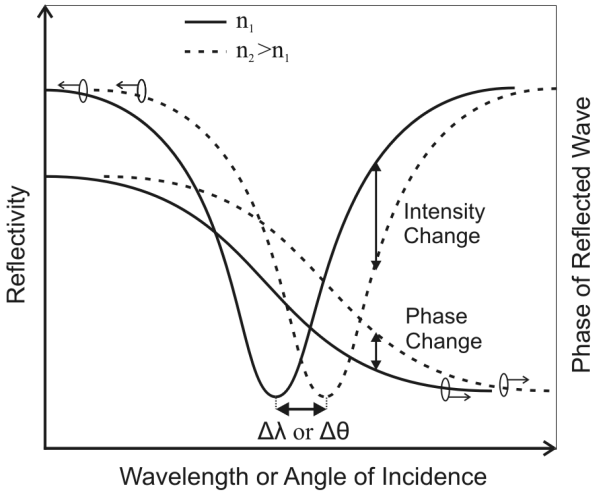

Fig. 14 SPR change caused by a refractive index change in spectrum of reflected wave characteristics.

SPR sensors relying on measurements of various characteristics of light exciting SPs were investigated [19]:

- Angular modulation (SPR is monitored using monochromatic optical wave under multiple angles of incidence. Variations of RI in sensing area are measured by tracking changes in position of SPR dip in angular reflectivity spectrum.)
- Wavelength modulation (SPR is monitored using polychromatic optical wave under fixed angle of incidence. Variations of RI in sensing area are measured by tracking changes in position of SPR dip in reflectivity spectrum of wavelength.)
- Intensity modulation (SPR is monitored using monochromatic optical wave under fixed angle of incidence. Changes of RI in sensing area are determined from variations of intensity of reflected optical wave.)
- Phase modulation (SPR is monitored using monochromatic optical wave under fixed angle of incidence. Changes of RI in sensing area are determined by measuring the variations of phase of reflected optical wave.)
- Polarization modulation (SPR is monitored using monochromatic optical wave under fixed angle of incidence. Changes of RI in sensing area are determined by measuring the reflected optical wave polarization changes.)

Majority of SPR sensors is used for detection of biological analytes. Up to now number of SPR sensors capable of measuring various analytes such as toxins [24], [25] herbicides [26], [27] and bacteria [28] were reported. In SPR biosensors, a sensitive layer with biological recognition elements, able to capture selected analyte, is used, see Fig. 15.

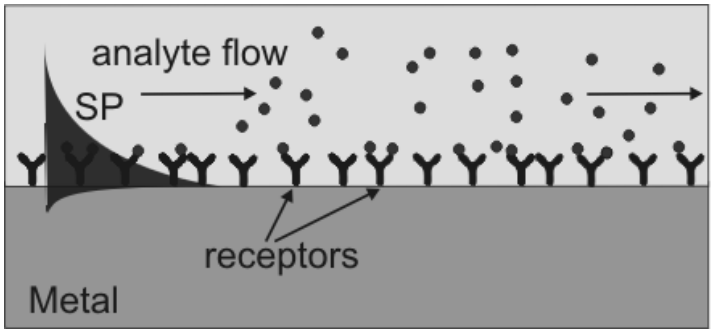

Fig. 15 Surface of SPR biosensor with layer of receptors as biological recognition element.

Up to now, SPR sensor devices were carried out using various optical arrangements. These include prism-based SPR sensors [29]-[33], grating-coupled SPR sensors [34], [44], [46]-[48], integrated optical SPR sensors [40]-[43] and optical fiber SPR sensors [35]-[39].

1.5.1 Prism-based SPR sensors

The configuration based on prism coupler was employed in first SPR sensors pioneered in the beginning of 80's [30] and later it has become the most popular one [29], [31], [32]. In these sensors, Kretschmann geometry for excitation of SPs is used as it allows bringing the samples in contact with the sensor surface directly (see Fig. 16, Fig. 17). In prism-based SPR sensors, numerous SPR modulations were employed. In Fig. 16 and Fig. 17, SPR sensors based on prism coupler with angular and wavelength modulation, respectively, are shown. In prism coupler-based SPR sensor with angular modulation of SPR, monochromatic light wave is made incident on the prism base under different angles of incidence. Changes in the resonant angle of incidence are measured from variations in the angular distribution of intensity of reflected light. In prism coupler-based SPR sensors with wavelength modulation (Fig. 17), collimated polychromatic wave is used to excite SPs. Changes in SPR are measured by the spectral analysis of the reflected light using a spectrograph.
Prism-based SPR sensor with angular modulation was demonstrated to be capable of measurements of refractive index changes as low as $3x10^{-7}$ RIU (refractive index units) [53].

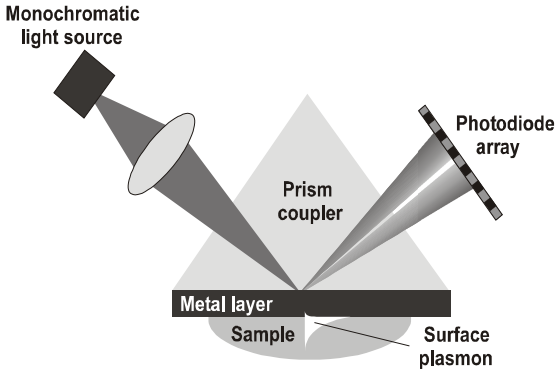

Fig. 16 SPR sensor with prism coupler and angular modulation (reproduced from [19]).

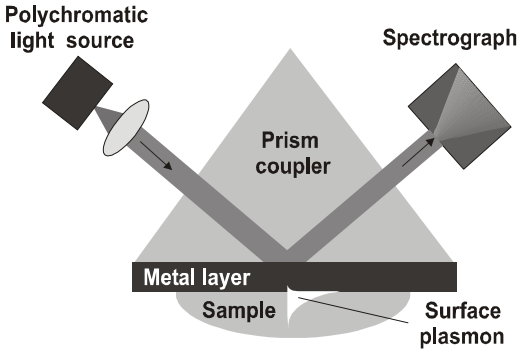

Fig. 17 SPR sensor with prism coupler and wavelength modulation (reproduced from [19]).

1.5.2 Optical fiber SPR sensors

SPR sensors based on optical fibers were investigated in order to exploit their potential for design of miniaturized and remote operating sensors. Up to now, numerous optical fiber SPR sensors based on multi-mode [35], [36] and single-mode [37]-[39] optical fibers were developed since the beginning of the nineties of the last century. In these sensors, surface plasmons are excited by guided modes of an optical fiber when the cladding of the fiber is locally removed and replaced by the SPR active metal layer. Example of sensing area of SPR sensor based on single-mode optical fiber is presented in Fig. 18. The resolution of optical fiber SPR sensor as low as $1x10^{-6}$ RIU, was achieved with SPR sensor based on single-mode optical fiber and wavelength modulation [39].

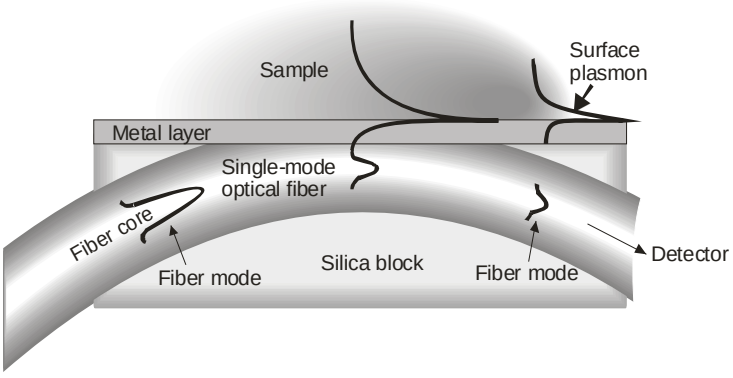

Fig. 18 Sensing structure of fiber optics SPR sensor (reproduced from [39]).

1.5.3 Integrated optical SPR sensors

The principle of integrated optical SPR sensors is similar to fiber optical SPR sensors. SPs are excited by guided mode of a waveguide such as slab or channel waveguide. Sensing structure used in this type of sensors is depicted in Fig. 19.

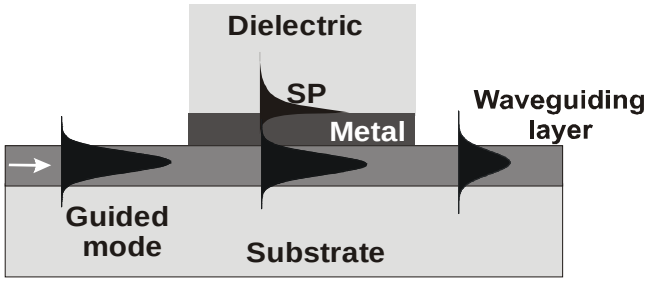

Fig. 19 Excitation of SP in integrated optics wave-guiding structure.

This type of sensor was first demonstrated in 1987 [40]. Later, several integrated optical SPR sensors were developed [41], [42]. Using integrated-optical sensor with wavelength modulation (see Fig. 20) resolution as low as 1.2×10^{-6} RIU was achieved [43].

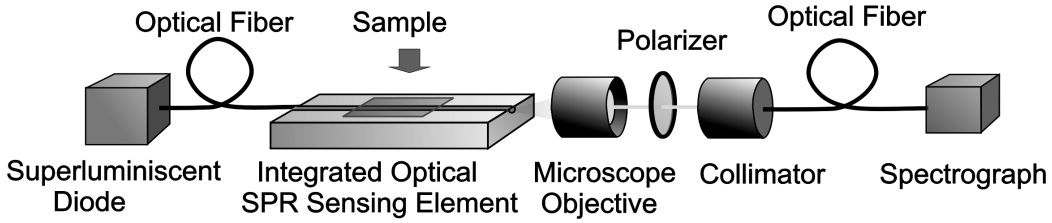

Fig. 20 Integrated optical SPR sensor with wavelength modulation (reproduced from [43]).

1.5.4 Diffraction grating-based SPR sensors

So far, diffraction gratings have been exploited in SPR sensors to a lesser extend than prism couplers. The reason for this lower interest is due to more complicated design of diffraction gratings. In addition, the necessity of excitation of SPs through analyzed samples can be assumed as a disadvantage. On the other hand, diffraction grating structures offer numerous features advantageous for applications in SPR sensors. These include the higher versatility of coupling of light to surface plasmons and possibility of integration of multiple diffraction-based optical components on the sensor chip. Additionally, the sensor chip can be fabricated from plastics by mass-production compatible technologies such as hot embossing or injection molding, [45].
Scheme of example of grating-based SPR sensor with wavelength interrogation is depicted in Fig. 21.

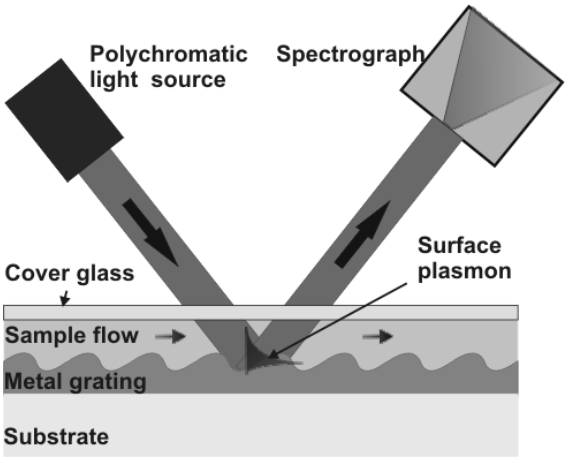

Fig. 21 SPR sensor with diffraction grating and wavelength modulation.

The first reported SPR sensor with diffraction grating relied on intensity modulation of SPR [44]. Later, wavelength and angular modulation was introduced to diffraction grating-based SPR sensors to achieve higher accuracy in SPR measurements [46]-[49]. Grating-based SPR sensor with wavelength modulation and improvement of resonant momentum detection using acousto-optical modulator was demonstrated to be capable to recognize refractive index changes as small as $1x10^{-6}$ RIU [54].

1.5.5 SPR sensors with long-range surface plasmons

So far, majority of SPR sensors employed SPs propagating along a single metal dielectric interface. In order to improve the accuracy of SPR sensors, excitation of long-range surface plasmons guided along thin metal films was explored.

In prism coupler-based SPR sensors, employing of long-range surface plasmons was shown to improve the sensor resolution, because this SP mode allows closer matching of its dispersion relation with that of excitation optical wave. This results in narower SPR reflectivity dip, which yields in higher accuracy in determination of SPR position [57]. In 2001, Nenninger et. al. demonstrated prism-based SPR sensor with long-range SPs allowing measurements of refractive index changes as small as 2.6×10^{-7} RIU [33]. Most recently, Slavík reported SPR sensor based on prism coupler and wavelength interrogation of long-range SPs capable of resolution of refractive index changes down to 4×10^{-8} RIU [60]. Further, prism-based SPR sensor based on long-range SPs imaging was reported in 2005 [61].

On diffraction gratings, possibility of excitation of LRSPs on asymmetric structure for sensor applications was demonstrated by Lyndin et. al. in 1999 [59]. However, no grating coupler-based SPR sensor with long-range surface plasmons was reported yet.

2. Aim of the work

Aim of this work investigation of special surface plasmon modes - long-range surface plasmon (LRSP) and short-range surface plasmon (SRSP) - for applications in grating-coupled surface plasmon resonance (SPR) sensors with wavelength modulation of SPR. The introduction of long-range surface plasmons to SPR sensors is expected to provide several important benefits. As losses of LRSP are lower then the ones of the conventional SP, narrower resonance can be observed in the wavelength spectrum of light exciting this mode. Therefore, measurement of changes in the resonant wavelength can be performed more precisely, which yields in higher resolution of SPR sensor. Furthermore, more sensing channels can be encoded in certain wavelength band in SPR sensors relying on wavelength division multiplexing (WDM) of sensing channels. In addition, the coupling of SP modes through the thin metal layer allows excitation of LRSP and SRSP through the substrate. This feature allows simplification of grating-coupled SPR sensor instrumentation, as the light does not need to pass through the flow-cell and analyzed sample.

This work encompasses both theoretical and experimental analysis of diffractive structure for excitation of LRSP and SRSP modes. In the theoretical part of this work, presented in Chapter 3, characteristics and optical excitation of LRSP and SRSP modes guided by slightly refractive index asymmetric structure is investigated. Furthermore, sensitivity of LRSP and SRSP to refractive index changes at the sensor surface is evaluated. In the experimental part of the work, presented in Chapter 4, fabrication and characterization of the diffractive structure followed is described. Finally, application of prepared diffractive structures for an SPR sensor is demonstrated.

3. Theory

In this chapter, theoretical analysis and optimization of multi-layer diffractive structure for SPR sensor with LRSP and SRSP modes is carried out. At first, theoretical analysis of guided modes supported by the slightly asymmetrical structure consisting of buffer layer (refractive index close to water), thin gold film and water-like medium is presented, followed by the optimization of grating profile parameters in order to achieve an optimal coupling between an optical wave and SP modes. After, the minimal thickness of AlF_3 layer and the sensitivity of considered sensor to refractive index changes are determined.
All numerical calculations in this chapter were made by using the commercial computer program "PC-Grate" [55] based on the modified rigorous integral method [50]. The SP field profiles were calculated by the computer program CAMFR [56] (Cavity Modeling Framework) based on the eigen-mode expansion method [56].
Because the proposed SPR sensor is considered to operate with aqueous samples, the dielectric "buffer" layer with refractive index close to that of water needs to be added into the diffractive structure (see Fig. 22). In this work, aluminum fluoride (AlF_3) is chosen to form the buffer layer as it has suitable mechanical and optical qualities.
In the following calculations, normal incidence of excitation optical wave is considered. The grating spatial period is chosen to establish the maximum coupling of SP with optical wave at λ=800 nm, where the gold exhibits smallest losses. Modulation profile of gold film surfaces is considered to be sinusoidal. Dispersion relations of materials, which are used in numerical model, are included in Appendix.

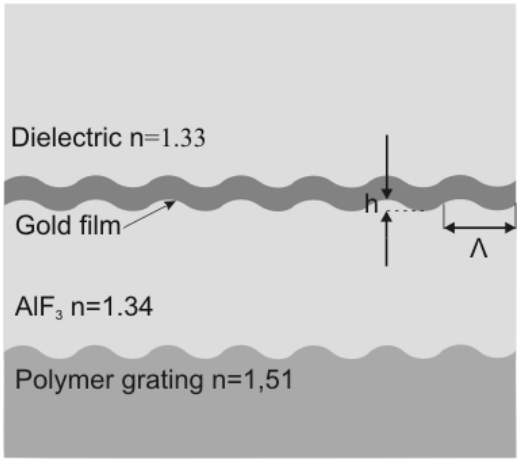

Fig. 22 Multi-layer diffractive structure, Λ denotes grating period, h is modulation depth. Refractive indices are given for λ=800 nm.

3.1 Modeling of SPR on metallic diffraction grating using integral method

Let us assume the geometry with Cartesian coordinates (see Fig. 23), consisting of semi-infinite metal (permittivity ε_M) with periodically modulated surface and semi-infinite dielectric (permittivity ε_D). The metal surface cross-section by the plane *xz* is described by a periodic function z=*f(x),* which is invariant along the *y* coordinate. Further, if we assume incident monochromatic plane wave impinging on grating in the plane of incidence *xz*, diffraction problem can be treated in two dimensions, because of the system homogeneity in *y* direction.

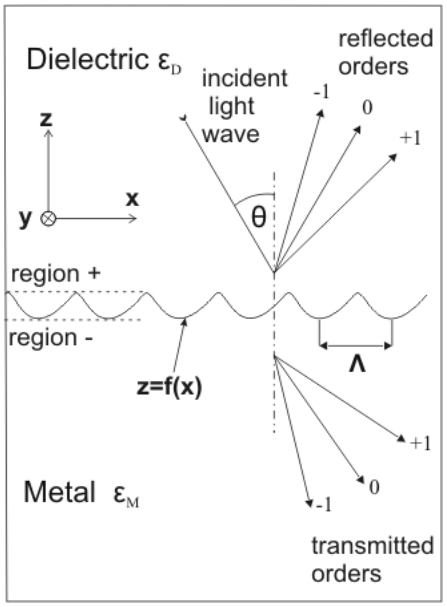

Fig. 23Geometry of diffraction problem on a metallic grating.

In general, total field in space above the grating can be expressed as superposition of incident and diffracted field. In case of TM polarization (magnetic intensity vector parallel to the grating grooves), magnetic intensity field can be expressed as:

$$H_y^{tot} = H_y^i + H_y^d, \tag{2.1}$$

where H_y^{tot}, H_y^{inc} and H_y^d denotes total, incident and diffracted magnetic field, respectively, θ is angle of incidence. Diffracted field in regions denoted as "+" (*z > max[f(x)]) and* "-" (*z < min[f(x)])* (Fig. 23) can be described in the form of Rayleigh expansion [52]:

$$H_y^{d+} = \sum_{m=-\infty}^{+\infty} R_m \exp[-i(k_{xm}x + k_{zm}^{+}z)], \tag{2.2}$$

$$H_y^{d-} = \sum_{m=-\infty}^{+\infty} T_m \exp[-i(k_{xm}x + k_{zm}^{-}z)], \tag{2.3}$$

where R_m and T_m are amplitudes of m^{th} reflected and transmitted order, respectively ,k_{xm} is x-component of m^{th} diffracted order, k_{zm}^{+} and k_{zm}^{-} are z-components of the m^{th} order in region "+" and "-", respectively. Components of wave vectors k_{xm}, k_{zm}^{+} and k_{zm}^{-} can be expressed as:

$$\begin{aligned} k_{xm} &= \frac{w}{c}\sqrt{e_D}\sin q + m\frac{2p}{\Lambda}, \\ k_{zm}^{+} &= \sqrt{e_D\left(\frac{w}{c}\right)^2 - k_{xm}^2}, \\ k_{zm}^{-} &= \sqrt{e_M\left(\frac{w}{c}\right)^2 - k_{xm}^2}, \end{aligned} \tag{2.4}$$

where ε_D, ε_M denotes permittivity of top (dielectric) and bottom (metal) medium, respectively and Λ is period of function $f(x)$. In order to find amplitudes of diffracted orders in Rayleigh expansion (2.2), (2.3), rigorous integral method (see [50]-[52]) was used. In the rigorous integral method, diffracted field is considered to be formed by a current flowing along the grating surface. This current is induced by the incident electromagnetic field. Diffraction problem is then reduced to finding the expression for the unknown surface current. Diffracted magnetic field in the dielectric medium can be expressed in the form of Helmholz-Kirchhoff integral (see [50]), when the integration is done over one grating period with respect to Floquet theorem [52]:

$$\mathrm{H_y^d} = \int_{\Lambda} \mathrm{G^+(x, x', y, f(x'))\Psi(x', f(x'))dx'}. \tag{2.5}$$

Here, function $\Psi(x,f(x))$ represents transformed current on the grating surface and G^+ is the so-called Green function of upper half space. Unknown scalar function $\Psi(x,f(x))$, which knowledge is necessary for retrieve the diffracted field by solving eq. (2.5), can be obtained when boundary conditions for total field and its normal derivatives on the metal-dielectric interface are taken into account. This yields in integral equation from which the function Ψ can be numerically calculated when the incident field, material constants and grating profile are known. When function Ψ is found, the Helmholz-Kirchhoff integral can be solved using point matching method (collocation method) [50]. For solving the

diffraction problem on multi-layer structures, integral method was extended to “modified integral method” [50], [51] few years ago.

3.2 Surface plasmon modes guided along slightly asymmetric structure

In this chapter, properties of long-range and short-range SP modes guided by the structure consisting of gold layer embedded between two semi-infinite dielectric media with refractive indices 1.33 and 1.34 RIU are presented.
Gold film thickness determines the coupling strength between SP modes propagating on the opposite sides of the metal film, which affects the propagation constant of long-range and short-range SP modes (see equations (1.7), (1.8) and Fig. 24). From TM reflectivity spectra, shown in Fig. 25 for three different thicknesses of the gold film, one can see that with decreasing the gold film thickness, difference in spectral position of reflectivity dips associated to LRSP (at lower wavelength) and SRSP (at larger wavelegth) are increasing which is in agreement with Fig. 24. Further, reflectivity dip caused by the resonance with LRSP exhibits smaller width with decreasing the gold film thickness, while the SRSP mode exhibits opposite dependence. This feature is given by the different distribution of LRSP and SRSP field (see Fig. 26). While the portion of LRSP field localized in lossy metal is decreasing with decreasing gold film thickness, the SRSP mode is localized more in metal for smaller gold film thicknesses which causes broadening of the SPR dip.

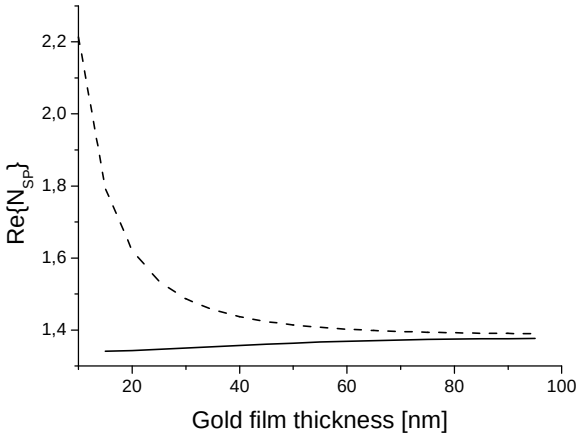

Fig. 24 Real part of effective refractive index of long-range (———) and short-range (– – –) SP modes as function of gold film thickness. Calculated at λ=800 nm, for structure consisting of semi-infinite dielectric with refractive index n=1,33 RIU, gold film and semi-infinite dielectric with refractive index n=1,34 RIU.

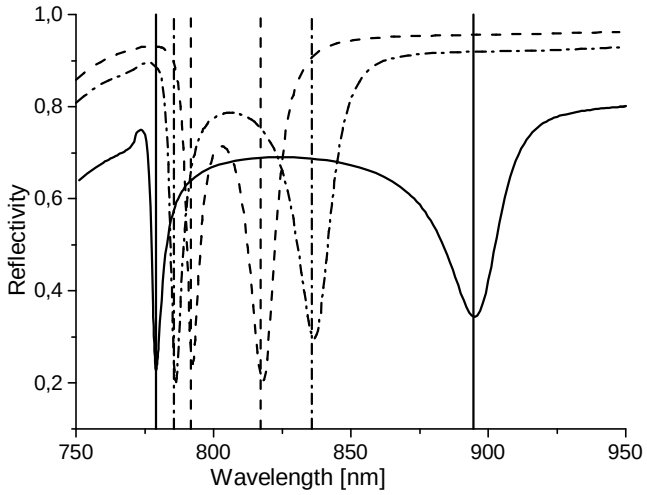

Fig. 25 Spectra of TM polarized normal incident optical wave, reflected from the structure consisting of 20 (———), 35 (– · –) and 50 (– – –) nm thick gold film with periodically modulated surfaces, surrounded by two semi-infinite dielectric media with refractive indices 1.33 and 1.34 RIU. Parameters of grating profile: period Λ=580 nm, modulation depth h=30 nm. Vertical lines represent the resonant wavelength of LRSP (lower wavelengths) and SRSP (larger wavelengths) in resonance with normal incident optical wave calculated using equations (1.7), (1.8) and (1.12) on structure consisting of periodically modulated gold film (Λ=580 nm) with thickness 20 (———), 35 (– · –) and 50 (– – –) nm surrounded by the semi-infinite dielectric medium with refractive index n_D=1.335.

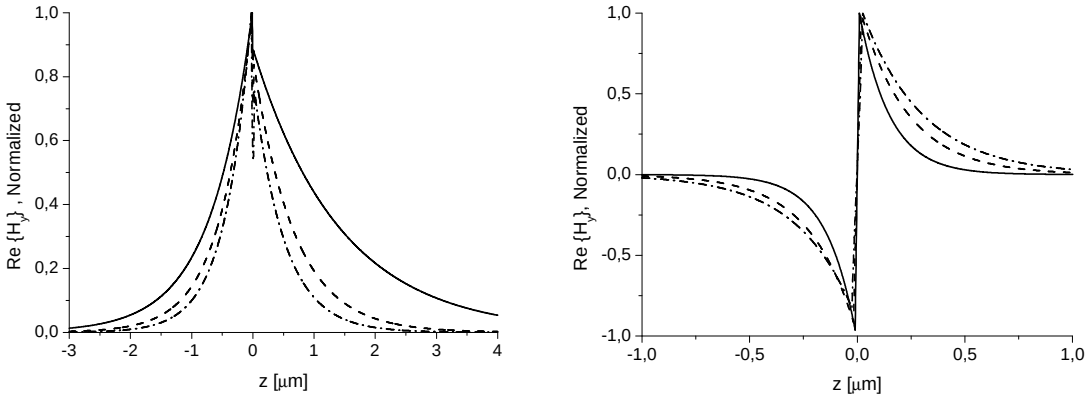

Fig. 26 Normalized real part of LRSP (left) and SRSP (right) magnetic intensity field calculated for structure consisting of dielectric (n=1.33 RIU), gold film with thickness 20 (———), 35 (– – –) and 50 nm (– · –) and dielectric (n=1.34) (from left to right).

3.3 Optimization of grating profile parameters

In order to excite SPs on desired wavelength, dependence of resonant wavelength on the grating spatial period was calculated for long-range and short-range mode on structure with 40 nm thick gold film embedded between semi-infinite AlF_3 and water media (see Fig. 27). This dependence was determined from positions of reflectivity dips, calculated using the integral method for several values of grating period Λ.

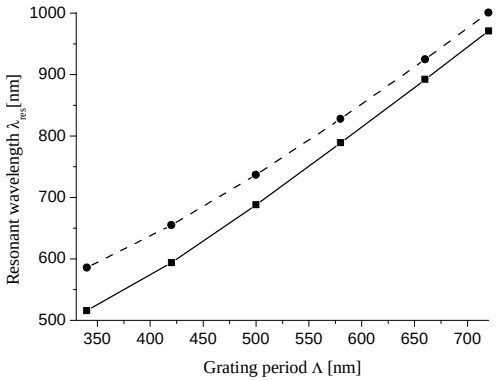

Fig. 27 Resonant wavelength of LRSP (——) and SRSP (– – –) mode as function of grating spatial period Λ in normal incidence geometry.

Efficiency of coupling between light wave and SP can be controlled through modulation depth of the grating. For purposes of SPR sensing, sharp and deep resonances in reflectivity spectrum are preferred as they allow determination of the resonant wavelength more precisely. Reflectivity spectra in normal incidence geometry were calculated for structures consisting of semi-infinite AlF_3 layer, gold film with periodically modulated surface (thickness 20 and 50 nm) and semi-infinite water. For each grating period, a set of reflectivity spectra with different modulation depths was calculated and parameters δR_{LR} and δR_{SR} (for illustration see Fig. 28) describing the depth of reflectivity dip caused by the coupling to long-range and short-range SPs respectively were determined.

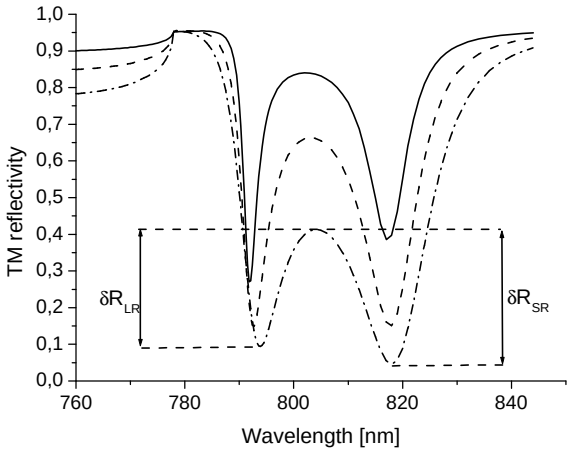

Fig. 28 Reflectivity spectra of TM polarized light wave in normal incidence geometry on structure consisting of gold film (thickness 50 nm) with periodically modulated boundaries (period of modulation 580 nm, modulation depth 20 (——), 30 (– – –) and 40 (– · –) nm) embedded in semi-infinite dielectric media -AlF_3 and water.

From calculated sets of spectra optimal modulation depths h were determined as those, for which parameters δR_{LR} (describing the coupling to long-range SP) and δR_{SR} (describing the coupling to short-range SP) are maximal. Obtained optimal modulation depths calculated for gold film thickness 20 and 50 nm at λ=800 nm are presented in Table 3.

	Optimal modulation depth h [nm]	
	LRSP	SRSP
Gold thickness 20 nm	25	45
Gold thickness 50 nm	22	27

Table 3 Optimal grating modulation depth calculated for gold film thickness 20 and 50 nm at the wavelength λ=800 nm.

3.4 Effect of finite thickness of aluminum fluoride layer

As in real sensing structure, AlF_3 is used to form the layer between the substrate and the gold layer, let us explore the effect of finite thickness of AlF_3 on SPR reflectivity. Objective of this chapter is to determine the minimal thickness of the AlF_3 layer, for which almost entire SP field is localized inside the AlF_3 – gold – sample structure. This condition should assure the independence of SPR on the AlF_3 layer thickness. For this purpose, the dependence of SPR properties on AlF_3 layer thickness was calculated for several values of thickness of the gold layer. The set of theoretical reflectivity spectra in

normal incidence configuration was calculated for each thickness of gold film with thickness of AlF_3 layer varying from 100 to 1500 nm. Then, we observed the value of reflectivity in the minimum of the spectral dip, caused by the coupling of light into long-range SP. Dependence of these resonant reflectivities on the thickness of AlF_3 layer is shown in Fig. 29 for several gold film thicknesses. The modulation of described curves in Fig. 29 is caused by the multiple reflections of light on the boundaries of aluminum fluoride with gold and substrate.

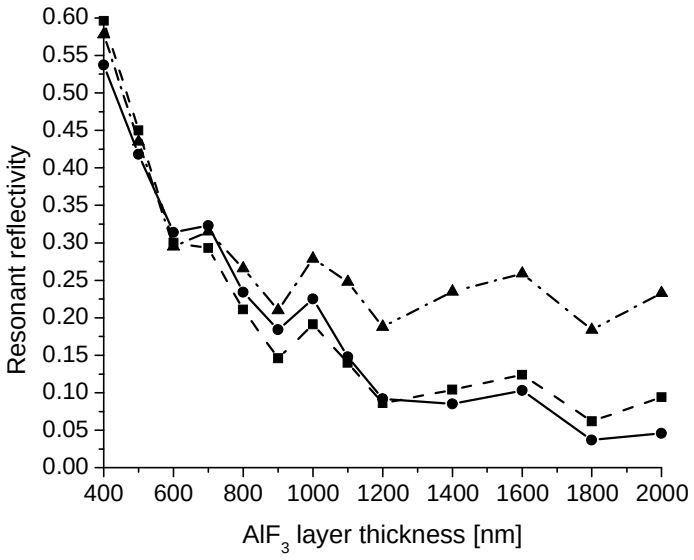

Fig. 29 Reflectivity of normal incident TM polarized optical wave in resonance with LRSP as function of the AlF_3 layer thickness. Diffractive structure consists of substrate (semi- infinite, refractive index 1.51RIU), AlF_3 layer with thickness 400-2000 nm, gold film with thickness 20 (——), 40 (– – –), 60 (– · –) nm. Period of grating profile modulation Λ was chosen to excite LRSP near the the desired wavelength (λ=800 ± 5 nm, Λ=595 ± 5 nm), grating modulation depth is 30 nm.

From data presented in Fig. 29, we assumed that in designed multi-layer diffractive structure, AlF_3 layer with thickness 1000 nm is sufficient to assure the localization of majority of LRSP field in AlF_3 - gold – sample structure.

3.5 Sensitivity of long-range and short-range SP modes to refractive index changes

In SPR sensor with wavelength interrogation, sensitivity of the sensor to refractive index changes is defined as:

$$S = \frac{d\,l_{res}}{d\,n}, \tag{2.6}$$

where $\delta\lambda_{res}$ denotes change in resonant wavelength caused by the small change in refractive index of sensed dielectric δn. Further, one can distinguish sensitivity to bulk refractive index changes (S_B, bulk sensitivity) and sensitivity to refractive index changes within a thin layer near the sensor surface with the thickness much smaller than SP penetration depth into dielectric (S_S, surface sensitivity). In order to evaluate the bulk sensitivity of SPR sensor based on studied diffractive structure, resonant wavelengths were calculated for two slightly different refractive indices of sample medium. This calculation was done for both SP modes - LRSP and SRSP, when the resonant wavelengths were set to be in interval λ_{res}=(800±5) nm. Bulk sensitivities calculated for the metal film thickness varying from 20 to 50 nm are shown in Fig. 30. The surface sensitivity was calculated for the same resonant wavelength and gold film thickness values, but change in refractive index was assumed to occur only within the 15 nm thick dielectric layer attached to the sensor surface (see Fig. 31).

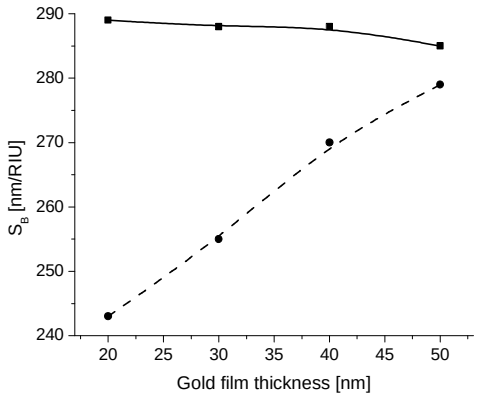

Fig. 30 Sensitivity of resonant wavelength to bulk refractive index changes as function of gold film thickness calculated for normal incident light wave in resonance with long-range (____) and short-range (_ _ _) SP, λ=800 nm. Sensing structure consists of semi-infinite AlF_3, gold film and semi-infinite sample (refractive index was varied from n=1.33 to n=1.34 RIU).

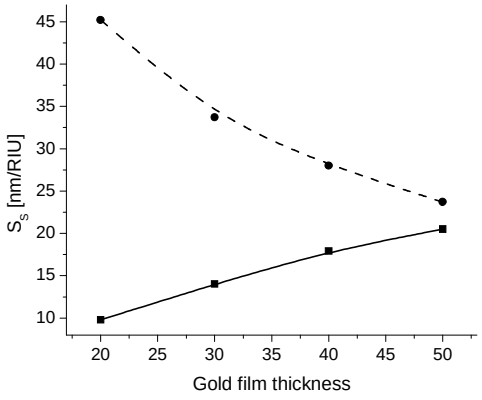

Fig. 31 Sensitivity of resonant wavelength to surface refractive index changes as function of gold film thickness calculated for normal incident light wave in resonance with long-range (____) and short-range (_ _ _) SP, λ=800 nm. Sensing structure consists of semi-infinite AlF_3, gold film, 15 nm sample (refractive index was varied from n=1.33 RIU to n=1.43 RIU) and semi-infinite dielectric (n=1.33 RIU).

Calculated dependences of sensitivities of long-range and short-range SP modes to bulk and surface refractive index changes correspond to the different field distribution of these SP modes. Long-range SP exhibit higher sensitivity to bulk RI changes than the SRSP as it has larger portion of its field stretched in sensed dielectric, while the SRSP mode has larger surface sensitivity, because its field is localized near the sensor surface.
Furthermore, the dependence of bulk sensitivity of LRSP and SRSP modes on resonant wavelength was calculated for normal incident excitation optical wave, while the gold film thickness was set to 20 nm. Different values of resonant wavelength were obtained by changing the grating spatial period *Λ*. Obtained dependence is shown in Fig. 32.

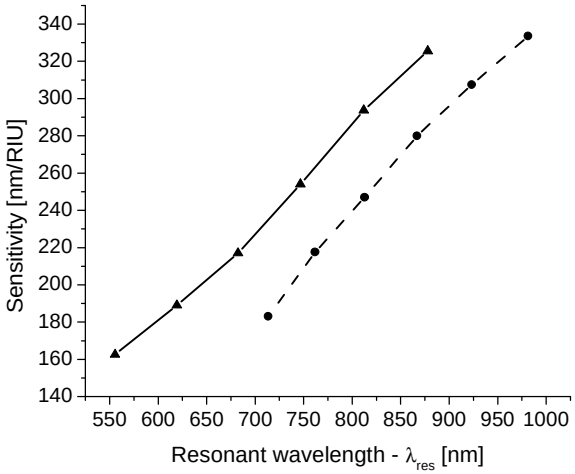

Fig. 32 Bulk sensitivity of SPR sensor with LRSP(——) and SRSP (– – –) modes as a function of resonant wavelength calculated on structure consisting of semi-infinite AlF_3 layer, gold film (thickness 20 nm) and semi-infinite dielectric (refractive index was varied from n=1.33 to n=1.34 RIU).

4. Experimental

In this chapter, fabrication and characterization of diffractive structure is presented. At the end of this chapter, prepared sensing structure is evaluated for SPR sensing in model refractometric experiment.

4.1 Fabrication of the multi-layer diffractive structure

The procedure of fabrication of the multi-layer diffractive structure consists of several steps including holographical preparation of master diffraction grating, its replication using soft-lithographical method and preparation of layers which supports the propagation of long-range and short-range SP modes by means of thermal evaporation in vacuum.

4.1.1 Master grating preparation

Master diffraction grating was prepared holographically into photoresist layer (SF 1813 from Shipley, USA) deposited on substrate - polished BK7 glass slide with dimensions 32x15x1,5 mm (from Schott glass technologies, Duryea, USA).
Before the photoresist deposition, substrates were cleaned with acetone and then placed into an ozone cleaner (UVO cleaner 42-220 from Jelight Company) for 20 minutes. The photoresist layer was deposited on substrate by means of spin-coating. Sufficient amount (200 μl) of photoresist was dropped on a rotating substrate while the rotation speed was set to 3500 rpm and rotation time to 15 s. Resulting thickness of photoresist layer was about 1 μm. After the deposition, substrates with photoresist layer were dried for 30 minutes at temperature 90°C.
The holographical exposition of the photoresist layer was realized using Mach – Zehnder interferometer arrangement. Substrate slides with photoresist layer on the front side were painted with black paint on its back side to avoid the back reflections during the holographical exposition. Such prepared samples were exposed to incidence of two coherent laser beams which were made incident on photoresist with angles of incidence $\theta/2$ and $-\theta/2$ (see Fig. 33). As source of the coherent light, an argon ion laser (type 165 from Spectra Physics, USA) operating at λ_L=457,9 nm was used. Exposition time was set to 2 minutes and intensity of optical wave in both interferometer arms were set to 13 μW/cm^2.

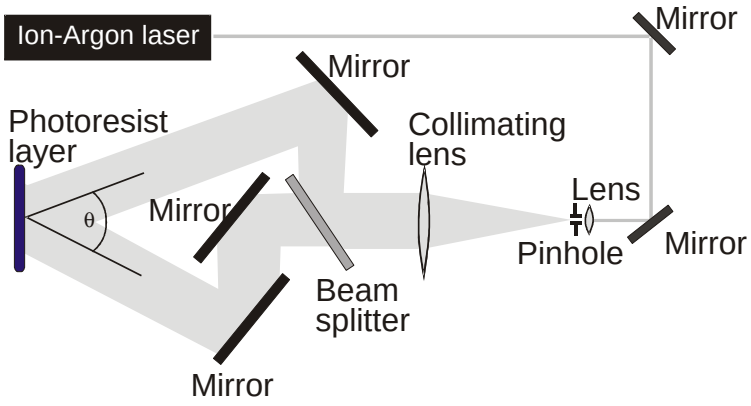

Fig. 33 Arrangement of the holographical grating exposition using Mach-Zehnder interferometer.

The grating period is given by the distance of interference fringes in the interference region, which is dependent on the angle of intersection of the laser beams θ and operation wavelength of laser λ_L:

$$\Lambda = \frac{l_L}{2\sin(q/2)}. \tag{3.1}$$

Substrates coated by the photoresist layer with recorded grating were developed in AZ 303 developer diluted in ratio 1:9 with distilled water. During the development, modulation depth of grating profile was controlled by measuring the efficiency of -1st diffracted order, which was compared with efficiency calculated using integral method for different modulation depths of the grating. The efficiency of -1st diffracted order was measured using Littrow configuration, when intensities of -1st and 0th diffracted order were measured (see Fig. 34) with He-Ne laser, operating at 632,8 nm. The total development time was varied from 30 to 100 s to obtain a desired modulation depth for each individual grating.

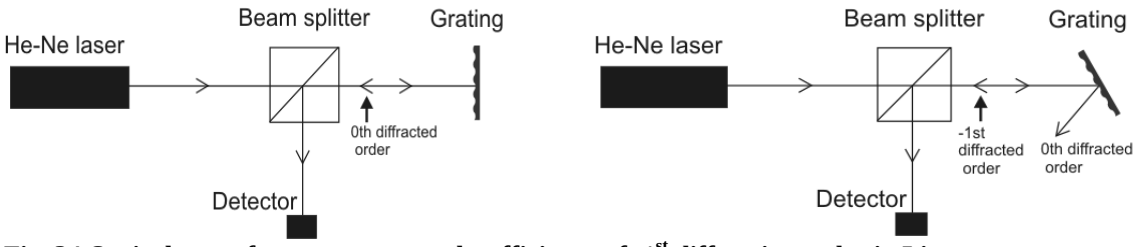

Fig. 34 Optical setup for measurement the efficiency of -1st diffraction order in Littrow configuration.

4.1.2 Replication of master diffraction grating

During the multi-layered structure preparation, samples are exposed to high temperatures (~250 °C). Because the photoresist layer instability at such temperatures, replication of master grating to polymer layer with higher thermal stability was used. Furthermore, this replication technique based on soft lithographic method make the process of the grating preparation less time consuming.
The replication procedure consists of several steps. At first, master grating profile was copied into special stamp, which was consequently used to imprint the grating profile to polymer layer, prepared on another substrate. For purpose of transfer the master grating profile to stamp, master grating was cast in liquid mixture of polymethyldisiloxane (PDMS, Sylgard 184 from Dow Cornig, USA) and curing agent, mixed with ratio 9:1. Then, the liquid PDMS was degassed and cured for 6 hours at 60°C to produce elastic PDMS stamp. These PDMS stamps were used to copy the master grating modulation profile to polymer (UV curable OG 146 from Epotek, USA) layer coated on cleaned glass slides. The polymer layer was deposited by spin-coating (rotation speed 10000 rpm, rotation time 10s), and then - in contact with PDMS stamp - was cured after the thermal stabilization in UV for 30 minutes using a mercury lamp. After this procedure, the PDMS stamp was removed and replica grating was heated for 30 minutes at 150°C to undergo the glass transition of OG 146 layer. Main steps in grating replication procedure are illustrated in Fig. 35.

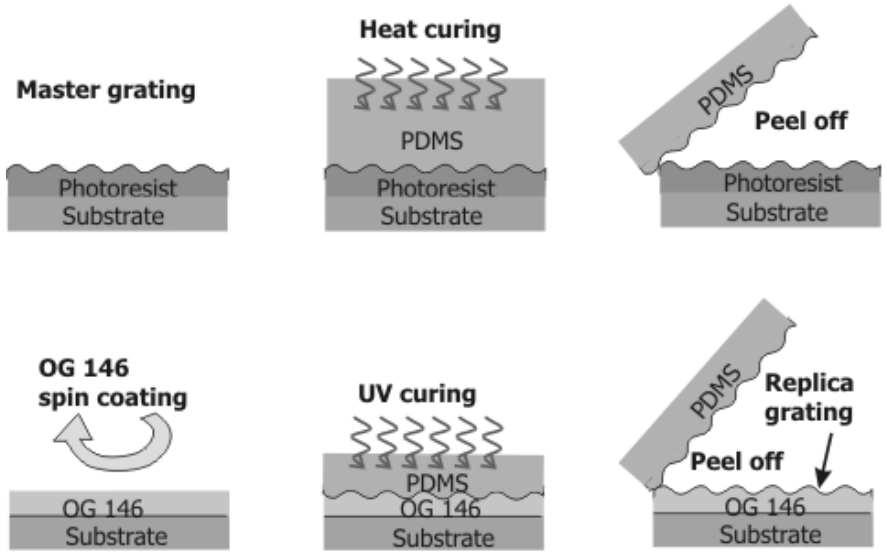

Fig. 35 Scheme of grating replication procedure. First row of pictures illustrates the transfer of master grating to PDMS stamp. Second row shows the imprinting of the PDMS stamp grating profile into replica grating.

4.1.3 Deposition of aluminum fluoride and gold layers

Aluminum fluoride (from Cerac, USA) and gold layers were both prepared by the thermal evaporation technique in PFEIFFER PLS 570 deposition chamber in vacuum better than 10^{-7}mbar. Thicknesses of deposited layers were continuously controlled by the quartz crystal oscillator. The AlF_3 layer was evaporated from molybdenum crucible (with deposition speed 0,2-0,3 nm/s) designed specially to reduce the spitting of evaporated material. Temperature was kept at 250 °C. After the deposition, sample was let for 30 minutes at the same temperature. Deposition of gold layer was done from wolfram crucible in the same vacuum while the temperature was decreased to 150 °C. Deposition speed was 0,4-0,5 nm/s. In order to establish better adhesion between AlF_3 and gold layers, several sensing structures were made with adhesion promoting titanium layer that was deposited AlF_3 layer by means of electron-beam gun. After deposition of Ti, gold layer was evaporated in the same manner as it is described above.

4.2 Characterization of developed sensing structure

In this chapter, characterization of developed sensing structures by means of measuring the reflectivity spectra or study of the surface quality of AlF_3 and gold layers by the atomic force microscope is given. The optimization of diffractive structure parameters presented in Chapter 3, resulted to structure consisting of substrate (RI=1.51), polymer layer with refractive index very close to that of substrate (thickness approximately 1 μm), AlF_3 layer with thickness 1 μm and gold layer (thickness 30-40 nm). The period of grating modulation profile was chosen to be about 600 nm to excite LRSP and SRSP modes near the desired wavelength λ=800 nm. Grating modulation depth was chosen to be 30-35 nm to reach optimal coupling of optical wave and SP modes.

4.2.1 Characterization of grating profile using atomic force microscopy

In order to characterize the properties of prepared multi-layer diffractive structure, surface of deposited layers – AlF_3 and gold were analysed using AFM (MultimodeTM from Veeco, USA). The set of several diffraction gratings was made with different modulation depth of the surface modulation to evaluate the smoothing of the original grating modulation profile after the evaporation of AlF_3 and gold layers. All measured gratings with original modulation depth from 38 to 65 nm exhibited after deposition of 1 μm thick AlF_3 layer and 30 nm gold layer lowering of the grating modulation depth by approximately 10 percent. Also the roughness properties of studied gratings did not change after the deposition of AlF_3 and gold layers significantly. The rms of the roughness of the polymer grating profile and gold grating profile were determined to be about 10 nm in both cases. Detail of grating surface before and after the deposition of AlF_3 and gold layers is in Fig. 36.

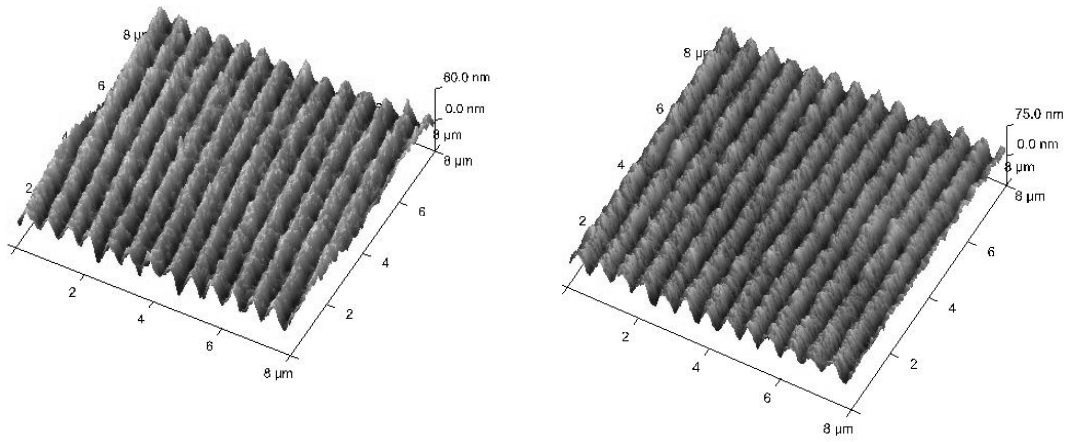

Fig. 36 AFM pictures of grating profile of replica grating before (left picture) and after (right picture) the deposition of AlF_3 and gold layers.

4.2.2 Characterization of long-range and short-range surface plasmon on diffraction grating

For purposes of evaluation of SPR on the developed diffractive structure, reflectivity of light wave in normal incidence was measured when the sensing structure was in contact with water. The experimental setup is shown in Fig. 37. Light from a polychromatic light source was coupled into a multi-mode optical fiber (FT-200 EMT from Thorlabs, USA) and on the fiber output was collimated using "Glass optics for parallel beam" (from Zeiss, Germany). Collimated beam was then passed through a polarizer (Polarcor 800-HC from Corning, USA) and a cube beam-splitter (from Linos, UK), where it hit the diffractive structure in contact with water. Optical wave reflected from the sensing structure was coupled into an optical fiber (FT-200 EMT from Thorlabs, USA) and transmitted to a spectrograph (MCS 500 spectrometer module from Zeiss, Germany) connected to a computer, where it was analysed.

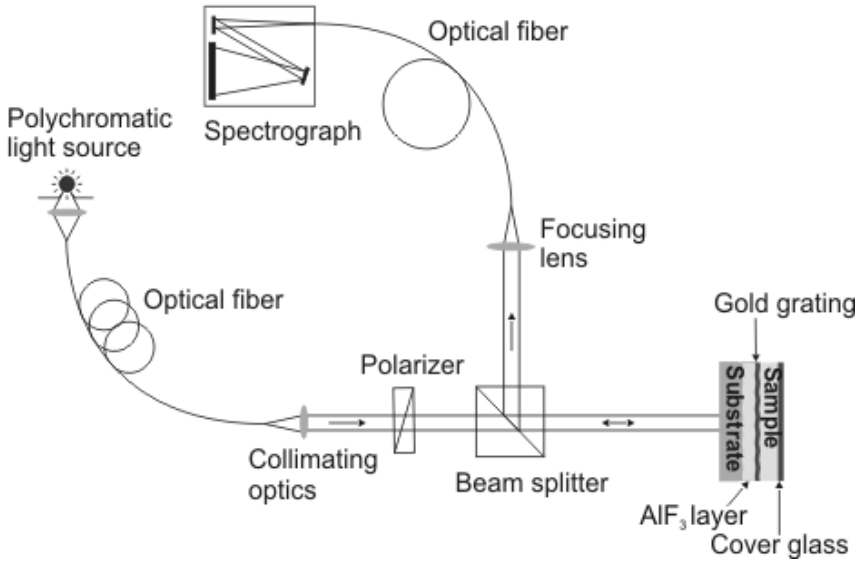

Fig. 37 Experimental setup used to observe excitation of LRSP and SRSP modes on a gold diffraction grating.

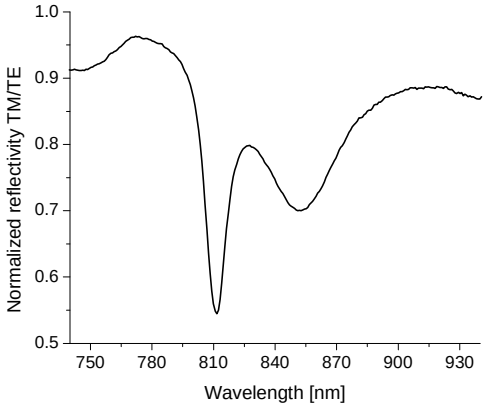

Fig. 38 Normalized reflectivity spectrum measured in normal incidence geometry on diffractive structure consisting of substrate (RI=1.51), polymer layer (RI = 1.51), AlF_3 layer (thickness 1µm), Ti layer (thickness ~ 0.5 nm) and gold layer (thickness 35 nm, modulation depth 31 nm, grating period 600 nm) in contact with water.

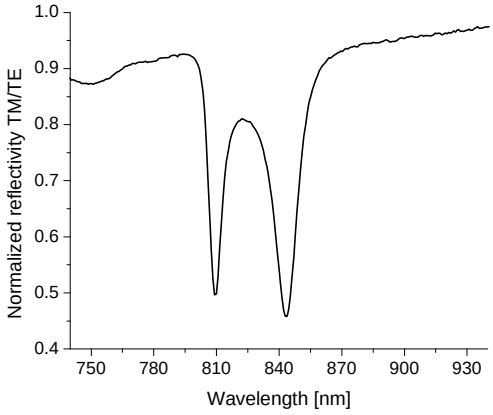

Fig. 39 Normalized reflectivity spectrum measured in normal incidence geometry on diffractive structure consisting of substrate (RI=1.51), polymer layer (RI = 1.51), AlF_3 layer (thickness 1µm) and gold layer (thickness 42 nm, modulation depth 31 nm, grating period 600 nm) in contact with water.

From measured spectra (Fig. 38, Fig. 39), one can see, that employing the lossy adhesion layer into sensing structure affects the SPR significantly even though the thickness of the fabricated layer has been chosen to be as low as possible (~0.5 nm). Besides that, we can see that influence of the titanium layer is stronger in case of SRSP mode due to its electromagnetic field localized mainly in the vicinity of the gold layer surface, where the

Ti layer is placed. While the full width at half a minimum (FWHM) of the resonant dip associated to LRSP changes approximately from 6 to 9.5 (see Table 4) nm by employing the Ti layer, FWHM of resonant dip caused by the SRSP will change from 11 to 25 nm. When we compare the reflectivity spectrum measured on a diffractive structure without the Ti layer with the spectrum calculated using integral method on the same structure (semi-infinite substrate – RI=1.51 / AlF_3 layer – thickness 1000 nm / gold layer – thickness 42 nm, grating period 596 nm, modulation depth 31 nm / semi-infinite sample - water) shown in Fig. 40, we can see that in comparison with theoretical model, measured reflectivity dips are shallower and have larger widths. This effect is probably caused by the grating inhomogeneity, roughness of the grating surface and also by a quality of optical wave collimation.

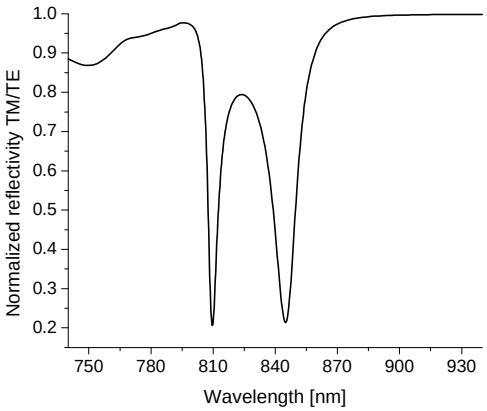

Fig. 40 Normalized reflectivity spectrum calculated in normal incidence geometry on structure consisting of semi-infinite substrate – RI=1.51, AlF_3 layer – thickness 1000 nm, gold layer – thickness 42 nm, grating period 596 nm, modulation depth 31 nm and semi-infinite sample – water.

	FWHM of LRSP	FWHM of SRSP [nm]
Theoretical (without Ti)	5.0	10.7
Measured (without Ti)	6.2	10.7
Measured (with Ti)	9.5	25.1

Table 4 Comparison of calculated and measured reflectivity dip widths (FWMH) for LRSP and SRSP modes. Data in second, third and fourth row of the table are determined from Fig. 40, Fig. 39 and Fig. 38, respectively.

4.3 SPR sensor based on developed sensing structure

In this chapter, we report results of model refractometric experiments based on developed diffractive sensing structure. The measurements were performed using sensor setup shown in Fig. 41, which is similar to one, that is described in Chapter 4.2.2. The samples with different refractive indices were made flow along the sensor surface by means of peristaltic pump (Reglo from Ismatec, Switzerland) with flow rates from 40 to 70 μl/min. Spectral properties of out-coming light were determined by the SD 2000 spectrometer (from Ocean optics, USA) with CCD array consisting of 2048 elements. The spectrometer working range was 740-975 nm. The spectra measured by the spectrograph were further processed using computer program, which tracks changes in the position of spectral dips [58].

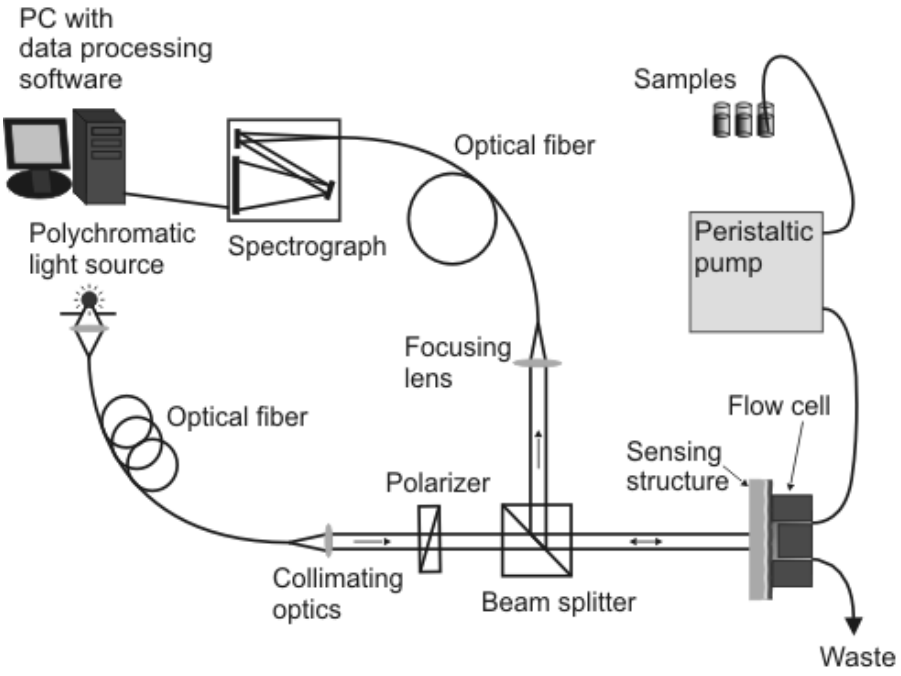

Fig. 41 Arrangement of grating-coupled SPR sensor setup with wavelength interrogation.

These model experiments were realized using two sensing structures, both fabricated from the same master grating, without (Fig. 42) and with the adhesion promoting titanium layer (Fig. 43).
The resonant wavelength was determined using special data processing software for SPR sensors based on tracking centroid method [58]. Typically, 50 spectra measured by the spectrometer during 5 seconds were averaged to obtain raw spectrum. The raw spectrum

was further smoothed and resonant wavelength was determined by the tracking centroid algorithm.

Measured data are shown in Fig. 42 and Fig. 43, where changes in positions of both resonances – caused by the LRSP and SRSP modes – were monitored, while the different mixtures of water and ethylene glycol with RI = 1.3330 1.3360, 1.3390 and 1.3419 were flowed along the sensor surface.

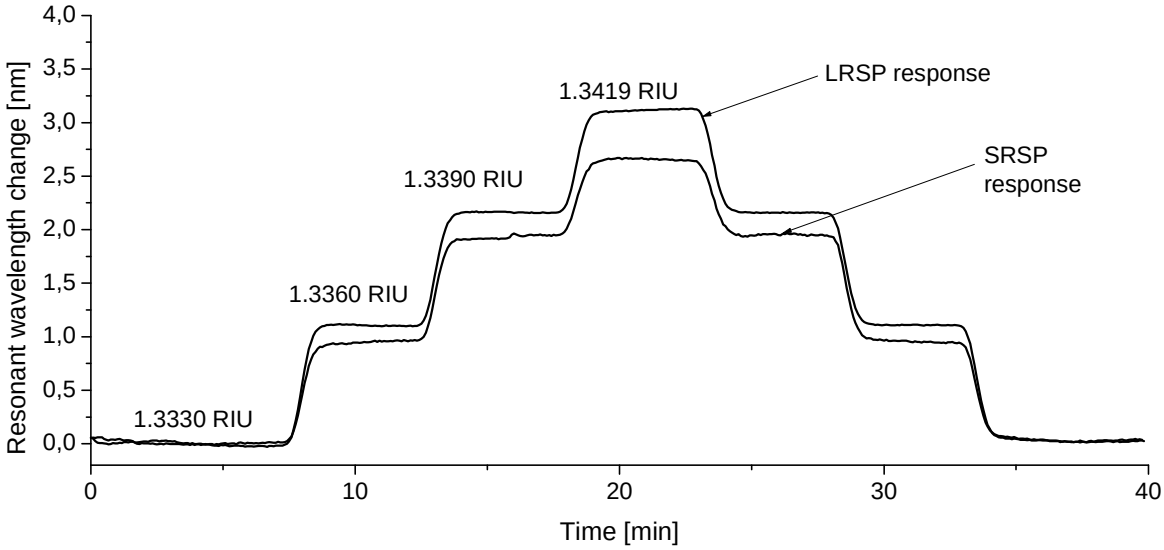

Fig. 42 Resonant wavelength of LRSP and SRSP as function of time, when samples with different refractive indices were flowed along the sensor surface. Used sensing structure consisted of substrate, OG 146 polymer layer (~1µm), AlF_3 layer (~1µm) and gold film (~40nm) and was illuminated by the normal incident optical wave through the substrate.

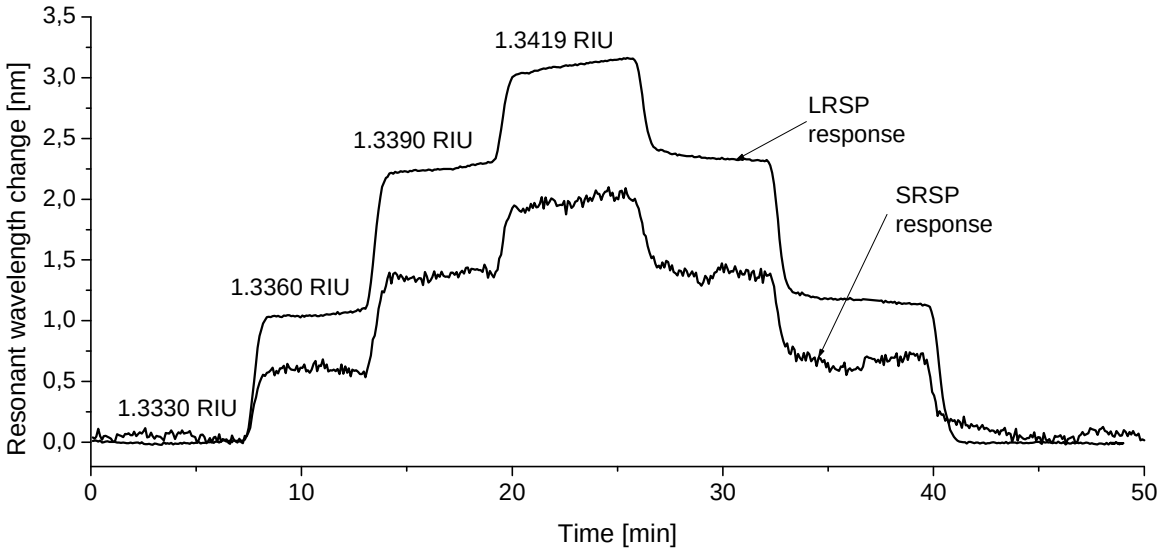

Fig. 43 Resonant wavelength of LRSP and SRSP as function of time, when samples with different refractive indices flowed along the sensor surface. Used sensing structure consisted of substrate, OG 146 polymer layer (~1µm), AlF_3 layer (~1µm), Ti (~0.5nm) and gold film (~35nm) and was illuminated by the normal incident optical wave through the substrate.

From measured sensor responses shown in Fig. 42 and Fig. 43, sensitivity to bulk refractive index changes S_B of SRSP and LRSP modes were determined for two fabricated sensing structures – with and without the Ti layer. The resolution of the sensor defined as a ration of the standard deviation of noise - N_{SD} and sensitivity: $RES = N_{SD} / S_B$, was also determined. Measured sensitivities, standard deviations of noise and resolutions associated to the LRSP and SRSP modes are summarized in Table 5.

	S_B [nm/RIU]	N_{SD} [nm]	Resolution [RIU]
LRSP, without Ti	350	0.002	$5{,}7 \times 10^{-6}$
SRSP, without Ti	330	0.005	$1{,}5 \times 10^{-5}$
LRSP, with Ti	350	0.005	$1{,}43 \times 10^{-5}$
SRSP, with Ti	~250	0.03	1.2×10^{-4}

Table 5. Measured sensitivities to bulk refractive index changes and sensor resolutions determined by the experiment on grating-coupled SPR sensor with interrogation of LRSP and SRSP modes and based on two different sensing structures – with and without adhesion promoting Ti layer.

Data presented in second and third row of Table 5 shows, that sensitivity of long-range SP propagating along structure without Ti to bulk refractive index changes is slightly larger than that of SRSP. Presence of the adhesion layer does not affect the sensitivity of LRSP mode, but noise characteristics of the sensor gets worse more than two times,

which is caused by the broadening the SPR dip and thus larger uncertainty in SPR dip position determination. The influence of Ti layer to SRSP properties is much more significant, because of the larger portion of its field is localized in Ti layer when compared to LRSP mode. This feature results in a decrease of sensitivity of SRSP mode as well as an increase of standard deviation of noise (almost ten times).
Unfortunately, sensing structures prepared without the Ti layer were not mechanically stable, which makes them less practical for SPR sensors.

5. Conclusions

Special surface plasmon (SP) modes- LRSP and SRSP, excited using a grating coupler on a thin gold film, were theoretically and experimentally studied for application in a surface plasmon resonance (SPR) sensor. For this purpose, a multi-layer diffractive structure with aluminum fluoride and thin gold layers, which supports coupled surface plasmon modes – long-range and short-range SP, was developed.

In the theoretical part of the work, excitation of coupled surface plasmons on the diffractive structure was simulated using the rigorous integral method. The analysis was focused on optimization of the diffractive structure in order to achieve the optimal coupling of light into SP modes and optimal properties of SP modes with respect to the sensor performance. Based on the carried out optimization of diffractive structure parameters, multi-layer diffractive structures with and without an adhesion promoting Ti layer were prepared and characterized.

Finally, the developed diffractive structure was tested in SPR sensor with wavelength modulation. The sensor based on LRSP interrogation, with diffractive sensing structure without Ti exhibited good resolution of bulk refractive index changes ($5{,}7 \times 10^{-6}$ RIU) comparable with standard grating-coupled SPR sensors. Unfortunately, due to the rather limited adhesion between AlF_3 and gold layers, this structure is not sufficiently stable for sensing applications. A thin (~0.5 nm) Ti layer was demonstrated to promote the adhesion between these two layers. The presence of lossy Ti in this multi-layer structure negatively affects the sensor resolution.

Currently, this structure is tested for biosensing applications [62]. Further development of this structure will be focused on finding alternative ways to improve the adhesion between AlF_3 and gold layers.

6. References

[1] J. Raiteri, M. Grattarola, H. J., P. Skladal: Micromechanical cantilever-based biosensors. *Sensors and Actuators B*, 79 (2001) 115-126.

[2] J. Shah, E. Wilkins: Electrochemical Biosensors for Detection of Biological Warfare Agents. *Electroanalysis*, 15 (2003), 157-167.

[3] Nguyen Quy Dao and M. Jouan: The Raman laser fiber optics (RLFO) method and its applications. *Sensors and Actuators B*, 11 (1993) 147-160.

[4] Ch. R. Yonzon, Ch. L. Haynes, X. Zhang, J. T. Walsh,Jr. And R. P.Van Duyne: A Glucose Biosensor on Surface-Enhanced Raman Scattering: Improved Partition Layer, Temporal Stability, Reversibility and Resistance to Serum Protein Interference. *Analytical Chemistry*, 76 (2004) 78-85.

[5] W. Trettnak, O. S. Wolfbeis: Fully reversibe fibre-optic glucose biosensor based on the intrinsic fluorescence of glucose oxidase. *Analytical Chimica Acta*, 221 (1989) 1995-203.

[6] D. Clerc and W. Lukosz: Integrated optical output grating coupler as refractometer and (bio-)chemical sensor. *Sensors and Actuators B,* 11 (1998) 461-465.

[7] J. Piehler, A. Brandenburg, A. Brecht, E. Wagner, and G. Gauglitz: Characterization of grating couplers for affinity-based pesticide sensing. *Applied Optics,* Vol. 36, No. 25 (1997) 6554-6562.

[8] A. Y. Johannes S. Kanger, R. Wijn, P. V. Lambeck, J. Greve: Development of a multichannel integrated interferometer immunosensor. *Sensors and Actuators B,* 83 (2002) 1-7.

[9] X. Liu, Z. Cao, Q. Shen, and S. Huang: Optical sensor based on Fabry-Perot resonance modes. *Applied Optics*, Vol. 42, No. 36 (2003) 7137-7140.

[10] B. Cunnigham, P. Li, B. Lin, J. Pepper: Colorimetric resonant reflection as a direct biochemical assay technique. *Sensors and Actuators B,* 81 (2002) 316-328.

[11] J. Homola, S. Yee, G. Gauglitz: Surface plasmon resonance sensors: review. *Sensors and Actuators B,* 54 (1999) 3-15.

[12] R. W. Wood: On a remarkable case of uneven distribution of light in a diffraction grating spectrum. *Phil. Magm.* 4, (1902) 396-402.

[13] R. W. Wood: Anomalous Diffraction Gratings. *Physical Review, 48 (1935)* 928-936.

[14] U. Fano: The Theory of Anomalous Diffraction Gratings and of Quasi-Stationary Waves on Metallic Surfaces (Sommerfeld's Waves), *J.O.S.A.*, 31 (1941) 215-222.

[15] R.H. Ritchie: Plasma losses by fast electrons in thin films, *Physical Review*, 106 (1957) 874-881.

[16] A. Otto: Excitation of nonradiative surface plasma waves in silver by the method of frustrated total reflection. *Z.Phys* , 216 (1968) 398-410.

[17] E. Kretschmann, H. Raether: Radiative decay of nonradiative surface plasmon excited by light. *Z.Naturf,* 23A: (1968) 2135-2136.

[18] H. Raether: Surface Plasmons on Smooth and Rough Surfaces and on Gratings. Springer tracks in modern physics, Vol 111, *Springer-Verlag, Berlin* (1983).

[19] J. Homola, S. S. Yee, D. Myszka: Surface plasmon resonance biosensors. In: Optical biosensors: Present and future. (Editor: F. S. Ligler), *Elsevier, Amsterdam* (2002) 207-251.

[20] M. C. Hutley: Diffraction gratings. *Academic press* (1982).

[21] J. Homola, G. Schwotzer, H.Lehman, R.Willish, W. Ecke, H. Barlert: A New Optical Fiber Sensor for Humidity Measurement. *Photonics' 95, Prague, Czech Republic, August 1995, EOS Annual Meeting Digest Series*, 2A, 225-248.

[22] A. Schilling, O.Yavas, J. Bischof, J. Boneberg, and P. Leiderer: Absolute pressure measurement on nanosecond scale using surface plasmons, *Appl. Phys. Lett.*, 69 (1996).

[23] B. Moslehi, M. W. Foster, P. Harvey: Optical Magnetic and Electric Field Sensors Based on Surface Plasmon Polariton Resonance Coupling, *Electronic Letters*, 27 (1991).

[24] A. Rasooly: Surface plasmon resonance analysis of staphylococcal enterotoxin B in food. *Journal of Food Protection*, 64 (2001) 37-43.

[25] J. Homola, J. Dostálek, S Chen, A. Rasooly, S Jiang and S. S. Yee: Spectral surface plasmon biosensor for detection of staphylococcal enterotoxin B in milk. *International Journal of Food Microbiology*, 75 (2002) 61-69.

[26] M. Minunni and M. Mascini: Detection of pesticide in drinking water using real-ime biospecific interaction analysis. *Analytical Letters*, 26 (1993).

[27] C. Mouvet, R. D. Harris, C. Maciag, B. J. Luff, J. S. Wilkinson, J. Piehler, A. Brecht, G. Gauglitz, R. Abuknesha and G. Ismail: Detemination of simazine in water samples by waveguide surface plasmon resonance. *Analytica Chimica Acta*, 338 (1997) 109-117.

[28] P. M. Fratamico T. P. Strobaugh, M. B. Medina and A. G. Gehring: Detection of Escherichia coli O157:H7 using a surface plasmon resonance biosensor. *Biotechnology Techniques*, 12 (1998) 571-576.

[29] B. Liedberg, I. Lundstrom and E. Stenberg: Principles of biosensing with an extended coupling matrix and surface plasmon resonance. *Sensors and Actuators B,* 11 (1993) 63–72.

[30] B. Liedberg, C. Nylander and I. Lundström, Surface Plasmon Resonance for Gas Detection and Biosensing, *Sensors and Actuators*, 4, (1983), 299-304.

[31] M. Zhang, D. Uttamchandani: Optical chemical sensing employing surface plasmon resonance. *Electronic Letters*, (1988) Vol.24 No.23, L.

[32] K. Matsubara, S. Kawata, S. Minami: Optical chemical sensor based on surface plasmon measurement. *Applied Optics* Vol.27 No.6 (1988).

[33] G. G. Nenninger, P. Tobiška, J. Homola, S. S. Yee: Long-range surface plasmons for high-resolution surface plasmon resonance sensors. *Sensors and Actuators B*, 74 (2001) 145-151.

[34] M. J. Jory, P. S. Vukusic and J. R. Sambles: Development of a prototype gas sensor using surface plasmon resonance on gratings. *Sensors and Actuators B,* 17 (1994) 1203–1209.

[35] R. C Jorgenson, S. S Yee, A fiber-optic chemical sensor based on surface plasmon resonance, *Sensors and Actuators B*, 12 (1993) 213-220.

[36] A. Trouillet, C. Ronot-Trioli, C. Veillas, and H. Gagnaire, Chemical Sensing by Surface Plasmon Resonance in a Multimode Optical Fiber, *Pure Applied Optics*, 5 (1996) 227 - 237.

[37] R. E. Dessy, W. J. Bender, Feasibility of a Chemical Microsensor Based on Surface Plasmon Resonance on Fiber Optics Modified by Multilayer Vapor Deposition, *Analytical Chemistry*, 66 (1994) 963 – 970.

[38] J. Homola: Optical Fiber Sensor Based on Surface Plasmon Excitation. *Sensors and Actuators* B, 29 (1995) 401 - 405.

[39] R. Slavík, J. Homola, E. Brynda: A miniature fiber optic surface plasmon resonance sensor for fast detection of staphylococcal enterotoxin B. *Biosensors and Bioelectronics,* 17 (2002) 591-595.

[40] H. J. M. Kreuewel, P. V. Lambeck, J. van Gent, T. J. A. Popma: Surface plasmon dispersion and luminiscence quenching applied to a planar waweguide sensors for measurement of chemical concentrations. *Proc. SPIE* , 789 (1987) 218–224.

[41] C. R. Lavers and J. S. Wilkinson: A waveguide-coupled surface-plasmon sensor for an aqueous environment. *Sensors and Actuators B,* 22 (1994) 75-81.

[42] C. Mouvet, R. D. Harris, C. Maciag, B. J. Luff, J. S. Wilkinson, J. Piehler, A. Brecht, G. Gauglitz, R. Abuknesha, G. Ismail: Determination of simazine in water samples by waveguide surface plasmon resonance. *Analytica Chimica Acta,* 338 (1997) 109-117.

[43] J. Dostálek, J. Čtyroký, J. Homola, E. Brynda, M. Skalský, P. Nekvindová, J. Špirková, J. Škvor, J. Schrőfel: Surface plasmon resonance biosensor based on integrated optical waveguide. *Sensors and Actuators B,* 76 (2001) 8-12.

[44] D. C. Cullen, R. G. Brown, C. R. Lowe: Detection of Immuno-complex Formation via Surface Plasmon Resonance on Gold-coated Diffraction Gratings. *Biosensors* 3 (1987/88) 211-225.

[45] M. T. Gale: Replication technique for diffractive optical elements. *Microelectronic Engineering*, 34 (1997) 321-339.

[46] M. J. Jory, G. W. Bradberry, P. S. Cann and J. R. Sambles: A surface-plasmon-based optical sensor using acousto-optics. *Meas. Sci. Technology*. 6 (1995) 1193-1200.

[47] J. M. Brockman, S. M. Fernandez: Grating-coupled surface plasmon resonance for rapid, label-free, array-based sensing. *Am. Laboratory* 33 (2001) 37-40.

[48] J. Dostálek, J. Homola, M. Miler: Rich information format surface plasmon resonance biosensor based on array of diffraction gratings. *Sensors and Actuators B*, 107, (2005) 154-161.

[49] P. Adam, J. Dostálek, J. Homola: Multiple surface plasmon spectroscopy for study of biomolecular systems. *Sensor and Actuators B*, 113 (2006) 774-781.

[50] L. I. Goray: Modified integral method for weak convergence problems of light scattering on relief grating. *Proc. SPIE,* 4291 (2001) 1-12.

[51] L. I. Goray and J. F. Seely: Efficiencies of master, replica, and multilayer gratings for the soft-x-ray–extreme-ultraviolet range: modeling based on the modified integral method and comparisons with measurements. *Applied Optics*, 41 (2002) 1434-1445.

[52] R. Petit: Electromagnetic theory of gratings. *Springer–Verlag Berlin Heidelberg New York* (1980).

[53] R. Karlsson, R. Stahleberg: Surface plasmon resonance detection and multispot sensing for direct monitoring of interactions involving low-molecular-weight analytes and for determination of low affinities. *Anal. Biochem.* 228 (1995) 274–280.

[54] M. J. Jory, G. W. Bradberry, P. S. Cann, J. R. Sambles: A surface plasmon-based optical sensor using acousto-optics. *Meas. Sci. Technol.* 6 (1995) 1193–1200.

[55] http://pcgrate.com

[56] http://camfr.sourceforge.net

[57] J. Homola, I. Koudela, S. S. Yee: Surface plasmon resonance sensor based on difraction gratings and prism couplers: sensitivity comparison. *Sensors and Actuators B*, 54 (1999) 16-24.

[58] G.G. Nenninger, M. Piliarik and J. Homola: Data analysis for optical sensors based on spectroscopy of surface plasmons. *Measurement Science and Technology*, 13 (2002) 2038-2046.

[59] N. M. Lyndin, I. F. Salakhutinov, V.A. Sychugov, B. A. Usievich, F. A.Pudonin, O. Parriaux: Long-range surface plasmons in asymmetric layered metal dielectric structures. *Sensors and Actuators B*, 54 (1999) 37-42.

[60] R. Slavík, J. Homola: A new surface plasmon resonance sensor with an ultra=high resolution: *Europt(r)ode VIII, Tubingen, Germany, April 2 – 5, 2006, Book of Abstracts,* pp. 112.

[61] A. W. Wark, H. J. Lee and R. M. Corn: Long-range surface plasmon resonance imaging for bioaffinity sensors. *Analytical Chemistry*, 77 (2005) 3904-3907.

[62] M. Vala, J. Dostálek, J. Homola: Long-range surface plasmon resonance biosensor based on difraction gratings. *The ninth world congress on biosensors, May 10-12, 2006 Sheraton Centre Toronto, Ontario, Canada, Accepted for presentation.*

[63] G. M. Hale, M. R. Querry: Optical constants of water in the 200-nm to 200-μm wavelength region, *Applied Optics,* Vol. 12, No.3, (1973) 555-562.

Appendix

Dispersion relations

Water:

$$e_{H_2O}(l) = (1.429331 - 0.403306\times10^{-2}\, l + 0.650493\times10^{-4}\, l^2 - 0.487305\times10^{-6}\, l^3 + 0.137143\times10^{-8}\, l^4)^2 ,$$

Ethylene glycol:

$$e_{EG}(l) = \left[1.42099+0.01516\exp\left(-\frac{l-439.06012}{173.61282}\right)\right]^2 ,$$

Gold:

$$\varepsilon_{Au}(\lambda)=[41.56403 - 0.2106\lambda + 3.98641\times10^{-4}\lambda^2 - 3.3293\times10^{-7}\lambda^3 + 1.03534\times10^{-10}\lambda^4 + i(-20.95173+0.0945\,\lambda + 1.44797\times10^{-4}\lambda^2 + 1.0889\times10^{-7}\lambda^3 - 3.09932\times10^{-11}\lambda^4)]^2 ,$$

AlF_3:

$$\varepsilon_{AlF_3}(\lambda)=(-0.36277 + 0.00932\lambda - 1.83679\times10^{-5}\lambda^2 + 1.5643\times10^{-8}\,\lambda^3 - 4.88843\times10^{-12}\lambda^4)^2 ,$$

Dispersion relation of water is taken from [63], while the dispersion relation of ethylene glycol is derived from data provided by the producer. Dispersion relations of gold and aluminum fluoride thin layers were determined using ellipsometer SE-850 (Sentech Instruments, Germany).